DESIGN, DEVELOPMENT AND OPTIMIZATION OF HIGH TEMPERATURE MOTORS FOR IN-SERVICE INSPECTION DEVICES

By

SREE RANJINI K S

Enrolment No: ENGG02201404011

Indira Gandhi Centre for Atomic Research, Kalpakkam, India

A thesis submitted to the

Board of Studies in Engineering Sciences

In partial fulfillment of requirements

for the Degree of

DOCTOR OF PHILOSOPHY

of

HOMI BHABHA NATIONAL INSTITUTE

January, 2019

Homi Bhabha National Institute[1]

Recommendations of the Viva Voce Committee

As members of the Viva Voce Committee, we certify that we have read the dissertation prepared by **Sree Ranjini K S** entitled **"Design, Development and Optimization of High Temperature Motors for In-Service Inspection Devices"** and recommend that it may be accepted as fulfilling the thesis requirement for the award of Degree of Doctor of Philosophy.

Chairman - **(Dr. K.Velusamy)**		**Date:** 3/2/2020
Guide / Convener - **(Dr. S. Murugan)**		**Date:** 03.02.2020
Co-guide - **(Dr. S. Sivakumar)**		**Date:** 3/2/2020
Examiner - **(Prof. Sydulu Maheswarapu)**		**Date:** 03/02/2020
Member 1- **(Dr. B.P.C. Rao)**		**Date:** 3/2/2020
Member 2- **(Dr. Anil Kumar Sharma)**		**Date:** 3/2/2020
Member 3- **(Dr. G. V. Prasad Reddy)**		**Date:** 3/2/2020
Technology Adviser: **(Dr. B. K. Nashine)**		**Date:** 03/2/2020

Final approval and acceptance of this thesis is contingent upon the candidate's submission of the final copies of the thesis to HBNI.

I/We hereby certify that I/we have read this thesis prepared under my/our direction and recommend that it may be accepted as fulfilling the thesis requirement.

Date: 03.02.2020

Place: Kalpakkam

Dr. S. Sivakumar
Co-guide

Dr. S. Murugan
Guide

[1] This page is to be included only for final submission after successful completion of viva voce.

STATEMENT BY AUTHOR

This dissertation has been submitted in partial fulfillment of requirements for an advanced degree at Homi Bhabha National Institute (HBNI) and is deposited in the Library to be made available to borrowers under rules of the HBNI.

Brief quotations from this dissertation are allowable without special permission, provided that accurate acknowledgment of source is made. Requests for permission for extended quotation from or reproduction of this manuscript in whole or in part may be granted by the Competent Authority of HBNI when in his or her judgment the proposed use of the material is in the interests of scholarship. In all other instances, however, permission must be obtained from the author.

Ranjini

Sree Ranjini K S

Date: 28.1.2019

Place: Kalpakkam

DECLARATION

I, hereby declare that the investigation presented in the thesis has been carried out by me. The work is original and has not been submitted earlier as a whole or in part for a degree / diploma at this or any other Institution / University

Ranjini

Sree Ranjini K S

List of Publications

Journals

1. "Memory based hybrid dragonfly algorithm for numerical optimization problems", **Sree Ranjini K S** and S. Murugan, *Expert Systems with Applications*, vol. 83, no. Supplement C, pp. 63 – 78, 2017.

2. "Design and Performance Comparison of Permanent Magnet Brushless Motors and Switched Reluctance Motors for Extended Temperature Applications," **Sree Ranjini K S** and S. Murugan, *Progress In Electromagnetics Research M*, Vol. 67, 137-146, 2018.

3. "A study on performance of MHDA in training MLPs," **Sree Ranjini K S,** *Engineering Computations, Vol.36, No:6, 2019*

4. "Design and development of automated test facility for high temperature motors", Saji Jacob George, **Sree Ranjini K S,** C Rajagopalan, S. Murugan , *Sadhana,* Vol. 45*, No: 6, 2020.*

5. "Intelligent design optimization of extended temperature permanent magnet motor using ANN and MHDA" **Sree Ranjini K S** and S. Murugan (Manuscript under review)

Conferences

1. "Design and Analysis of Brushless Servomotor for In-service inspection of PFBR," **Sree Ranjini. K. S**, R. Chellapandian, S. Murugan, and S. Venugopal, presented in *2015 Annual IEEE India Conference (INDICON)*, held at Jamia Millia Islamia on Dec 2015.(IEEE Xplore doi: 10.1109/INDICON.2015.7443307)

2. "Electromagnetic and Thermal analysis of Permanent Magnet motor for Extended Temperature Applications", **Sree Ranjini. K. S**, S. Murugan presented in *4th International Conference on Electrical Energy Systems* (ICEES), held at SSN College of Engineering, Chennai on Feb 2018.(IEEE Xplore doi: 10.1109/ICEES.2018.8442359)

Awards

1. Best technical paper in 'Control Applications-I' presented in 2015 Annual IEEE India Conference (INDICON) held at Jamia Millia Islamia, New Delhi

Ranjini

Sree Ranjini K S

I dedicate this thesis

to my loving family

Acknowledgements

A doctoral dissertation is usually considered to be a personal accomplishment. However, it would not have been possible for me to finish this work without the inspiration, encouragement, and support from many people.

First of all, I would like to express my sincere gratitude to thesis supervisor, ***Dr. S. Murugan****, Professor HBNI, Associate Director, Components Development & Hydraulics Group, Reactor Design & Technology Group, IGCAR, Kalpakkam. I am grateful to my other doctoral committee members –* ***Dr. K. Velusamy****,* ***Dr. S. Sivakumar****,* ***Dr. B.P.C Rao, Dr. A.K Sharma****,* ***Dr. B.K Nashine****,* ***Dr. G.V.P Reddy*** *for their valuable suggestions, reviewing the work progress and proof reading the synopsis. I am also thankful to former committee members,* ***Dr. S. Venugopal*** *and* ***Dr. M. Saibaba*** *for their support and discussions. I am thankful to* ***Dr. Anish Kumar****, Dean Academic, Engineering Sciences, IGCAR and former Dean* ***Dr. G. Sasikala*** *for valuable guidelines in the completion of thesis work.*

I would like to thank ***Mr. Saji Jacob George****,* ***Mr. R. Chellapandian*** *and* ***Mr. Jobby C Johnson*** *for the close and continuous collaboration throughout our research. I am also thankful to Indira Gandhi Centre for Atomic Research, Kalpakkam and Board of Research in Nuclear Sciences, India for my fellowship to make my PhD financially stable.*

Most important of all, I owe my sincere and heartfelt gratitude to my husband, ***Praveen K and*** *my twin boys****, Naithik and Naman*** *for their unconditional love and support. My heart is filled with deepest gratitude to all my family members and friends for creating a peaceful and encouraging atmosphere. Without their great love, encouragement and understanding, everything would not have been possible. Thank you everyone*

Contents

List of Figures

List of Tables

Chapter 7

Conclusions

The key points and major outcomes of the thesis are summarized in this chapter. The design of a high temperature motor of ISI application, its experimental validation, and optimization is studied. This suggestion for future work is also included in this chapter.

7.1 Summary

In this thesis, a 1HP surface mounted permanent magnet motor capable of delievering rated torque of 2Nm at rated speed of 3500 rpm under high ambient temperature of 150ºC was designed. Strict operational and spatial constraints of ISI application demand super compact motors with a torque density of 20KNm/ m^3. A review has been conducted between permanent magnet and switched reluctance machines. Special care has been taken in the selection of materials used for each motor component. Stator and rotor laminations were built from iron cobalt vanadium alloys having high saturation flux density and low iron loss at high temperatures. This helps in scaling down the size of the motor. Samarium cobalt magnets, which can operate upto temperatures of 350ºC were used in the motor to make them more resistant to possible demagnetization caused by high temperature. Polyimide insulation which can withstand a temperature of 240ºC was used as winding insulation. Design of motor is validated by coupled electromagnetic-thermal analysis run iteratively until a convergence is reached. The design satisfies the major goal of the research delievering rated torque of 2Nm and efficiency of 85% at an ambient temperature of 150^{o}C and at the rated speed of 3500rpm. The performance of the motor has been validated experimentally using indigeniously designed high temperature motor test bench. Prototpe motor was experimentally tested by keeping the oven temperature at 150^{o}C and performance parameters such as speed, torque,winding temperatures were noted. It was found that experimental results were agreeing well with experimenal results.

After verifying the initial design, an attempt was made to improve the performance of high temperature motor adopting an efficient optimization strategy. A novel optimization algorithm namely Memory based Hybrid optimization was proposed. It is a hybridized version of Dragonfly algorithm and PSO algorithm with an additional feature of memory concept. Due to its excellent balance between exploration and exploitation capabilities, MHDA proves to be an effective optimization algorithm in locating near global optimal solution. The efficiency of algorithm is proved in standard test functions and engineering benchmark problems. It is also found that performance of MHDA is better compared to conventional algorithm in terms of accuracy, convergence and consistency and is recommended for optimization in design of high temperature motor.

The main aim of optimization process is to minimize the winding temperature of motor satisfying the constraints of torque,saturation flux density and efficiency. Inorder to save the computational time on optimization using coupled electromagnetic -thermal model, an Artificial Neural Network (ANN) based surrogate model is proposed. This ANN model is trained by MHDA with the set of intelligently chosen data points using Latin hypercube sampling technique. MHDA trained ANN based model is designed and is compared with Kriging based model and found to be more accurate. Further, MHDA is used in optimizing the design parameters of the ANN based model with winding temperature as the objective function to be minimized and torque, efficiency and flux density as constraints. The optimization results are successfully validated using coupled EM-Thermal analysis. The temperature rise in optimized design is 7$^{\text{o}}$C lesser than the original design which approximately corresponds to 20,000 hours increase in life time of insulation. The surrogate based optimization in the design of high temperature motor helps in arriving at fast and accurate optimized model. The main contributions of this thesis are summarised as follows:

1. From the work explained in this thesis, it evident that the high temperature motor design is having high reliability and thereby saving the operating life of motor in the absence of any cooling mechanism. Though the thesis is focused on the application of ISI of Fast breeder reactor, the design methodology adopted in design of motors can be extended to any critical applications. Hence, this work has contributed an in-house designed methodology in the area of high temperature motor design. If there is a relaxation in the space constraints, peek and ceramic insulation having high temperature capabiliy of 500$^{\text{o}}$C can be considered.

2. Most commercial testbenches for motor available today, are designed for operation only under normal temperature. Hence an innovative test bench suitable for testing different types of motors at elevated temperature is presented. The proposed system is capable of evaluation of steady state and dynamic performance of system. Test bench can be used to test latest technology in control algorithms for electrical machine drives and analyze their transient behavior. Test bench can be also used for accelerated life test where the motor is operated at high temperature, thereby subjecting to severe thermo-mechanical stress. This on-line monitoring/data analysis gives valuable information regarding the calculation of reliability and possible failure modes. It is designed to enable a wide variety of electric machine configurations and applications, as it provides

a platform for testing of innumerous projects especially at high temperature.

3. MHDA proposed in the thesis can be applied to any real world optimization problem. Presently it has been applied to Vertical Electrical Sounding (VES) Data[169], power flow analysis[170] etc.

4. The proposed methodology of surrogate modelling combined with optimization algorithm can be helpful in various multiphysics applications since computational cost and effort is reduced.

7.2 Future work

The work explained in the thesis opens up a few areas for further investigation and exploration:

- Manufacture of optimized high temperature motor and validating the optimization strategy with hardware results.
- Studies on MHDA in different levels of applications and other practical problems of different dimensionality.
- The accuracy of thermal analysis can be improved by incorporating Computational Fluid Dynamics (CFD) techniques to estimate the temperature rise.
- Further investigation of multi-objective and multi variate optima to solve complex problems such as efficiency improvement and cost reduction can be considered.
- Study of alternative design topologies for harsh environmental conditions and their performance enhancement are some of the topics that can be considered for further enhancement.
- Application of ANN surrogate model in condition monitoring and fault diagnosis of high temperature motors.

SUMMARY

The demand for compact, high torque density motors capable of operation under high ambient temperature conditions has increased over past few decades. High ambient temperature alters the physical properties of the materials used in motor thereby affecting its performance characteristics. In-Service Inspection (ISI) of Fast Breeder Reactor using semi-automated device is such an application characterized by an ambient temperature of 150°C. The main objective of the research is to develop a high temperature motor for traction of ISI device and to propose methods for design optimization. Special care has been taken in the selection of motor configuration, materials and also in design equations to account for operation at high ambient temperature. A coupled electromagnetic-thermal analysis is done to examine the performance and a 12/10 slot/pole surface mounted permanent magnet motor is selected for development. In order to experimentally validate the design of motor, an automated high temperature test facility is fabricated. The proposed design is validated experimentally in this test set up. For minimizing winding temperature and to improve future design of high temperature motors, a surrogate assisted optimization technique is proposed. Artificial Neural Networks based surrogate model was proposed for approximating the non-linear relationship between the design variables and objective function. A novel hybrid optimization algorithm - Memory based Hybrid Dragonfly Algorithm (MHDA) is proposed and its potential benefits compared to other reported methodologies is demonstrated. MHDA was also used to train ANN based model. Optimized model gave temperature reduction of 7°C satisfying all the design constraints thereby increasing the life time of insulation and reliability of high temperature motor.

Chapter 1

Introduction

This doctoral thesis focuses on researching a novel approach to the design, development and optimization of high temperature motor for In-Service Inspection(ISI) device of Fast Breeder Reactor. This chapter gives an overview of the research background and motivations drawn for research work. The objective of research and thesis organization is also explained.

1.1 Background

With increasing demands of per capita energy due to industrialization and urbanization of world's increasing population, nuclear power plants are poised to augment the conventional energy sources by being safe, environmentally benign and economically viable[1]. In order to assess the integrity of the structures and components while the plants are in service, continuous monitoring and inspection of critical components is necessary. Extremely hostile and hard to reach environmental conditions make manual inspection of plant impossible. In this context, robotics and automation plays a significant role in in-service inspection, maintenance and repair of plant facilities more frequently with higher accuracy. Semi -automated devices, where actions are performed by robots but cognitive decisions are still taken by skilled operator, are excellent choice for ISI of nuclear power plant [2]. In traditional industrial robots, electrical motors of a few hundred to a few thousand watts are most common. However, for newer developments e.g. in service or humanoid robotics, smaller and more lightweight motors with high power density and high functional density are needed. The weight of the complete drive system is required to be low because it is moved along with the robot. This can be achieved by appropriate dimensioning and the choice of high performance motors. In certain safety critical applications apart from operational and spatial constraints, environmental factors also play a major role in design and performance of motor. The demand for electro mechanical actuators operating under harsh environmental conditions has increased with the increasing applications in high performance actuation systems of aerospace and nuclear industries.

High temperature is one of the harsh environmental constraint that influences the operation and lifetime of electrical machine. Electrical and magnetic loading of electrical machine is greatly affected by temperature. Electrical loading is mainly determined by the property of winding insulation to withstand the prescribed temperature rise over an ambient temperature whereas magnetic loading depends upon the magnetic flux density that can be produced by magnets without irreversible demagnetization, which again is a function of temperature. Every electrical motor is characterized by a specific ambient temperature and allowable temperature rise. Most manufacturers do not recommend the operation of motor beyond the specified temperature as it adversely affect the performance of machine and reduces its life time. Motors for typical industrial application are rated for 40°C and any operation beyond this temperature requires either special considerations in design or additional cooling methodologies or both.

In Service Inspection (ISI) of Fast Breeder Reactor (FBR) using semi-automated device is a typical application characterized by an ambient temperature of 150°C. Strict spatial and environmental constraints limit the use of any advanced cooling mechanism. Hence the only method of thermal management in motor can be realized with the use of high temperature materials. With the use of high temperature materials, the overall performance is compromised due to the overall poorer electrical and magnetic properties. Hence an effective optimization methodology is essential to make a proper trade off between all the properties in the design stage. This thesis focuses on the design, analysis, development, experimental validation and optimization methodology of high temperature motor working at an ambient temperature of 150°C.

1.2 In-Service Inspection

ISI plays an important role in maintaining the safety of equipments in nuclear power plant. In this thesis, ISI of nuclear reactor specifically, a FBR is considered. FBRs utilize natural uranium fuel very effectively (∼75%) through breeding and thus provide a rapid energy growth potential (300GWe for about 30 years) [3]. They constitute a clean source of power unlike fossil fuel power stations.

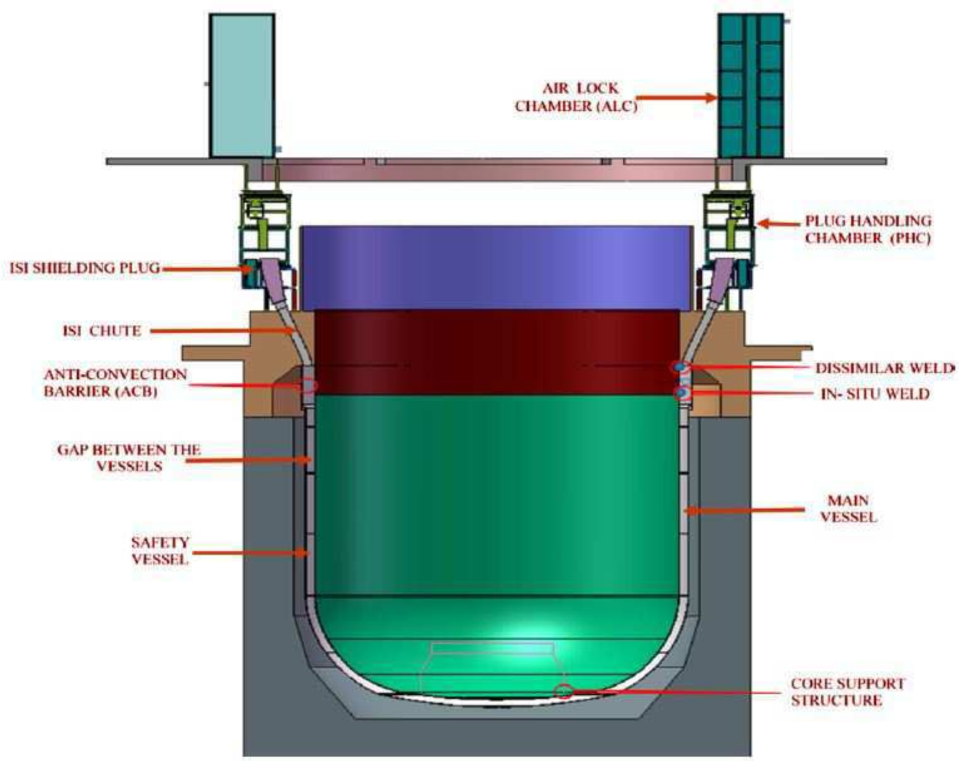

Figure 1.1 – Critical areas of FBR requiring ISI[1]

One of the main objectives of ISI is to monitor the external boundary of main reactor vessel for liquid sodium leakage. ISI is usually carried out in a narrow space between the Main Vessel (MV) and Safety Vessel (SV) of FBR which is filled with nitrogen. Figure 1.1 shows the critical areas of a typical FBR requiring ISI [1]. ISI is usually carried out under offline conditions and the effect of radiation is considered to be minimum. High ambient temperature of 150°C makes manual inspection of the plant infeasible. Thus, any inspection under these circumstances can only be carried out by customized remote inspection techniques coupled with semi-automated vehicles. A typical four wheeled semi-automated device driven by compact, high temperature traction motor is proposed for ISI application. Figure 1.2 shows the CAD model of ISI device.

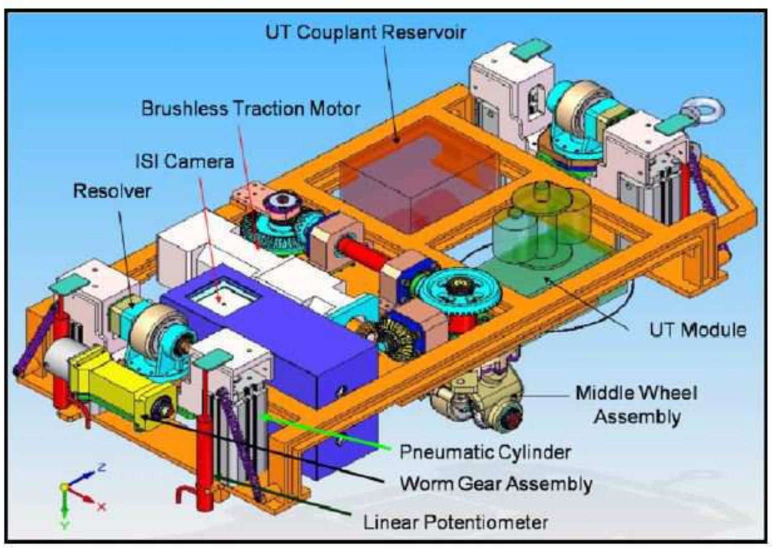

Figure 1.2 – CAD model of ISI device[1]

After inserting the device in interspace for testing, it has to positioned against gravity, pressing continuously on the walls of vessels. Collapsing/expanding mechanism in the ISI vehicle helps in adjusting the real time variations of the interspace which is in the order of ±50 *mm.* The mechanical assembly as well as the actuators for steering and traction for the device must withstand temperature of 150°C in the interspace. The controller and associated drive electronics are housed in a modular-sealed-airlock chamber kept at room temperature approximately at a height of 6.5m above the reactor vault[3]. Figure 1.3 shows the block diagram of the servo mechanism for traction motor of the device.

Due to limited spatial conditions, a compact, high torque density traction motor with high temperature operating capability and low weight is required to drive the semi-automated device. Operating conventional motors at this high ambient temperature can result in partial or complete demagnetization of permanent magnets and deterioration of insulation which further leads to thermal runaway and stalling of motor. Stalling of motor can cause the risk of device getting jammed in the annular space, which is highly undesirable. Hence it is very necessary that the traction motor must be capable of withstanding high temperatures and providing required torque, meeting the space constraints of the device.

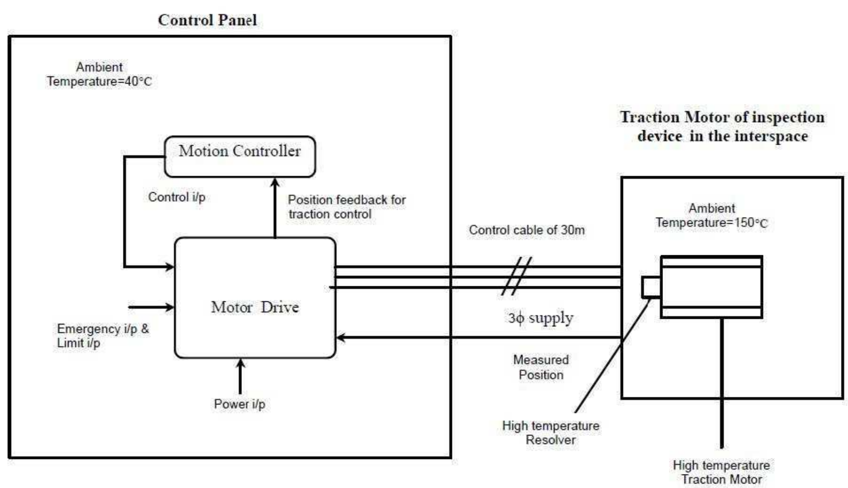

Figure 1.3 – Block Diagram of the servo mechanism for traction motor

Apart from application in ISI device, high temperature motors are also used in jet engines or deep-sea drilling equipment. The possible applications of high temperature motors also includes pumps and valves for liquid metal cooling systems[4], material lifting from oil and geothermal wells[5], gimbals for expendable launch vehicle engines and components of spacecraft that operate near extremely hot sources such as the sun, gas turbine starters/generators for aircraft engines[6], robotic exploration vehicle systems that operate in and around terrestrial volcanoes[7] and deep ocean hydrothermal vents[8].

1.3 Motivation and Objectives

Literature review shows that there have been considerable efforts in the design of electrical machines operating under harsh environmental conditions. A short duty permanent magnet motor operating at an ambient temperature of 80°C was proposed for aviation industry [9]. Japan Atomic Power Company has proposed a design of high temperature servomotor operating at a temperature of 220°C [10]. A high temperature motor capable of operating at high temperature of 460°C was proposed for Venus drilling mission [7]. However, these design of high temperature motors fails to meet the stringent operational as well as spatial requirements of ISI device and an attempt has been made to design and develop a compact high temperature motor with high torque density and high efficiency without any cooling method.

The market availability of high temperature motors matching the specifications is also rare which demands an indigenous technology development of these motors. Moreover the knowledge gained from the design and development of high temperature motors can be further extended for different other applications in nuclear reactor such as actuation of control rods[11], under sodium scanners[12], submersible linear pumps[13].

High temperature motor for ISI application is realized with the proper selection and utilization of high temperature materials in the design. But these high temperature materials have poorer electrical and magnetic properties which necessitates an efficient optimization strategy with fast computational capability to make a proper trade-off between electrical, thermal and other material properties in the design stage [14]. The proposed research is also aimed to develop a fast and efficient method for the design and optimization of high temperature motor operating at temperature of 150°C. In this way, an advanced methodology, replacing outdated design practices, that would allow designers to optimize electromagnetic devices that meet the needs of any given specific application is developed. The objectives of research can be summarized as follows.

1. To understand the application requirements and to design an extended temperature permanent magnet motor operating at a temperature of 150°C for In-Service Inspection device of Fast Breeder Reactors. The motor is expected to meet the operational and spatial constraints in the absence of any cooling mechanism.

2. To compare permanent magnet and permanent magnet free motor topologies for extended temperature applications.

3. To analyze the design of motor using coupled electromagnetic-thermal analysis and accurately predict the temperature rise in different parts of motor.

4. To validate the initial design with experimental results.

5. To optimize the design using an appropriate optimization algorithm.

6. To develop a surrogate assisted evolutionary optimization technique for minimizing the winding temperature by optimal selection of design parameters.

7. To validate the optimal results with coupled FEA-thermal simulations.

1.4 Structure of thesis

This thesis presents the research work conducted for the design, analysis, development and optimization of high temperature permanent magnet motor working at an ambient temperature of 150°C. Thesis is divided into 7 chapters. The description of following chapters are given below.

Chapter 2 details on the basic necessity and general applications of high temperature motors. A broad literature review of current developments in high temperature motors is also explained. The challenges in the design of high temperature motors is reviewed along with the relevance of optimization strategy in the design of such motors.

Chapter 3 focus on application specifications of high temperature motor for traction of ISI device used in Fast Breeder Reactors. First of all, the selection of materials compatible with high temperature is carried out and verified the performance with a coupled electromagnetic -thermal analysis. A detailed survey of motor topologies suitable for high temperature applications is also explained. The chapter explains the detailed design of SMPM motor for high temperature applications. Following the design, a coupled electromagnetic-thermal analysis for estimating the electromagnetic and thermal performance of the motor is explained.

Chapter 4 describes the development of prototype high temperature motor and its experimental validation using automated test bench. The performance of prototype is validated by testing the motor characteristics in this test bench under different temperatures.

Chapter 5 details on the design of novel hybrid optimization algorithm known as MHDA developed for solving numerical optimization problems such as motor design. The chapter gives a detailed survey on reported optimization algorithm and the need of developing a hybridized algorithm. The chapter describes operating mechanism of MHDA and also analyses the relation between the algorithm parameters, search space boundaries and the variables in the optimization problem and their impact on the overall search performance. The efficiency of MHDA in solving engineering problems is also demonstrated by standard design problems which proves its credibility for applying it to multiphysics design optimization task of electric motor design.

Chapter 6 proposes a novel method of constructing a surrogate model based on Artificial Neural Networks(ANN) for high temperature motor. MHDA is used in ANN training for finding the optimal set of weight and biases. The performance of ANN trained by MHDA is also compared with kriging based surrogate model. Followed by the performance analysis, ANN based surrogate model is used for sensitivity analysis and optimized for minimum hot spot temperature. The performance of optimized high temperature motor is also validated by finite element analysis.

Chapter 7 summarizes the key points and major conclusions drawn from the research work towards the design and development of high temperature motor. The suggestion for future scope of the research is also explained.

Chapter 2

Literature Survey

This chapter gives a comprehensive literature review of main topics treated in this thesis. An overview of applications characterized by harsh operating conditions is provided in the beginning. An up-to-date survey of high temperature motors is presented along with their design challenges followed by an overview of traditional design analysis methods and the latest progress in optimization of electric machines design.

2.1 Robotics for harsh environmental conditions

Harsh environment is any environment that is hazardous or challenging to agents within it. It can be characterized by high levels of radiation, high explosive risk, extreme temperature or pressure[15]. In such conditions, Robotics and Autonomous Systems (RAS) play a significant role to avoid human exposure to hazardous environment and tasks ranging from scrutiny and general maintenance to decontamination and post accidental activities. Rapid decrease in cost, flexibility and integration of artificial intelligence have enabled robots to be successfully deployed in many critical applications. There are different forms of robotic system with different functionalities and intended for different applications. Wheeled mobile vehicles, unmanned aerial vehicles, humanoid robots, serial-link manipulators, snake robots and legged robots are some of them. Based on control, robotic systems are divided into manual, semi-automated and fully automated system. For critical systems, semi-automated systems where the human operator is in loop for providing cognitive assistance for safe execution of operation is recommended. Some of the applications deploying these systems are automation industries, oil and gas industry, nuclear power plants, space exploration system, and pipeline inspection system. In nuclear power plants, robotic systems are used for radioactive material handling, inspection of reactor assemblies, pressure vessels, pipelines and also assistance in examination. Deploying robots at nuclear power plants can reduce the risk of human exposure to hazardous radiation and temperature; at the same time helps to execute specific task with more precision and without interruption [16].

In this thesis, robotic system used for ISI of Fast Breeder Reactor is considered. A free roving four-wheeled semi-automated device is used for the inspection of Main Vessel (MV) and Safety Vessel (SV) of FBR for any possible sodium leakage. The four-wheeled remote-controlled robotic device is designed to carry non destructive testing equipment into the inter-space (which is the gap between MV and SV) for enabling volumetric examination of welds and visual examination of external surface and internal surface of the MV and SV respectively. The temperature of inter-space is expected to be in the range of 150°C at the time of inspection [17]. The semi-automated device will be maneuvered by means of four independently driven wheels with steering capability, two resting on each vessel. Each wheel will have traction and steering motors with encoders for position feedback. ISI is usually carried out under shut down conditions and effect of radiation is considered negligible [1]. Since the ambient temperature is characterized by 150°C, traction and steering motors or actuators must be able to withstand this high temperature and provide necessary torque for the movement of the device.

Over the years, there has been considerable research in the design and development of electrical machines operating at adverse environmental conditions. However, all these known solutions generally lead to an increase of the overall weight and volume, which could then have a significant impact on the machine's suitability for the application.

2.2 Electrical machines for high ambient temperatures

Electrical machines that can survive harsh environmental conditions have been an interesting research topic in recent years due to increasing applications in aerospace, mining and nuclear industries. For high performance applications, reliability, high torque density, high efficiency and lower weight are of high importance. Electrical machines generate torque either electromagnetically or by reluctance principle[18]. In the first category, motion is produced by the interaction of two magnetic fields, one generated by the stator and the other by the rotor. Two magnetic fields, mutually coupled, produce an electromagnetic torque tending to bring the fields into alignment. The same phenomenon causes opposite poles of bar magnets to attract and like poles to repel. The vast majority of motors in commercial use today operate on this principle. Some of the familiar ways of generating these fields are through energized windings, with permanent magnets, and through induced electrical currents. In the second category, motion is produced as a result of the variable reluctance in the air gap between the rotor and the stator. When a stator winding is energized, producing a single magnetic field, reluctance torque is produced by the tendency of the rotor to move to its minimum reluctance position. This phenomenon is analogous to the force that attracts iron or steel to permanent magnets. In those cases, reluctance is minimized when the magnet and metal come into physical contact. Switched reluctance motor and synchronous reluctance motor falls into this class of machines. Synchronous reluctance motor require variable frequency drive and construction is more complex than switched reluctance motor. Hence, only Switched Reluctance(SR) motor is considered for comparison with Permanent Magnet(PM) motor.

2.2.1 Switched Reluctance (SR) Machines

The concept of SR machines has been already known for more than 150 years, and with availability and improvement of cost effective high power fast semi-conductor switches and extensive use of microcontrollers and integrated circuits, SR machines have become popular. SR motors consist of doubly salient structure having stator with excitation windings and rotor without any windings. Absence of permanent magnets makes SR motors a simple, mechanically robust and cost-effective solution for high temperature applications provided appropriate stator winding insulation materials are used. Another advantage is their phase independent operation making them a fault tolerant solution for critical applications[19]. There are number of works reported regarding high ambient temperature operation of SR motors. High temperature light weight switched reluctance motors and generators were designed for aircraft engine application and lunar exploration light rover. However operation under extreme temperatures were not fully tested. A four phase 8/6 SR motor, with a frame size of NEMA 23 was designed and developed for Venus drill application where the ambient is filled with carbon dioxide and characterized by a temperature of 460°C and atmospheric pressure greater than 90 bars[20]. But it's torque output was in th range of mNm. A high temperature SR motor operating at 280°C was designed for hybrid electric vehicles [21]. Size was not a constraint for this application, hence higher electrical loading was done to achieve higher power density.

2.2.2 Permanent Magnet (PM) Machines

PM brushless motors have dominated the motion control applications which demand high positional accuracy. They have the advantages of high torque density, high efficiency and compact size as demanded by most of robotic applications. The presence of permanent magnets imparts a strong and independent excitation system but their performance at high temperatures needs to be investigated. Permanent magnet brushless machines based on their mode of excitation are divided into brushless dc motor and brushless ac motor. Based on position of permanent magnets, PM machines are divided into Surface Mounted PM (SMPM) machines and Interior PM (IPM) machines. SMPM configurations can achieve higher torque density than IPM machines with low weight and mass density. Due to sinusoidal flux distribution, they have low rotor losses and high efficiency. IPM machines have higher inductance and high saliency ratio that makes them suitable for field weakening applications. There have been reported works in literature regarding the design of PM machines for harsh operating conditions. This is realized either by effective cooling system or by using high temperature materials. A high temperature IPM motor was designed for ambient temperature of 150°C through effective oil cooling system for hybrid electric vehicle[22]. The design of PM motor with wide operating temperature ranging from -60°C to 300°C using high temperature materials was discussed in [23]. Design of high temperature brushless dc motor for oil well detecting system where the ambient temperature is 175°C was explained in [24]. However fabricated prototype was not tested under high temperature conditions. A high-temperature BLDC fan rated for 250°C was designed for forced air-cooling of advanced automotive power electronics [25]. Special focus was put on the design of the integrated BLDC machine for an ambient temperature of 250°C, including magnetic material selection and winding material selection. Wang [26] proposed a high temperature version of PM synchronous motor using phase change materials applied in the actuator systems of aircraft. A short duty PM brushless dc motor was designed for ambient temperature of 70°C for aerospace application was proposed by Sciascera in [9]. A PM machine was selected and designed adopting integrated electromagnetic and thermal models within a GA optimization tool.

2.3 Electromagnetic and Thermal Modelling Techniques

2.3.1 Electromagnetic field models and Finite Element Analysis

Classical analytical design equations are useful for initial design and sizing of electrical machines as they provide very fast and rapid solutions. However, flux leakage effects and change in the permeability of materials cannot be accounted as the magnetic circuit is considered to be linear[27]. Hence for accurately predicting the performance, the initial design by analytical equations is verified using set of magnetostatic simulations which correspond to different time instances, rotor positions and stator current distributions. These magnetostatic simulations are governed by Maxwell's equations which includes:

$$\nabla \times H = J \tag{2.1}$$

$$\nabla \times E = 0 \tag{2.2}$$

$$\nabla . B = 0 \tag{2.3}$$

where H is the magnetic field intensity, J is the current density, E is the electric field intensity, B is the magnetic flux density.

The magnetic non-linearity of materials is expressed as

$$B = B_r + \mu H \tag{2.4}$$

where B_r is the remanent flux density and μ is the permeability of the material.

Since magnetic field are solenoidal, they can be studied using Magnetic Vector Potential (MVP) equation[28] defined as

$$\nabla.(\nabla \times A) = 0 \tag{2.5}$$

where $A$is the magnetic vector potential.

Equation 2.5 can be rewritten into Poisson's vectorial equation as

$$\nabla(\frac{1}{\mu}\nabla \times A) = J + (\frac{1}{\mu}\nabla \times B_r) \tag{2.6}$$

In the case of non-linear magnetostatic field and isotrophic materials, equation 2.6 can be rewritten as

$$\frac{\partial}{\partial x}(\frac{1}{\mu}\frac{\partial A}{\partial x}) + \frac{\partial}{\partial x}(\frac{1}{\mu}\frac{\partial A}{\partial x}) = -J - [\frac{\partial}{\partial x}(\frac{B_{r,y}}{\mu}) + \frac{\partial}{\partial y}(\frac{B_{r,x}}{\mu})] \tag{2.7}$$

By applying anti-periodic or periodic boundary conditions, cross-sectional area for field analysis is reduced and the study of the flux distribution is by dividing the circuit into smaller pieces including the surrounding air into very small bits such as triangles and solving for MVP. Correct material properties must be used in the field equation solutions to achieve accurate results[29].

Based on the magnetic vector potential solution, the x and y components of the magnetic flux density are derived from the previous equations and the radial and tangential components can be calculated as

$$B_r(r,\theta) = B_x cos\theta + B_y sin\theta \tag{2.8}$$

$$B_t(r,\theta) = -B_x sin\theta + B_y cos\theta \tag{2.9}$$

The energy, W_m and co-energy, W_m^* per unit of axial length is calculated as

$$W_m = \int_s \int_0^B (HdB)ds \tag{2.10}$$

$$W_m^* = \int_s \int_0^H (BdH)ds \tag{2.11}$$

The electromagnetic torque per unit axial length, T_e can be calculated with Maxwell stress tensor as

$$T_e = \frac{D_g}{2\mu_0} \int_0^{\Pi D_g} B_r B_\theta \tag{2.12}$$

or by differentiating energy with respect to angular co-ordinate at constant flux linkage

$$T_e = -\frac{\partial w}{\partial \theta} \tag{2.13}$$

2.3.2 Thermal Modelling using equivalent circuits

Thermal modeling of electrical machines is generally divided into two methods- numerical methods and lumped parameter equivalent circuits. Numerical method of analysis can estimate temperature distribution in any part of electrical machine leading to prediction of hot spot temperatures. Numerical method involves combination of thermal Finite Element Analysis (FEA) in solid components and Computational Fluid Dynamics (CFD) to determine flow in complex parts such as air gap or motor end windings.

Method of analysis using thermal circuits is very fast to calculate and simple to model. This method gives only lumped distribution of temperature and does not give detailed estimation of hot spot temperatures in complex parts of machine[30]. Due to easy implementation and fastness in calculation, it is usually incorporated in optimization routine in industry. MOTORCAD is a commercially available software that incorporates detailed analytical thermal model for thermal analysis of electrical machine. Figure 2.1 shows the example for steady state heat transfer network of brushless motor as given by MOTORCAD software.

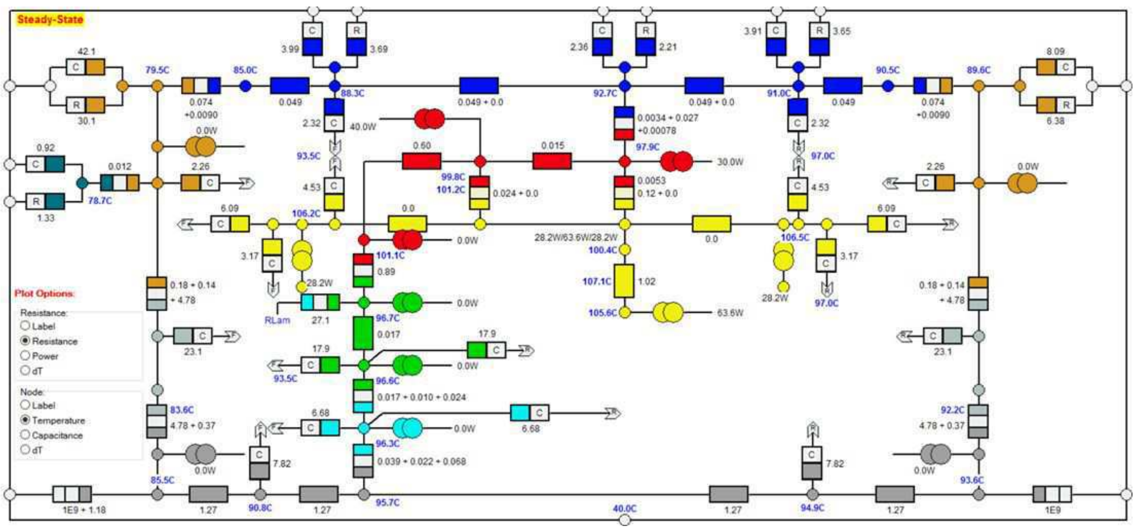

Figure 2.1 – Steady state heat transfer network of MOTORCAD

The analysis using MOTORCAD was found to be computationally effective as well as fairly accurate for estimation of temperature and have been widely used[31]. It involves heat transfer analysis and flow network analysis for estimation of temperature[32]. Thermal circuits of different parts of motor have been combined to obtain a complete thermal model of motor. Heat transfer analysis is analogous to electric circuit analysis where nodal temperature differences corresponds to voltages, power losses corresponds to current sources, power flow through resistances corresponds to current, and thermal resistance corresponds to electric resistance. Only thermal resistances are used to model heat transfer path for steady state analysis. Heat transfer occurs by conduction within solid and laminated components, where as it occurs by convection within air or any other cooling fluids. For thermal modelling, stator and rotor of electric motors are considered as hollow cylinders, whereas stator teeth and rotor teeth are considered as partial hollow cylinders. Axial shaft is modelled as long beam and heat transfer is taken along axial direction. Conductive heat transfer in a hollow cylinder containing heat sources can be solved using Fourier's law[33].

$$\frac{1}{r}\frac{\partial}{\partial r}[k_r\frac{\partial T}{\partial r}] + \frac{1}{r^2}\frac{\partial}{\partial \theta}[k_\theta\frac{\partial T}{\partial \theta}] + \frac{\partial}{\partial z}[k_z\frac{\partial T}{\partial z}] + q = \rho c_p\frac{\partial T}{\partial t} \tag{2.14}$$

where q represents the heat source represented by losses, $(k_r, k_{\theta,}k_z)$ represents the thermal conductivity in cylindrical co-ordinate system(r, θ, z), ρ represents density, c_p denotes specific heat capacity and T represents temperature.

There exist a number of conductive paths inside machine such as from winding copper to stator tooth and back iron, from stator back iron nodes to stator bore. Conductive thermal resistance, R_{cond} is calculated as

$$R_{cond} = L/KA \tag{2.15}$$

where $L(m)$ and $A(m^2)$ denotes length and path area from geometry and $K(W/m/°C)$ denotes thermal conductivity of material.

Convection heat transfer is realized through natural convection and forced convection. Natural convection arises due to buoyancy forces arising from density changes caused by fluid motion in the vicinity of surface where as forced convection is caused due to fluid motion produced by fan or pump[29]. Convective thermal resistance is calculated as

$$R_{conv} = \frac{T_{surface} - T_{ambient}}{q} = 1/(h_c.A) \tag{2.16}$$

where $T_{surface}(°C)$ denotes surface temperature, $T_{ambient}(°C)$ denotes ambient temperature, $h_c(W/m^2/°C)$ denotes convection heat transfer coefficient and A denotes surface area.

Convection coefficient, h_c is usually made dimensionless and is derived from equation 2.17

$$N_u = \frac{h_cL}{k_f} = f(R_a, P_r) \tag{2.17}$$

in case of natural convection and in the case of forced convection, from equation 2.18

$$N_u = \frac{h_c L}{k_f} = f(R_e, P_r) \tag{2.18}$$

where L is the characteristic length, N_u is Nusselt number, R_e is the Reynold's number, R_a is Rayleigh's number and P_r is the Prandtl 's number[33].

Radiation heat transfer is realized through energy transfer by electromagnetic waves. Radiation resistance, R_{rad} value is calculated as

$$R_{rad} = 1/(h_r.A) \tag{2.19}$$

$h_r(W/m^2/°C)$ denotes radiation heat transfer coefficient and $A(m^2)$ denotes surface area. Radiation heat transfer coefficient is calculated using the formula:

$$h_r = \sigma \varepsilon F_{1-2} \frac{T_1^4 - T_2^4}{T_1 - T_2} \tag{2.20}$$

where σ is the Stefan- Boltzmann's constant, ε is the emissivity of the radiating surface, $T_1(K)$ is the absolute temperature of radiating surface, $T_2(K)$ is the absolute temperature of surface radiated to (ambient) and F_{1-2} is the view factor for dissipating surface 1 to the absorbing surface 2.

Thermal resistance values are automatically calculated from motor dimensions and material data.

Flow network analysis is used to predict the flow velocity for fluid through the machine which is a function of forced convection heat transfer from the surface. Fluid mechanics counterpart is analogous to electric circuit analysis with pressure drop corresponds to voltage, volume flow rate corresponds to current, and fluid-dynamic resistance corresponds to electrical resistance. The fluid-dynamic resistance is governed by the equation 2.21

$$R = \frac{k\rho}{2A^2} \tag{2.21}$$

where, ρ is the air density, A is the flow area, and k is the dimensionless coefficient of local fluid resistance.

2.3.3 Coupled electromagnetic-thermal analysis

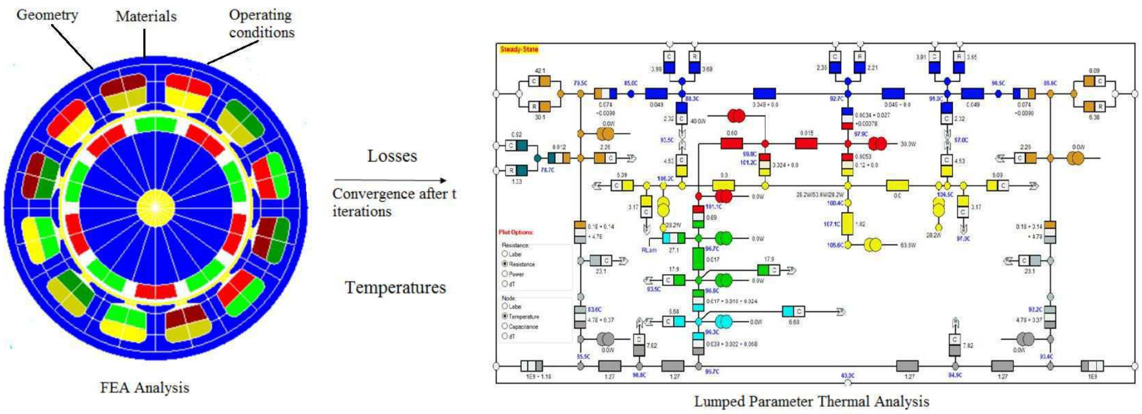

Figure 2.2 – Coupled EM-Thermal analysis

Electromagnetic and thermal simulations are directly linked due to the temperature dependent properties of the materials including copper, lamination steels, and coolant. With increase in temperature remanent flux density of permanent magnet reduces where as resistivity of copper increases. A coupled electromagnetic thermal simulation can accurately predict the electromagnetic and thermal performance of the electrical machine[34]. Electromagnetic analysis predicts the performance parameters of motor such as flux density distribution, saturation, and torque. It also predicts the amount of losses in the machine which acts as heat sources to the thermal model. Thermal model then predicts the temperature rise in different parts of motor. This procedure is iteratively continued until difference of losses computed from thermal and electromagnetic model is converged to less than 5% error[35]. Figure 2.2 shows the multiphysics coupled analysis.

2.4 Design Optimization of Electrical Machines

Electrical machine design is a comprehensive multiphysics phenomenon comprising electromagnetic, insulation, mechanical design. In critical applications such as aerospace, mining and nuclear industries, stringent requirement specifications such as torque, power density, volume and weight have to be met in addition to sustaining harsh environmental conditions. Energy efficiency of electrical machines is another crucial parameter for energy conservation, environment protection, and global sustainable development. Consequently, improving motor performance is of great significance to both the environment protection and the energy sustainability[36]. The design methodology of electrical machines has undergone different design changes with the recent developments in power electronics, new magnetic materials, manufacturing process and computational algorithms. Traditional design methods based on rules of thumb and empirical formulas have slowly become outdated and has often not made use of progress to improve machine performance. Therefore, there is an absolute requirement for a modern design method that is flexible, reliable and reflects up-to-date improvements in modern science and technologies [9].

In any optimization process, there are three important features to be considered. They are models, strategies and optimization algorithms [36]. Based on number of objectives to be optimized, there are single objective optimization model and multi-objective model. Strategies or methods correspond to the methods of execution of optimization. Some of the popular methods are direct, indirect, sequential, multi-level and space mapping. Direct optimization method involves optimization using analytical models. In-direct optimization uses surrogate models for optimization purpose. Surrogate model or metamodel is a black box model that reflects a complex model outputs in a limited context. There are several types of surrogate models, such as Response Surface Methodology (RSM), Kriging model, Radial Basis Function (RBF) model, Support Vector Machine (SVM) model, and Artificial Neural Network

(ANN) model[37]. Electric machine design optimization is a non-linear process involving large number of parameters, data, material properties and different domains. In order to reduce the computational complexity of optimization process, surrogate based optimization is becoming very popular. Sequential level optimization process is another method of optimization that reduces initial design space to interested subspace containing optimal solution. Multi-level optimization, which divides the initial high dimensional space into several subspaces by using sensitivity analysis methods is also very effective. The parameters with higher sensitivities will be optimized before those with lower sensitivities thereby reducing computational complexity and improving efficiency of the optimization process. Space Mapping (SM) method of electrical machines involves fine and coarse model spaces[38]. For electrical machines, the fine analysis model can be a FEA model or an analytical model; the coarse model can be a magnetic circuit model or a surrogate model. The optimization is conducted in the coarse model space only. However, the optimization solution is not good due to the less accuracy of the coarse model [36]. Therefore, several optimization loops may be required in the implementation of SM method.

Optimization algorithms play a very important role in finding global optimal solutions. Multiphysics and non-linear of objective function make optimization process complex. Therefore, an efficient optimization tool is necessary to make trade off between design objectives and search for optimal design parameters. With advancement in computational intelligence and optimization algorithm, there has been several reported works in the design optimization of electrical machines. As per No-Free Lunch theorem[39], there is no single algorithm that outperform other algorithms on all optimization problems. However, in practice, certain algorithms are more effective in solving certain problems and it is important to identify them. The search space of a problem is defined by the type of response, number and range of design variables.

Optimization algorithms are classified into conjugate gradient algorithms and intelligent algorithms. Now a days, electric machine design optimization is based on finite element analysis rather than analytical or mathematical models, which involves large data samples hence intelligent algorithms are used in the design optimization of electrical machines[36]. Among intelligent algorithms, swarm based algorithms have been widely used in solving engineering constrained problems. A swarm is characterized by a group of self-organized and decentralized system of non- complex individuals or agents interacting among themselves and with their environment for survival, hunting, navigation or foraging. It can be school of fish, flock of birds,colonies of ants etc. Swarm Intelligence models the collective behavior of these individuals to solve complex optimization process. Even though as individuals, these agents have limited operational capability, they tend to outperform in accomplishing the desired task by interacting among themselves and with the environment using their own specific behavioral patterns. Bat algorithm[40], Firefly algorithm[41], Krill Herd[42], Whale optimization algorithm[43], Grey wolf optimization[44], Competitive optimization algorithm [45], Dragonfly algorithm[46] are some of the recently developed swarm based meta heuristic algorithms.

2.5 Recent studies on design optimization of electrical machines

There have been many reported works in the design optimization of electrical machines using analytical methods. An analytical model of fractional slot brushless PM machines was developed and optimized using Particle Swarm Optimization (PSO) in [47]. An axial flux PM synchronous machine was designed using analytical method and optimized using Evolutionary Computation in [48]. Metamodel or surrogate based optimization have great potential in reducing computational complexity of optimization process and has been gaining popularity in engineering design problems[49]. Line start permanent magnet motor was optimized using neural network and Imperialistic

Competitive Algorithm[50]. A switched reluctance generator was optimally designed using Kriging based surrogate model and genetic algorithm [51]. Zheng Tan [52] proposed a surrogate based optimization for maximizing the power output of doubly fed induction generator. A permanent magnet flux switching generator was optimally designed using Artificial Neural Network and multi-objective PSO [53]. A number of design optimization works based on sequential optimization methodology has been reported in the literature [54][55]. A multiobjective sequential design optimization of PM-SMC motors for six sigma quality manufacturing was discussed in [55]. Techniques for multilevel design optimization of permanent magnet motors are presented in [56]. Space mapping optimization of the magnetic circuit of electrical machines including local material degradation was explained in [57] and Kriging output space mapping technique for electromagnetic design optimization was explained in [58].

Relevance of considering multiple domains in the design optimization of electrical machines has been discussed in [59]. A multiphysics modelling of permanent magnet synchronous machine was carried out using lumped models of magnetic, electrical, electronic, thermal whereas vibro-acoustic and mechanical parts are represented by analytical models [60]. A new technique for coupling the electromagnetic, thermal, and airflow analysis is proposed particularly for electric machines that exhibit reduced dependence of core losses with temperature and load and have low rotor losses [61]. An implicit constrained multiphysics system for motor wheels of electric vehicle was modelled and optimized using stochastic optimization algorithm in [62]. Multi-physics analytical model for a saturated permanent magnet assisted synchronous reluctance motor consisting of electromagnetic model, electrical model, loss model, and thermal model was discussed in [63]. A multiphysics design methodology combining electromagnetic and thermal models was applied to a high force density short duty linear actuator [64]. The design of high-speed permanent-magnet (PM) electrical machine for centrifugal air blower application with consideration of the multiphysics constraints, including the mechanical strength, rotor dynamics, mechanical losses, and thermal field was explained in [65].

2.6 Inspiration for the present work

The literature review reveals that there are worldwide developmental activities carried out for the design and development of high temperature electrical motors. It has been found that high temperature motors reported in the literature have certain disadvantages for application to ISI, either due to the additional cooling system or due to inadequate torque to weight ratio. The overall objective of this project is to theoretically and practically investigate an improved permanent magnet brushless motor for an ISI application with the specific aim to operate at high ambient temperature of 150°C without any cooling mechanism. This involves basic design, development and experimental validation of high ambient temperature motor in a high temperature test facility. Since the characteristics of these type of applications are exploited by employing high current densities for the stator windings, the windings' electrical insulation system will experience critical temperature cycles during operations which can adversely affect the lifetime of the insulation[9]. Hence it is required to minimize winding temperatures. A coupled electromagnetic thermal analysis, which can be computationally expensive, is necessary to accurately estimate the rise in temperature. Taking account of this, a structured design methodology based on a novel optimization algorithm and an efficient surrogate model is proposed to minimize the winding temperature meeting the requirements of torque, efficiency and flux density. This research will be of interest to aerospace, automotive, geothermal and mining industries which requires motors operating under harsh environmental conditions. The proposal of novel optimization technique using surrogate model and novel hybrid optimization algorithm can be highly useful for industries for reducing the computational cost and speeding up the large scale optimization process.

2.7 Conclusion

- In this chapter, a literature review of the main topics concerning the design of high temperature motors for ISI devices is presented.
- A review of robotic applications for harsh environmental conditions is discussed.
- A survey of electrical machines, with special focus on permanent magnet machines and switched reluctance machines is carried out. Clearly, each machine technology has distinct advantages and depending on considerations of cost, eco-friendliness, and utilization, the selected machine technology can be optimized to meet the required specifications.
- A brief review of the design optimization methods for electrical machines, including design analysis methods and models, optimization models, algorithms and methods/strategies is presented.
- Recent design optimization studies of electrical machines is reviewed and objectives of present work are summarized.

Chapter 3

Design and Performance Analysis of High Temperature Motor for ISI Application

---

This chapter deals with details of application specifications and selection of appropriate motor configuration for traction of semi-automated device used for In-Service Inspection (ISI) of Fast Breeder Reactors. A comparative performance analysis of permanent magnet and permanent magnet free configuration for high temperature environment is carried out. Choice of design is made based on analysis results taking all the critical factors into consideration and making the required trade off. The design of selected motor configuration is completed using conventional analytical equations. And finally, the performance of the machine is predicted with coupled FEA- thermal analysis.

3.1 Introduction

The demand of electrical machines operating at a high ambient temperature (i.e. 100^{o}C and above) is gaining significance with increased applications in automotive, mining, aerospace and nuclear industries [7]. At this high temperature environment, the performance of electrical machines gets degraded predominantly due to failure of insulation and demagnetization of permanent magnets (as in the case of permanent magnet motors). Hence, to ensure the safe operation as well as intended performance of electrical machines, several factors must be considered in the initial design stage. One amoung the globally used techniques to address the issues at high temperature is an effective design of cooling system. The cooling system can be either natural or forced convection with gaseous or liquid coolant. But, in aerospace and nuclear applications, having strict restrictions on the operational and spatial constraints, provision of cooling system in most cases seems to be an infeasible option. In such cases, use of materials that can sustain higher temperatures is a plausible option. In-Service Inspection (ISI) of Fast Breeder Reactor (FBR) using semi-automated vehicle is such an application characterized by an ambient temperature of 150ºC[1]. This chapter details on the application requirement specification of traction motor, selection of motor configuration, design by analytical equations and performance analysis using coupled electromagnetic-thermal simulation.

3.2 Application specifications

The specifications of traction motor of ISI device is framed based on (i) torque (ii) temperature and (iii) weight of the application.

3.2.1 Torque

The torque required for drive motor of robotic device, can be derived by applying principles of vehicle dynamics[66]. According to vehicle dynamics, the total tractive effort is equal to the sum of forces due to Grade Resistance (GR), Rolling Resistance (RR), and Force required for Acceleration (FA). The free body diagram of vehicle moving up an inclined plane is shown in Figure 3.1. Following are the inputs provided by the mechanical designers of the ISI device which are considered for determining the torque of traction motor[1][67].

1. Weight of robotic vehicle is 70 kg

2. Maximum slope at which the vehicle is expected to climb is 45°.

3. Coefficient of rolling friction between vessel steel and wheel is 0.3

4. Radius of the wheel is 40mm

5. Friction loss factor is 1.

6. Maximum acceleration of vehicle is 0.2 m/s^2

7. Gear Ratio is 50:1

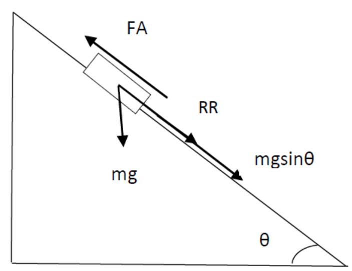

Figure 3.1 – Free Body Diagram of vehicle moving up an inclined plane

Grade Resistance(GR) is the force necessary to move a vehicle and it is given by

$$GR = 70\,kg \times 9 \cdot 8\frac{m}{s^2} \times \sin 45 = 485 \cdot 5\,N \tag{3.1}$$

Rolling Resistance (RR) is the opposing force that the vehicle has to overcome during rolling motion. In case of ISI vehicle, force on wheels was found to be 3300N[1] and rolling resistance can be calculated as

RR= Force exerted on the wheels x coefficient of rolling friction

$$RR = 3300N \times 0 \cdot 3 = 990N \tag{3.2}$$

Force required for acceleration (FA) is given by

FA=Mass x Acceleration

$$FA = 70kg \times 0 \cdot 2\,\frac{m}{s^2} = 14N \tag{3.3}$$

According to vehicle dynamics, the torque required by the motor is given by

$$T_m = R_f \times (GR + RR + FA) \times r_{wheel} \tag{3.4}$$

whereR_f denotes the friction loss factor and r_{wheel} denotes the radius of the wheel. Assuming the outer radius of the traction motor as 40mm, torque can be calculated as

$$T_m = 1\,(485 \cdot 57N + 990N + 14N) \times 0 \cdot 04 = 59 \cdot 58Nm \tag{3.5}$$

Torque required by the motor considering gear ratio is given by

$$T_m = 59 \cdot 58/50 = 1 \cdot 2Nm \tag{3.6}$$

A de-rating of 60% is considered for safe operation of vehicle and the Torque required by the motor,T_m is be set to $2Nm$.

3.2.2 Ambient conditions

In service inspection is a procedure which is performed during the shut down of reactor. Though the temperature during operation is higher than 500^{o}C, during the inspection the maximum expected temperature is 150^{o}C. Hence, the machine has to withstand a temperature of 150^{o}C, delivering the rated torque. The effect of radiation during inspection is also considered to be negligible. The space for inspection is filled with gaseous Nitrogen to provide an inert atmosphere.

3.2.3 Size and Weight

The robotic vehicle is designed to be compact so that it can be positioned and moved in the limited space of about 300mm. The volume of the motor is decided by the space allocation in the vehicle.The maximum outer diameter and length of the motor can be 100 mm and 100 mm respectively. The weight of motor must be kept as minimum as possible to increase the payload capacity of vehicle. Based on the above factors, the specifications of drive motor are derived and summarized in Table 3.1[1].

Table 3.1 – Application requirements

Parameter	**Value**
DC bus voltage	310V
Rated Torque	2Nm
Rated Speed	3500rpm
Maximum Outer Diameter	100mm
Maximum Length	100mm
Ambient Temperature	150°C
Efficiency at ambient temperature	>75%
Weight	Minimum
Excitation	Sinusoidal
Atmospheric medium	Nitrogen

3.3 Selection of High temperature materials

The major concerns in high temperature motor design is the selection of stator core laminations, permanent magnets and proper insulating materials for windings.

3.3.1 Stator Lamination

The selection of lamination steels in motors is based on the factors such as core loss, cost, saturation flux density and permeability. Most commonly used materials for stator laminations in electric motors are nickel steel, iron cobalt vanadium alloy and silicon steel [68]. For motion control applications, popular choice is M19 silicon steel which has lowest core losses with smaller cost impact. But it tends to saturate at higher temperatures. Iron cobalt vanadium (FeCoV) alloys offer high saturation density and lower core losses and are considered to be best materials for compact design of motor working at high temperatures. Hiperco-50, a commercially available iron cobalt vanadium alloy, has high saturation flux density of 2.3T at normal room temperature and Curie temperature of 940°C. Due to its superior performance under high ambient temperatures, laminations of Hiperco-50 of 0.15mm thick have been selected for this analysis.

There are a variety of materials that are used for lamination coating like Nomex paper, Mica, Ceramic, Epoxy etc. Nomex paper can withstand a temperature of 180 ºC. Mica insulation can withstand higher temperatures of 500 ºC. Due to size constraints Nomex paper and mica insulation were not used. Ceramic coating can withstand higher temperatures of 500 ºC, but it can considerably increase in the size of machine and it is difficult to get a uniform coating. Hence, Ceramic coating is not preffered. High temperature Epoxy (of Jotatemp make) is used in prototype motor which can withstand continuous temperatures up to 250°C and peak temperatures as high as 300°C.

3.3.2 Permanent Magnet

High remenant flux density and coercivity are desired characteristics of permanent magnets operating at high temperatures. Neodymium Iron Boron (NdFeB) and Samarium Cobalt (SmCo) are two suitable choices. Alnico has better thermal properties, but its energy product is small making size of magnet as well as the motor bulky. NdFeB magnets are brittle and have poor thermal performance compared to SmCo magnets[68]. Fig 3 shows the temperature dependent remanence of SmCo and NdFeB magnets[69]. SmCo has lower magnetic remanence than NdFeB at room temperature, but possesses much higher Curie temperature than NdFeB which makes them appropriate for high temperature applications. It also offers high thermal stability and magnetic output at elevated temperatures of even 550°C. The remanence loss at temperature of 150°C of bulk magnets can be calculated from the approach used in [70]as follows

$$B_{r(150°C)} = B_{r(20°C)} \left[1 + \alpha_{PM}(150°C - 20°C)\right] \tag{3.7}$$

where $B_{r(150°C)}$ and $B_{r(20°C)}$represents the residual flux density of magnet at 150°C and 20°C respectively, and α_{PM} is the linear coefficient of temperature dependence of permanent magnet. The typical values of α_{PM} is -0.016 to -0.035%/^{o}C. The temperature coefficient of remanence of commercially available SmCo magnet, Vacoflux 240HR is-0.035%/^{o}C. Magnets are retented to the surface of rotor using magnet bonding adhesives which have high temperature resistance, high impact and shear strength and high thermal conductivity in order to keep pace with high temperature working condition and vibration. Cyanoacrylate adhesives that can withstand temperature of 250°C is used to hold the magnet. Metallic sleeve or non-metallic sleeve was not used since mass of the magnets was small and can be sufficiently retained by high temperature adhesive. Ceramic ball bearings having high temperature withstanding capability is used.

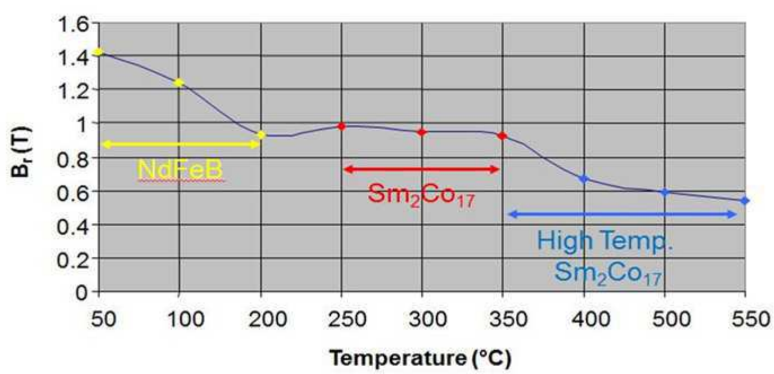

Figure 3.2 – Temperature dependent remanence of SmCo and NdFeB magnets

3.3.3 Winding

As the motor operates continuously temperature increases in the coil due to Joule losses. So the temperature of winding can rise up to 240°C depending upon the operating speed and losses. Oxygen Free High Thermal Conductivity (OFHC) copper conductors with organic insulation may fail at these temperatures. Hence, inorganic insulation such as polyimide, amide-imide or ceramic have to be used. Ceramic windings and Nickel clad copper windings can withstand a temperature of 500 ºC but they have small bending radius due to which number of conductors that can be accommodated in slot decreases thereby decreasing the output of the machine. Moreover they require special bobbin to wind. Ceramic windings if wound like regular motors, fiber coating will detach leading to break down of coil. Hence polyimide insulation, that can withstand temperatures of 240°C is used for the design. Impregnation with high performance epoxy can further enhance the heat dissipation from windings. The following equation describes the change in resistance of the windings with respect to temperature

$$R_{(150°C)} = R_{(20°C)}(1 + \alpha(150° - 20°C)) \tag{3.8}$$

where $R_{(150°C)}$ and $R_{(20°C)}$ represents the resistance of the winding at 150°C and 20°C respectively, and α is the coefficient of temperature dependence of stator coils. The bearings also have to function at high temperatures. Special types of greases are available that can withstand temperatures up to 250 ºC [25].

The details of material selected in the construction of the prototype motor is tabulated in Table 3.2

Table 3.2 – Materials used in components of prototype motor

Component	Materials
Shaft	Nickel chromium alloy
Rotor Laminations	Iron cobalt vanadium alloy
Magnet grade	Samarium Cobalt Sm_2Co_{17}
Stator Laminations	Iron cobalt vanadium alloy
Wire winding & insulation	Polyimide insulated Cu
Magnet Retention	High temperature Cyanoacrylate glue
Ground wall insulation	High temperature Nomex insulation

3.4 Comparison of machine configuration: PM Vs SR motors

Brushless Permanent Magnet (PM) motor is widely used for high ambient temperature applications. Switched Reluctance (SR) motor, that works on reluctance principle for torque generation can be considered as an alternative candidate for brushless PM motors. Absence of permanent magnets, robust structure and phase independent operation makes SR motor more attractive than PM motor. This section aims to compare SR motor with PM motor for ISI application in terms of output torque, losses, efficiency, weight, material cost and average temperature. The design of SR motor having torque, power, speed range and efficiency values competitive to those of PM motor has been investigated for hybrid electric vehicles in [71]. Comparison studies for SR and PM motors have also been carried for electric bicycles[72] and electric brakes[73]. However, the feasibility of replacing PM motor with SR motor for high temperature, compact, high torque density application is not reported and demands a thorough investigation of electromagnetic and thermal performances. A standard PM benchmark design was taken as reference and SR motor was designed to meet the same torque requirements of PM motor using the same material for stator, rotor, magnet and armature winding. The detailed dimensions of SR motor designed for high temperature using standard equations/software is shown in Table 3.3. The flux density of designed SR motor is shown in Figure 3.3.

Table 3.3 – Dimensions of SR motor

Parameter	**Value**
Outer radius (mm)	60
Shaft radius (mm)	15
Rotor outer radius(mm)	32.5
Rotor pole arc	23^{o}
Stator pole arc	21^{o}
Number of turns	50

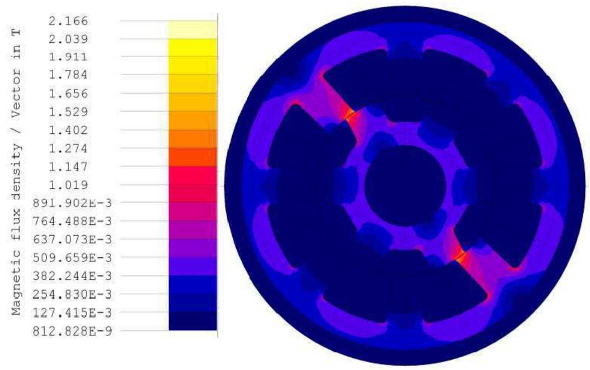

Figure 3.3 – Flux density of SR motor

3.4.1 Torque comparison

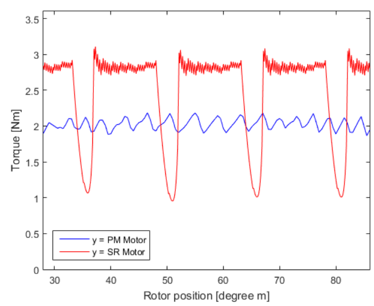

Figure 3.4 – Torque waveform of SR and PM motor

To meet the output torque requirements, the outer diameter and stack length of SR motor was increased to 120mm and 88mm respectively. SR motor requires a greater dimensions when compared to brushless permanent magnet motor for producing the required torque.This can ultimately increase the envelope size of traction motor in the inspection vehicle. The torque characteristics of SR motor and PM motor is shown in the Figure 3.4 respectively. It is found that, at rated speed of operation, the torque ripple is high for SR motor compared to brushless motors.

3.4.2 Efficiency comparison

In permanent magnet motors, permanent magnets act as a source of excitation in addition to the stator windings. Hence torque generation is contributed partly by permanent magnets and partly by stator excitation current. SRM on other hand, require greater amount of stator windings to generate equivalent torque. Moreover, high ambient temperature can also cause an increase in resistance of windings which further add to copper losses. Copper loss contributes major part to the total losses thus reducing the efficiency of SR motor to about 73.5% at 150°C while that of permanent magnet motor is about 85.84% . Figure 3.5 shows the comparison in terms of losses of SR and PM motor.

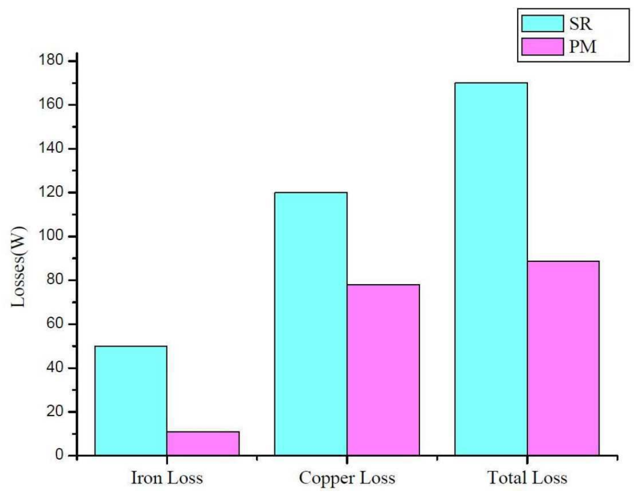

Figure 3.5 – Loss comparison of SR and PM Motor

3.4.3 Weight and cost comparison

Due to its increased weight of iron and windings, net weight of SR motor is on higher side when compared to permanent magnet motor. Table 3.4 shows the weight of active parts of PM motor and SR motor (excluding weight of shaft and housing). The difference in weight is about 0.6 kg which is insignificant as compared with the weight of ISI vehicle, which is around 70 kg

Table 3.4 – Weight comparison between SR and PM motors

Active parts	SRM	PM
Iron(Kg)	2.5	1.9
Magnet(Kg)	-	0.2
Copper(Kg)	0.7	0.5
Total(Kg)	3.2	2.7

3.4.4 Temperature rise

Table 3.5 – Temperature comparison between SR and PM motors

Motor Part	natural cooling	forced cooling	natural cooling
	SRM($^\circ C$)	SRM($^\circ C$)	PM($^\circ C$)
Winding	216.77	141	185.1
Housing	214.24	134	190
Rotor	215.27	89	182
Stator	203.53	134	181
Shaft	191.94	134	177
Bearing	213.09	125	174

To determine the temperature rise in various parts of motor, thermal analysis of SR motor is performed and compared with that of PM motor. For the sake of completion, the analysis is inclusive of both natural and forced cooling in SR motor. Without cooling, temperature in various parts of SR motor is found to be higher than PM motor as shown in Table 3.5. A forced cooling system with Nitrogen as coolant, can reduce the temperatures of SR motor. The winding temperature of SR motor with cooling is found to be 44.1ºC lesser than PM motor. But this provision of additional cooling system can also increase the cost of SR motor up to 30%.

To summarize, the designed SR motor is attractive in terms of cost and simplicity but it has disadvantages of high torque ripple and increased dimensions. SR motor is slightly heavier than PM motors; however difference in weight is insignificant in the context of ISI application. Efficiency of SR motor is less than PM motors due to increased copper losses. Temperature rise in different parts of SR motor is on higher side compared to PM motor, but this can be improved by with forced cooling. SR motor is a potential candidate for this application if proper cooling is provided. Though SR motor is inferior to PM motor in terms of size, efficiency and torque ripples, it has key advantages such as no risk of demagnetization at high temperature, low cost and easy availability. PM motor is recommended for high efficiency, lower weight and good thermal performance, in lieu of high cost and uncertainty in availability of magnets. Considering all the factors above, PM motor is selected for the present application.

3.5 Design equations for Permanent Magnet (PM) motor

Permanent magnet motors are the fastest growing machine/drive market share, even in the increasing prices of rare earth materials and magnets. PM motors are broadly divided into brushless AC motors and brushless DC motors. They share the same configuration except that they are excited by different nature of voltages. Brushless DC motor is fed with a trapezoidal waveform and synchronized with the rotor angular position, allowing only two phases to conduct. Brushless AC motors on the other hand, is fed with sinusoidal waveform and synchronized with rotor angular position, allowing three phases to conduct. The main advantage of brushless AC motors over DC is its robustness and ability to produce smooth torque.

The sizing constraints of motor have been arbitrated by the space that it has to occupy in the robotic vehicle. For enhanced performance of servo drives, the Torque per Rotor Volume (TRV) falls in the range of 14 KNm/m^3-50 KNm/ m^3[69]. The torque of the motor is directly related with the air gap flux density. Increasing the air gap flux density demands an increased length of permanent magnets or reduced air gap length. However too small air gap length is hard to realize and it increases the amount of cogging torque.

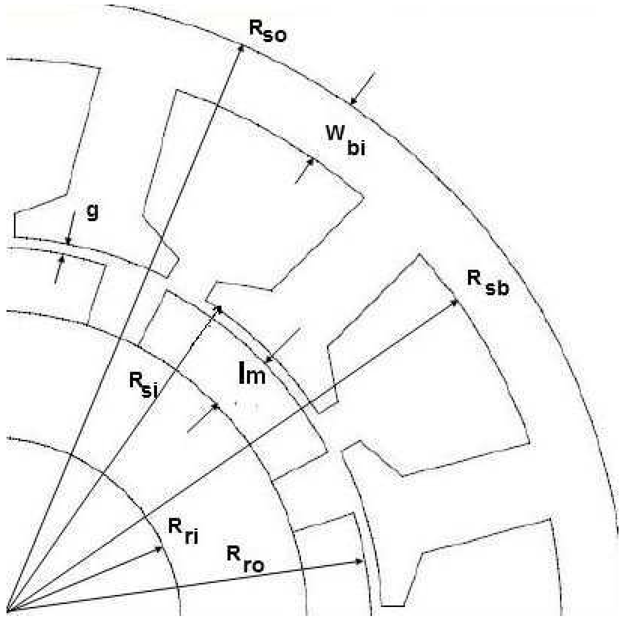

Figure 3.6 – Geometric cross-section of PM motor

The magnetic circuit of motor is built from the analytical equations explained in [74]. Figure 3.6 shows the geometric cross-section of PM motor. Some of the major design and sizing equations are explained below.

Permeance coefficient (PC) is computed from the length of magnet l_m, flux concentration factor $C_\Phi$and air gap length g [74].

$$PC = \frac{l_m}{gC_\Phi} \tag{3.9}$$

The average air gap flux density, B_g is calculated as[74]

$$B_g = \frac{C_\Phi B_r}{(1 + \mu_R K_c K_{ml}/PC)} \tag{3.10}$$

where $\mu_R$is the permeability of the magnet, K_c is the Carter's Coefficient, B_r is remanent flux density of magnet and K_{ml} is the magnet leakage factor.

Back iron width, $w_{bi}$is given by

$$w_{bi} = \frac{\phi_g}{(2B_m K_{st} L)} \tag{3.11}$$

where $\phi_g$is air gap flux, K_{st} is stacking factor and L is the motor axial length.

Assuming frame size of R_{so} other geometrical parameters are calculated as[74]

$$R_{sb} = R_{so} – w_{bi} \tag{3.12}$$

$$R_{si} = R_{ro} + g \tag{3.13}$$

$$R_{ri} = R_{ro} - l_m - w_{bi} \tag{3.14}$$

where $R_{sb}, R_{si}, R_{ri}, R_{ro}$ represents back iron radius, stator inner radius, rotor inner radius and rotor outer radius respectively.

Total slot depth ,d_s is given by

$$d_s = R_{sb} - R_{ro} - g \tag{3.15}$$

Given the desired torque total slot current,

$$I_S = n_s i \tag{3.16}$$

where n_s is the number of slots and I is the current per slot.

$$I_s = \frac{T}{(N_m K_d K_p K_s B_g N_{spp} R_{ro} L)} \tag{3.17}$$

where N_m represent number of poles, K_d, K_p represent winding factors, N_{spp} represent number of slots per pole and L represent motor length. Increase in the number of phases always increases the fault tolerance and reliability of the entire drive system. After finalizing the dimensions, power losses which include copper loss and core loss are computed neglecting mechanical losses. In this paper, standard Jordan model of iron losses as shown in the equation below is used for analysis.

$$P_{Fe} = K_h f B_{pk}^2 + K_{ec} B_{pk}^2 f^2 + K_{ex} B_{pk}^{1.5} f^{1.5} \tag{3.18}$$

where K_h is hysteresis coefficient, K_e is eddy current coefficient, K_{ex} is excess loss coefficient, B_{pk} is peak flux density and f is frequency.

The copper power loss, P_{cu} in SR motor is calculated as

$$P_{cu} = m I_{rms}^2 R_{r(T_{ref})} (1 + \alpha_r (T°C - T_{ref}°C)) \tag{3.19}$$

where I_{rms} denotes rms current, T denotes operating temperature, $R_{r(T_{ref})}$ denotes the resistance at temperature T_{ref} and α_r denotes the linear coefficient of temperature dependence of resistance.

Due to high ambient temperature and number of phases, copper loss is prominent and contributes to major part of the total losses. Once the losses are estimated from electromagnetic model, values are exported to thermal model for finding temperature rise.

The efficiency of motor producing rated torque, T at rated speed w_m is given by

$$\eta = \frac{(T w_m)}{(T w_m + P_r + P_c l + P_S)} * 100 \tag{3.20}$$

where P_r is the ohmic motor loss, P_{cl} is the core loss and P_s is the stray load loss.

3.5.1 Choice of SMPM vs IPM

Based on the position of permanent magnet on rotor, PM machines are classified as Surface Mounted Permanent Magnet (SMPM) motor and Interior Permanent Magnet (IPM) motor. Surface mounted machines are characterized by presence of magnets on the surface of the rotor whereas interior mounted machines have permanent magnets embedded within the rotor. SMPM motors have the advantage of high torque density, low torque ripple, reduced weight and volume[75]. IPM motors on the other hand are recommended for high speed applications where field weakening operation is required[76]. Considering the application of ISI vehicle, SMPM motors are more suitable in terms of higher torque density and lower weight. Hence SMPM motors are only considered in the rest of the analysis.

3.5.2 Choice of number of phases, slots and poles

Three phase motors have better conductor utilization factor, reduced torque ripple without any starting problems. However, they require three pair of power semiconductor switches which increases the total cost. Basically, the number of slots is chosen based on fundamental winding factor and Lowest Common Multiple (LCM) between number of poles and slots. Winding factor determines torque constant and LCM gives number of cogging periods per mechanical revolution[77].

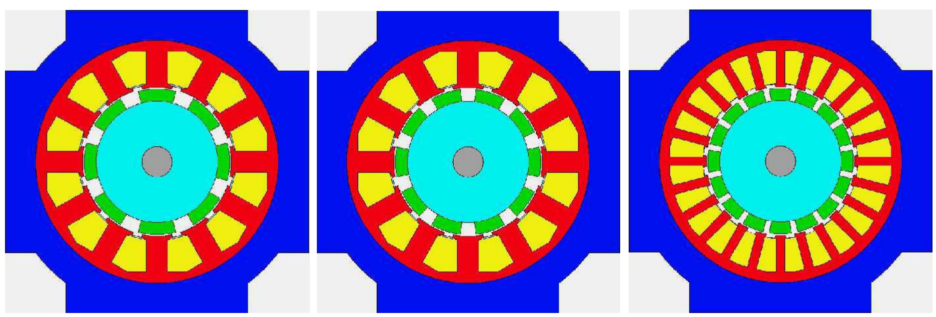

Figure 3.7 – Typical Cross-section of 12/8, 12/10 and 24/16 configuration

Single layer concentrated windings is a common choice due to its simple manufacturing process and reduced copper loss. Fractional-slot non overlapping winding is widely used in high performance applications because of high torque density, high efficiency, and low cogging torque[29]. Three widely used configurations of surface mounted brushless motor with slot /pole of 12/8, 12/10, 24/16 satisfying the application requirements, are studied and compared. The cross-section of 12/8, 12/10, and 24/16 are shown in Figure 3.7.

Table 3.6 – Performance metrics of three configurations

Parameter	**12/8**	**12/10**	**24/16**
Stack Length(mm)	55.3		
Outer Diameter(mm)	80		
Shaft diameter(mm)	10		
Air-gap (mm)	0.5		
Slot Fill factor	0.40		
Ambient temperature (^{o}C)	150		
Current density(A/mm^2)	5		
Slot Depth (mm)	12		
Torque (Nm)	1.8	2.35	2.12
TRV(KNm/m^3)	18.8	20	19
K_{w1}	0.866	0.933	0.866
LCM	24	60	48
Cogging Torque(Nm)	1.14	0.18	0.62
Weight(Kg)	3.81	2.35	1.99
Efficiency at 3500 rpm (%)	84.42	84.78	83.98
Average Winding Temperature (^{o}C)	188.8	188.1	186.6

For each solution, a preliminary design has been carried out using the procedure proposed in previous section. Three machine configurations are designed against specifications mentioned in the Table 3.6. For a fair comparison, stack length, slot fill factor, current density, air gap diameter and outer diameter are kept constant for all three cases. The electromagnetic and thermal behaviour are closely interrelated with each other due to temperature dependent properties of copper, lamination steel and magnet. The coupled analysis is carried out taking the effect of ambient temperature into consideration.

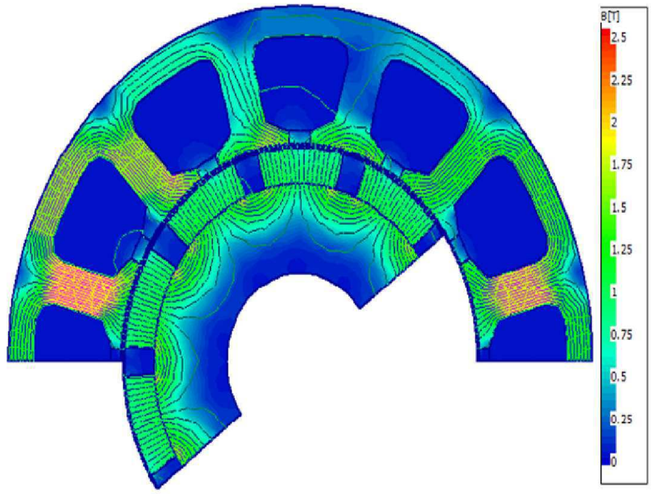

Figure 3.8 – Flux distribution of 12/10 configuration

Losses from the electromagnetic model are passed on, as heat sources to the thermal model. Thermal model predicts the temperature rise in various parts of motor. Increase in temperature again leads to increase in losses and the process is iteratively repeated until the solution is converged. A coupled electromagnetic-thermal simulation using MOTORCAD software is carried out to determine the performance characteristics of three configurations. Structural variation of motor with temperature is neglected in the analysis. In this study, a fixed supply voltage of 310V and current density of 5A/mm^2 is applied to determine the electromagnetic performance characteristics such as torque, weight and efficiency. The key characteristics of machine are tabulated in Table 3.6. Since all the three configurations have same diameter, total length, air gap and current density, comparison between the designs can be made directly looking at performance parameters.

The back emf and torque waveform are shown in Figure 3.9and Figure 3.10 respectively.

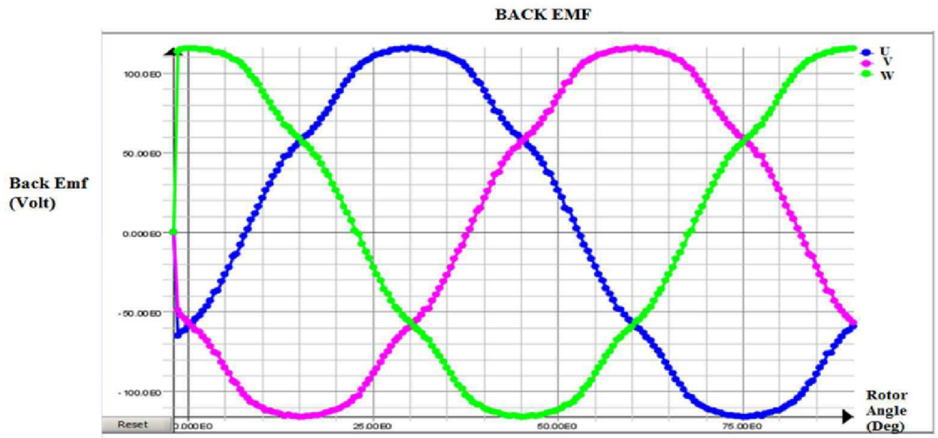

Figure 3.9 – Back emf waveform of 12/10 configuration

Efficiency of 12/10 was found to be better than 12/8 and 24/16. The configuration of 12/10 also has slightly better Torque per Unit Rotor volume compared to 12/8 and 24/16. 12/10 configuration was found to be lighter than 12/8 but heavier than 24/16 by 0.36 Kg. Thermal performance is one of critical parameters in the selection of motor configuration. It can be inferred from Table 3.6, the average temperature in all configuration was below the limit imposed by insulation. However, 12/10 exhibited improved thermal performance over 24/16 and more or less same performance as 12/8. The comparison among the proposed designs points out that all the solutions can satisfy the application requirements as shown in Table 3.1. Nevertheless, good thermal performance and lower losses were primary concerns; amount of torque ripple, cogging torque and weight must be also considered while making the final selection of topology. Hence 12/10 having lowest torque ripple, low cogging torque and lowest temperature among three is considered for application. Total iron losses in 12/10 machine was computed as 12W and Copper losses were found to be 58W.

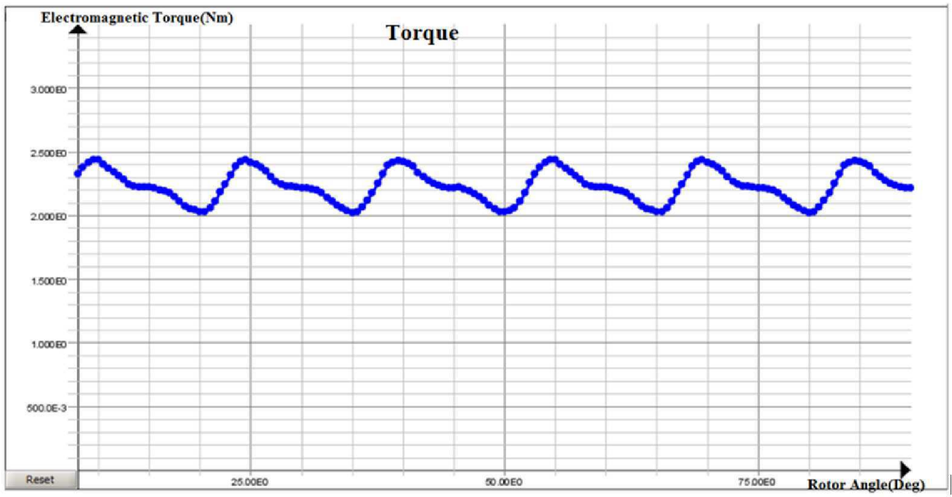

a

Figure 3.10 – Torque waveform of 12/10 configuration

The temperature distribution is shown in Figure 3.11

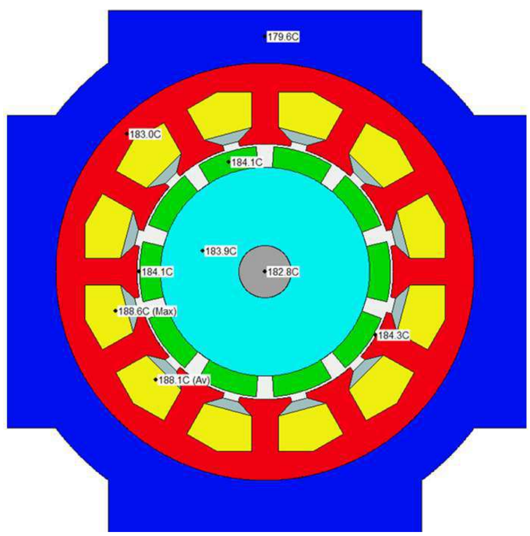

Figure 3.11 – Temperature distribution of 12/10 configuraation

The contents of this work are published in [78], [79] and [80].

Therefore surface mounted permanent magnet configuration was selected as final configuration. The design and winding details from simulation are tabulated in Table 3.7

Table 3.7 – Basic design parameters of 12/10 surface mounted permanent magnet motor

Parameter	**Value**
Outer rotor diameter	48mm
Rated Speed	3500rpm
Continuous torque	2Nm
Number of slot/pole	12/10
Stack length	90mm
Stator phase resistance	1.55ohms
Stator outer diameter	80mm
Stator slot depth	12mm
Stator back iron thickness	3.8mm
Coil winding gauge	21AWG
Air gap flux density	0.85T
Continuous Power Rating	746W
Air gap length	1mm
Ambient temperature	150ºC
Slot fill factor	40%
Current density	5A/mm^2
Magnet angle	140degrees
Magnet thickness	4mm
Shaft diameter	12.5mm
Rotor back iron thickness	14.5mm
No of turns/coil	36
No of strands	1

3.6 Conclusion

Following inferences can be made from this chapter.

- Application specifications for traction motor of ISI vehicle are framed following rules of vehicle dynamics.
- Materials capable of withstanding high temperature are selected for motor parts.
- A feasibility study of switched reluctance motor replacing permanent magnet brushless motor for high temperature application is explained. It is found that the designed SR motor is attractive in terms of cost and simplicity but it has disadvantages of high torque ripple and increased dimensions. Considering the above factors PM motor has been selected.

- A comparative study of widely used slot/pole configurations is studied and slot/pole of 12/10 is recommended for current application based on torque, cogging torque and efficiency requirements.

- Performance is further analyzed by coupled electromagnetic -thermal simulation and it is found with a frame size of 80mm and current density of $5A/mm^2$ the designed motor could achieve a torque of 2.35Nm which is satisfying the requirements of ISI vehicle.

- The maximum flux density found from magnetic analysis was 2.25 T which was below the saturation flux density of stator material and winding temperature was recorded to be 188.6^{o}C which was below the temperature limit of the insulation used in the design.

- The simulation results of basic design were found to be promising for the application. However in order to experimentally validate the results, a high temperature motor based on initial design needs to be built and tested.

Chapter 4

Development of High Temperature Motor and its Experimental Validation

---

This chapter deals with the development of prototype high temperature motor and its experimental validation using indigenous built automated test facility. The aim of the tests is to experimentally evaluate the performance of initial design of high temperature motor, as well as to compare the experimental results with the simulation results. All the attributes and purposes of test facility are explained in detail. Before testing the actual prototype, performance of the test facility is verified with commercially available high temperature stepper motor.

4.1 Introduction

The results produced by software simulations are usually optimistic and must be backed up by experimental results for confirmation, before their use for real time applications. A high temperature motor based on initial design and materials as explained in chapter 3 was developed and its performance characteristics at high temperature were tested in motor test bench. Electric motor test bench is an off site test facility used for evaluating the performance of motor. Most of these test bench as available in the market do not have a facility to test the performance of the motor under different ambient temperatures[81][82][83]. Hence a novel high temperature test bench suited for testing different types of motors at elevated temperature is considered.

4.2 Development of Initial Prototype of High Temperature Motor

Figure 4.1 – Prototype high temperature motor

A surface mounted permanent magnet motor is developed based on initial design. The developed machine has a rated speed of 3500 rpm and rated power of 1HP. The stator and rotor laminations are made from Hiperco 50 alloys. The stator has 12 slots with fractional distributed windings. Polyimide coated magnet wire having high heat absorption capability is used as the winding material. The rotor design consists of surface mounted permanent magnets with a pole arc of 140° using SmCo magnets having remanent flux density of 1.12T.

Figure 4.1shows the developed prototype of high temperature motor.The performance of the motor is verified in an indegeniously designed motor test bench.

4.3 Structure of motor test bench

The design of test bench is carried out keeping special attention on individual modules to withstand high temperature conditions. The developed test bench consists of a high temperature oven with stainless steel frame, fixtures for holding the motor under test, torque sensor and a braking mechanism. A work table with provisions for holding the drives, power supplies, accessories like panel meters for the measurement, and personal computer (PC) with control software and graphical user interface (GUI) for display of the motor parameters are also provided. Figure 4.2 shows the block diagram of the high temperature test set up.

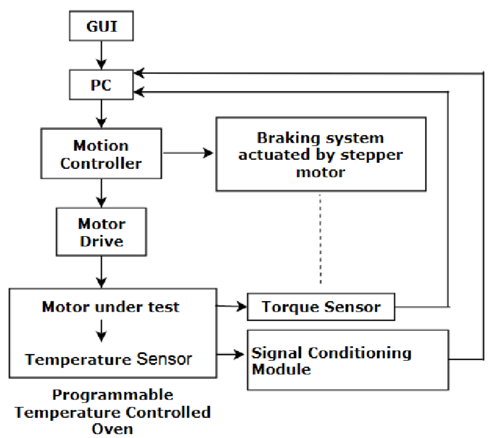

Figure 4.2 – Block diagram of test bench

The main components of test bench include

1. High temperature oven
2. Torque Sensor
3. Braking System
4. Control Panel
5. Software

4.3.1 High temperature oven

A programmable, temperature-controlled oven for carrying the characteristic tests of motor at high temperatures up to 250°C is the main component of this test bench.

High temperature oven has a capacity of 216 litres. Inner dimensions of oven is 600 x 600 x 600mm and outer dimensions is 900 x 900 x 900mm Inner chamber is made of stainless steel while outer chamber is made of mild steel. A ceramic blanket insulation is placed between the walls, covering top, sides and bottom. This insulation helps in preventing the loss of heat and thus increasing the efficiency of oven. Heating elements are located on sides of oven and a fan is provided on the top of oven. Fan circulates air through air-guides located over the heating elements and around the chamber. This ensures uniform temperature distribution inside the oven. The temperature settings of oven are adjusted externally by a microprocessor based PID controller. The accuracy of oven is ± 1°C. Suitable penetrations (˜100mm diameter) with leak tight high temperature mineral insulation are provided for motor and sensor cables. An insulated door is provided for oven with safety latch and 180 degree opening hinges for easy mounting of the motors inside the oven. The front panel door is provided is provided with double layer glass window and lighting for viewing the motor under test.

4.3.2 Torque Sensor

Torque sensor is a very important component in the measurement system. For ISI application, torque-speed characteristics is a major parameter that need to be measured at different temperatures. A commercially available dual range Kistler make torque sensor shown in Figure 4.3 is used for torque and speed measurement in the test bench. Torque sensor has two ranges for torque measurement, 0-2 Nm and 0-20 Nm, which can be selected based on the torque of the motor under test. The measurement is based on strain gauge technology. The torque and speed measurement accuracy are in the range of 0.25% and 0.01% of true value respectively. Torque sensor is attached to the shaft of motor using two flexible (RADEX make) couplings, one inside the oven that can withstand temperatures up to 350C, another outside the oven that can operate up to 280C. Since these couplings are provided on the motor output shaft, conductive heat reaching the torque sensor is fully attenuated. They can accommodate 10 of angular as well as radial misalignment and its homokinetic nature helps in delivering the same speed at input and output making it ideal for the purpose. Moreover, the system is laser aligned to minimize the alignment errors.

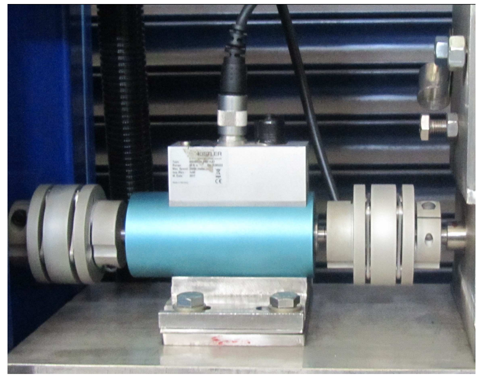

Figure 4.3 – Torque Sensor

4.3.3 Braking system

A disc-type braking system of Kateel make, model KA-H-180 is intended for applying load torque. Braking system is attached to the motor through high temperature bearings, torque sensor and flexible coupling. As the shaft rotates, heat generated is dissipated through high temperature bearings, and flexible couplings attached to both ends of torque sensor hence special thermal insulation is not required for braking system. Brake pads are electrically actuated by a stepper motor and screw and nut mechanism. Actuation and release of brake is implemented with help of software.

4.3.4 Control Panel

Figure 4.4 shows the components of control panel. The motion controller has sufficient digital inputs and outputs to interface emergency inputs, and other control inputs and outputs. The digital I/Os of the motion controller are optically isolated for better noise immunity from the field. The motion controller generates control signals for operating different types of motors such as stepper, brushless DC, permanent magnet DC and brushless AC motors and also have quadrature encoder inputs for receiving the encoder signal. Motion controller receives the commands from motor testing software pre-loaded in industrial PC for various mode of operation. The motion controller also controls the operation of disc brakes actuated by stepper motor system. The specifications of motion controller are tabulated in Table 4.1.

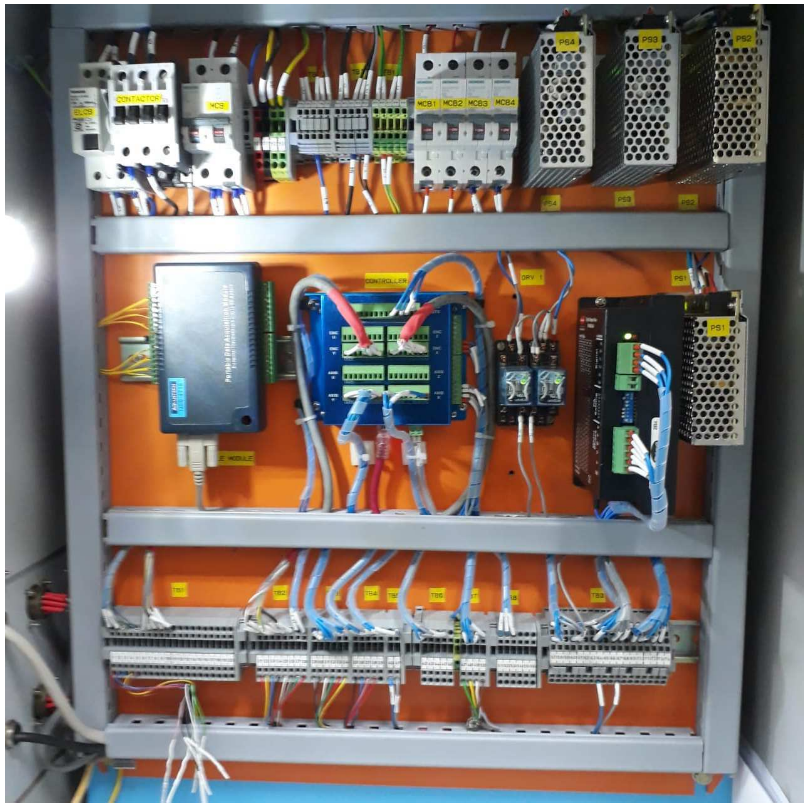

Figure 4.4 – Control Panel

The motion controller in the control panel is 4 axis controller suitable for DC, BLDC, Stepper and BLAC motors. The motion axis can be configured for any control technique. For each motor under test, drive of the corresponding motor is interfaced with the motion controller to perform the test. Power supply and isolation transformers are provided for powering the drives, which are to be used for motor under test. For testing different types of motor, suitable commercial drives are used. The speed and torque output from torque sensor is in digital format and represents real values of torque and speed. Hence no signal conditioning unit is required for processing the sensor output. This output can be interfaced to the data acquisition software for display of torque and speed component. However, thermocouple needs a separate signal conditioning module to convert the temperature data in digital format. A 8 channel isolated thermocouple signal conditioner with 16 bit resolution and 0.1% accuracy is used to acquire temperature data.

Additionally, each input channels of the signal conditioner can be individually configured to handle multiple sensor types. Therefore the temperature of different parts of motors can be acquired by the data acquisition system effectively without any additional modules. An emergency stop push button is provided in the control panel to activate safety relay.

Table 4.1 – Specifications of motion controller

No of axis	4,User selectable
Serial interface	USB/RS485/Ethernet
Motor type	DC, BLDC, Stepper and BLAC
Feedback type	Analog, Encoder
Absolute position range	±231 counts
Velocity range	1 to 20,000,000 counts/sec (servo)
Velocity range	1 to 4,00,000 counts /sec (stepper)
Servo control loop modes	PID, PIV
PID gains	0 to 32767
PID update rate	less than 80us (single axis)
Stepper output rate	4MHz (Full, half, micro stepping)
Stepper output mode	Step / direction or CW/CCW
Velocity profile	Trapezoidal or S curve
Coordinated motion support	Yes
Analog output	±10V(16 bit)
Programmable torque limit	±10V
Encoder Input rate	20MHz
Encoder	Incremental, Differential, Quadrature
Forward, reverse, home inputs	12 (4*3 per axis)
Trigger inputs	4(1 per axis
Output enable	4 (1 per axis)
Digital I/O	4port,8 bit, bit configurable
PWM output	4 channel, 50KHz
Power supply	12-36VDC

4.3.5 Software

A software based GUI is developed in C# and loaded in the industrial PC which communicates with the motion controller via Ethernet interface. The software issues various commands initiated by user and communicates with motion controller to drive the motor. During the testing, real time values of torque, speed, position, and temperature are acquired by the data acquisition system and read by the software at sampling rate of 300 data samples/second, displayed and printed in tabular formats at the user interface.

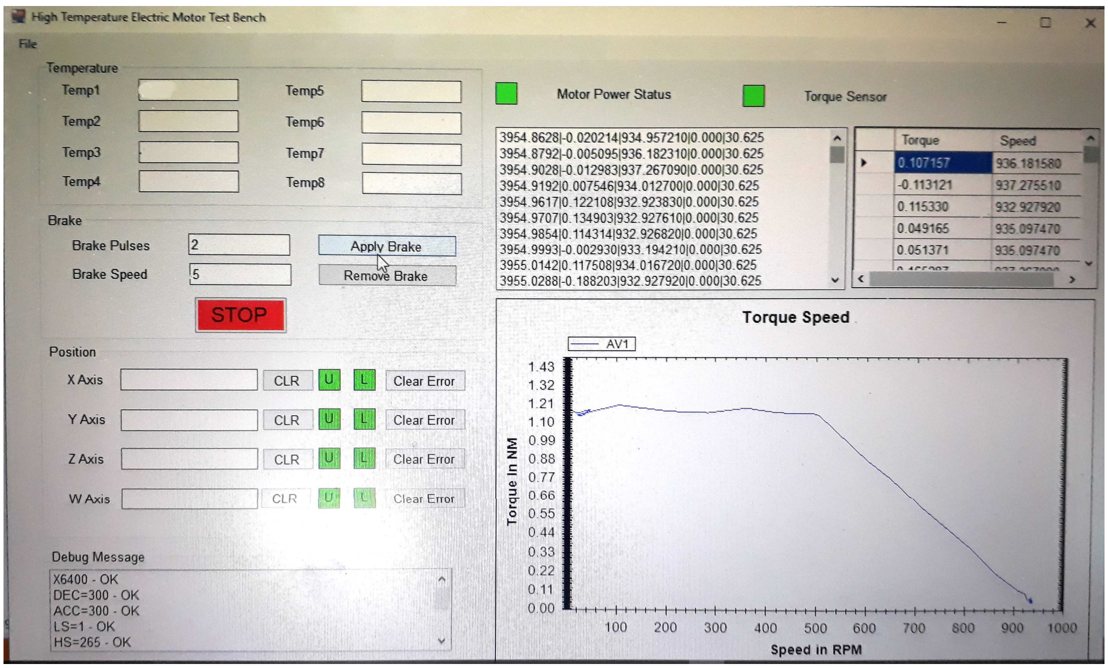

Figure 4.5 – Graphical User Interface

Software also has the ability to test variety of motors in different configurations and to modify PID controller setting during various tests. Soft controls for enabling/disabling drive, start, homing, stop, speed selection, jogging and directions for each motor are also provided in the software. Stepper control tab in the software also has the option to select the type of stepping sequence. The status of operation and healthy communication between PC and motion controller is indicated in the GUI for an error free operation. Figure 4.5 shows the snapshot of GUI.

Figure 4.6 shows the complete experimental set up of high temperature motor test facility.

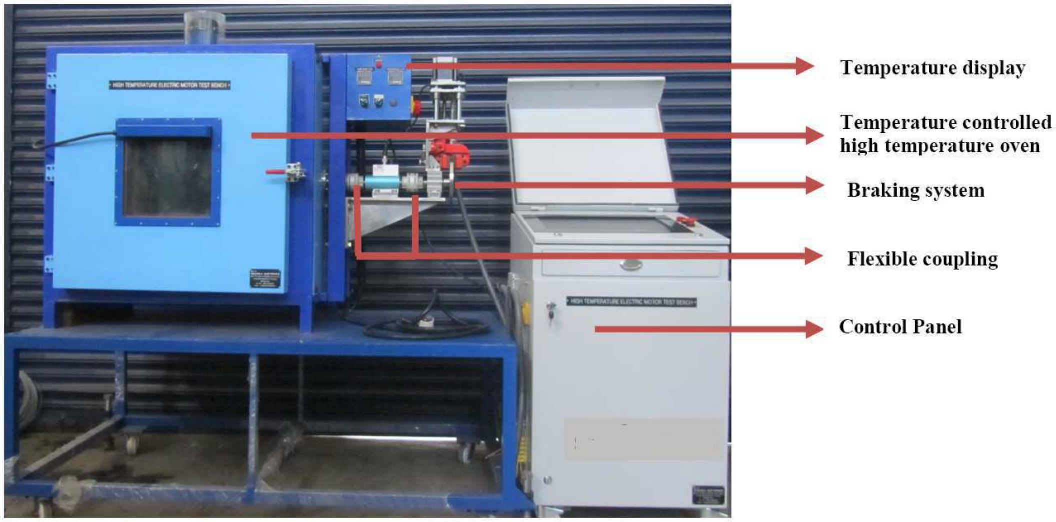

Figure 4.6 – High temperature motor test bench

4.4 Verification of test bench using high temperature stepper motor

In order to verify the performance of test bench, two phase, 1.8° Arun Microelectronics Limited (AML) make high temperature stepper motor shown in Figure 4.7 was tested.

Figure 4.7 – AML D42.3 Stepper Motor

Torque-speed characteristics is one of the major criteria that needs to be verified for high temperature motor. The performance of motor at high temperature without drastic decrease in torque is a necessary condition to be met. This test basically verifies the accuracy of torque sensor, temperature feedback and encoder, operation of different modules of control panel, functionality of software and overall integrity of the test facility. The name plate details of stepper motor are shown in Table 4.2

Table 4.2 – Characteristics of Stepper Motor

Holding Torque (mNm)	450
Detent Torque (mNm)	20
Rotor Inertia(gcm^2)	102
Mass(g)	610
Current/phase(A)	1
Resistance/phase at 20°C(Ω)	8.5
Phase Inductance(mH)	19.5

4.4.1 Testing sequence

Testing procedure is enumerated as follows.

1. The motor is mounted inside the oven with the help of suitable bracket size.

2. Over temperature control and ambient temperature of oven is set to 40°C and the set up is left undisturbed for 1 hour until the temperature builds uniformly.The ambient temperature of oven is also verified with thermocouple reading from the oven.

3. A DC voltage of 25V and rated current of 1A is provided for testing of motor. The values of torque,speed and winding temperature are noted.

4. Experiment is repeated for temperatures of 70°C, 100°C, 130°C, 160°C under different speeds in the range of 40-90 rpm.

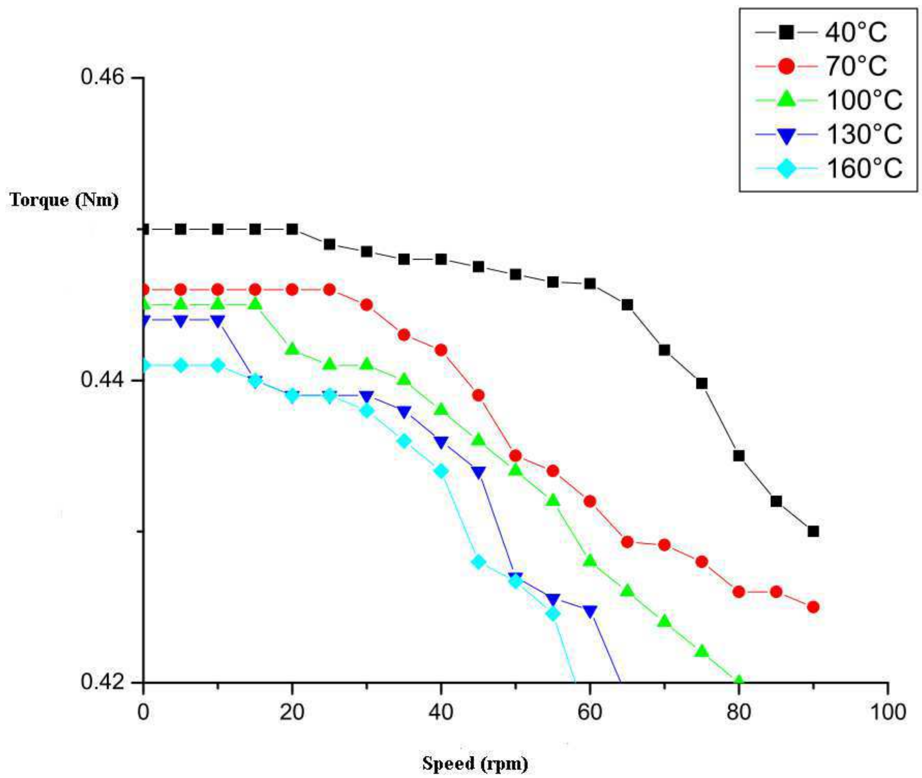

Figure 4.8 – Torque speed characteristics of stepper motor

Torque as function of speed and temperature is obtained. It is found that with increase in temperature from 40°C to 160°C , there is a decrease of 2.22% in torque output of the machine at speed of 20-50 rpm where as there is a decrease of 7% in torque at higher speed of 50-90 rpm which is in accordance with the information provided in the datasheets. Thus the experimental results validates the performance of motor test bench.Figure 4.8 shows the torque speed characteristics of AML make stepper motor

4.5 Experimental Validation of Prototype Motor

Table 4.3 – Characteristics of Brushless ac drive

Power output	2kW, 3ϕ PWM
Maximum current	20A
Serial interface	RS232/Ethernet- user selectable
Feedback devices	Resolver, Encoder
Position output	Simulated encoder output for resolver, differential quadrature output
Commutation	Sinusoidal, Trapezoidal commutation
Digital Input	4 Programmable inputs
Digital output	4 Programmable outputs
Command inputs	Pulse + direction, analogue velocity and torque input (± 10V)
Power supply	1ϕ 230VAC

Subsequent to the verification of test bench using commercially available stepper motor, the test bench is used to validate the performance of prototype motor. In this section, results collected from test performed on high temperature surface mounted permanent motor is presented. The developed motor is tested on high temperature test bench shown in Figure 4.6. Experimental validation is necessary to verify the performance of initial design and to compare the simulated as well as measured performance characteristics. The oven temperature is set to 150° C and the torque performance is noted for different speeds ranging from no-load to 6000rpm. Testing was carried out using standard brushless ac drive. The specification of drive is tabulated in Table 4.3. Winding temperature was taken from end windings. Leads from stator end winding were connected to thermocouple for temperature measurement. Rotor temperature was not measured due to practical difficulty of attaching thermocouple over the magnet. The phase resistance was measured using digital multimeter (Model:8808 Fluke) and found to be 2.1Ω against predicted value of 1.55Ω. It was found that simulated values were agreeing well with measured results.

4.5.1 Torque Speed Characteristics

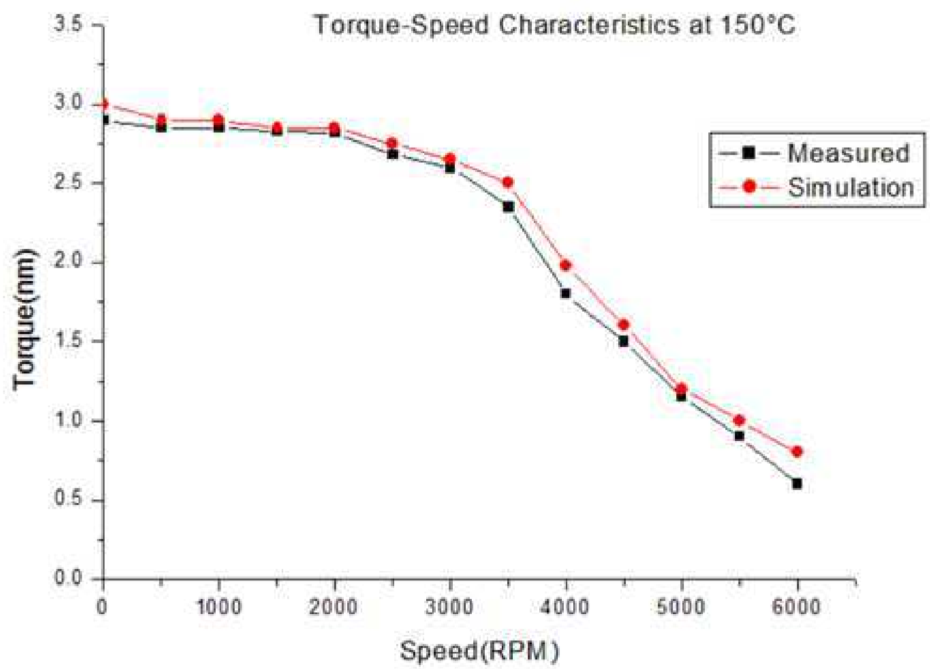

Figure 4.9 – Torque Speed Characteristics

The simulated results have been obtained from coupled electromagnetic-thermal simulation of 12/10 motor at different rated speeds ranging from 0 to 6000 rpm under constant temperature of 150°C and rated current of 4.5A. The machine has been tested under different conditions of speed ranging from 0 to 6000 rpm under the same conditions of temperature and current. At speed of 3500rpm the value of torque was found to be 2Nm. Over temperature control and ambient temperature of oven is set to 150°C and the set up is left undisturbed for 1 hour until the temperature builds uniformly. The ambient temperature of oven is also verified with thermocouple reading from the oven. The simulated and measured torque-speed characteristics of high temperature motor is shown in the Figure 4.9. It was found that the reduction in torque at higher speed is attributed to increased losses corresponding to temperature and eddy current losses in iron laminations, stator windings, and PMs corresponding to the higher supply frequencies.

4.5.2 Winding temperature

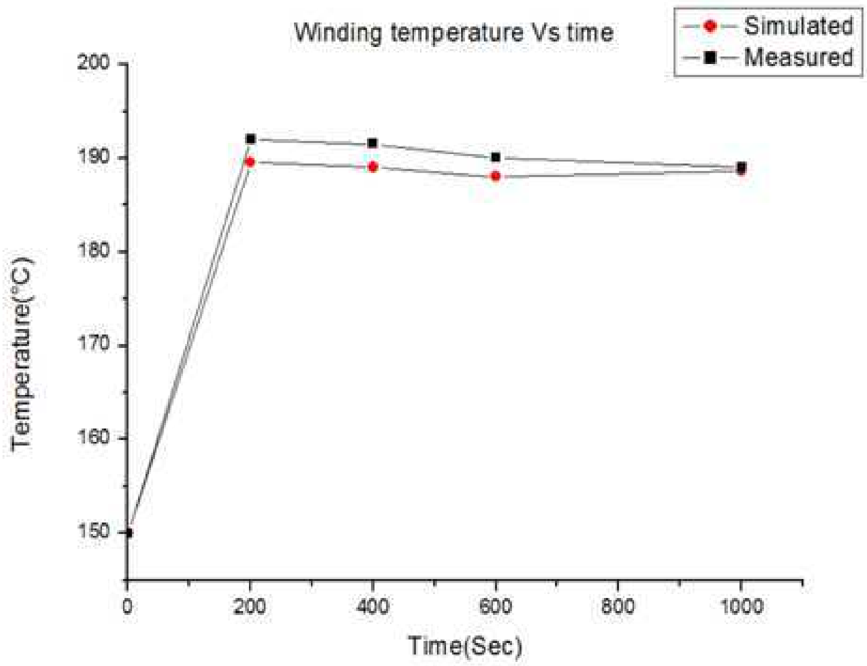

Figure 4.10 – Average winding temperature rise

The average winding temperature was obtained from the coupled electromagnetic thermal simulation using Finite Element Analysis (FEA) and lumped parameter thermal software, carried out under ambient temperature setting of 150° C. The developed motor was run at a rated speed of 3500 rpm with a constant current of 4.5A. The temperature of the oven was set to 150°C and temperature rise in the winding was noted for 1000 sec using 'K-type' thermocouple connected to stator end winding. The experiment was repeated and average value of readings were noted. It was found that average temperature rise at the end of 1000 seconds was converging to 188.6° C. The simulated and experimental results is shown in Figure 4.10.

4.6 Conclusions

- A high temperature surface mounted permanent magnet motor based on initial design and high temperature withstanding materials is developed.
- The design of a novel automated test facility for testing the performance of motor at different temperatures is discussed and realized.
- The performance of automated test facility is verified by testing the performance of the test bench using a standard commercially available motor.
- After verification of the functionality of test bench, torque-speed characteristics and average winding temperature of prototype high temperature motor is experimentally evaluated and compared with simulation results.
- It was found that experimental results were agreeing well with simulation results. The torque was found to be 2Nm at a rated speed of 3500 rpm and average winding temperature after 1000 seconds of operation was found to be 188.6°C.
- Though the winding temperature of designed motor is within the requirement specifications, it is an important factor which decides the lifetime of insulation and in turn the reliability of the entire system. Further reduction in winding temperature is possible by optimizing the dimensions and current density. Hence in continuation with design, development and experimental validation of high temperature, an attempt is made for developing a optimization methodology by incorporating novel optimization algorithms and surrogate model which is explained in following chapters.

Chapter 5

A Novel Optimization Algorithm-Memory based Hybrid Dragonfly Algorithm

This chapter details the survey of reported optimization algorithms, their advantages, disadvantages and application in design optimization of high temperature motor. The need for developing a hybridized algorithm combining advantages of two or more algorithms for application is explained. A novel hybridization algorithm known as "Memory based Hybrid Dragonfly Algorithm" inspired by Dragonfly Algorithm (DA) and Particle Swarm Optimization (PSO) algorithm is proposed. It combines the exploration capability of DA and exploitation capability of PSO to achieve global optimal solutions. The operating mechanism of the proposed method is explained with the help of flowchart and pseudocode. The superior performance of algorithm is verified using standard benchmark functions and the comparison of results with other algorithms have been proved statistically. The analysis and computational complexity of MHDA in carrying out optimization tasks is also explained.

5.1 Introduction

Optimization process has become an integral part of engineering and business problems. The purpose of the optimization can be for the maximization of efficiency, performance, productivity or social welfare. Many real world engineering problems are highly non-linear and complex involving many design variables and complex constraints. Potentialities offered by modern optimization techniques are of interest for industry year after year, giving the reason for their massive penetration into design chain[84]. The electric machine design optimization problem is one such problem characterized by the complex relationships between different domains such as electromagnetic, thermal and structural. The non- linearity often results in a multimodal search space making the problem difficult to solve. Gradient based algorithms fail in this context due to the presence of multiple local optimal solutions. Hence for the global optimization of such problems, the selection of proper optimization routine plays a significant role. In recent years stochastic algorithms have been gaining significance in producing fast, low cost and robust solution to complex optimization problems [85]. Compared to conventional deterministic approach, they do not require any gradient information and are simple and easy to implement [86]. Among the stochastic optimization algorithms, swarm intelligence (SI) based optimization techniques have attracted the attention of researchers worldwide. A swarm is characterized by a group of self-organized and decentralized system of non-complex individuals or agents interacting among themselves and with their environment for survival, hunting, navigation or foraging. It can be a school of fish, flock of birds, colonies of ants etc. SI based algorithms models the collective behaviour of these individuals to solve complex optimization process. Even though as individuals, these agents have limited operational capability, they tend to outperform in accomplishing the desired task by interacting among themselves and with the environment using their own specific behavioural patterns. Literature review on the SI based optimization algorithm reveals their effectiveness in solving complex optimization problems in different fields of study. Ant colony optimization inspired by the foraging behaviour of the ants was found to be very effective in solving structural optimization problems [87], traffic area control problems [88] and also in the field of genomics[89]. Particle swarm algorithm (PSO) is well known optimization algorithm mimicking the social behaviour of bird flocking or fish schooling [90].The effectiveness of PSO in solving bi-level programming problems[91], electric power systems[92], offshore heavy oil reservoir[93], and image processing [94] is clearly explained in the literature. Bat algorithm[40], Firefly algorithm[41], Krill Herd[42], Whale optimization algorithm[43], Grey wolf optimization[95], Ageist Spider Monkey optimization[96], Moth Search optimization[97], Competitive optimization algorithm[45]are some of the popular swarm based meta heuristic algorithms.

5.2 Importance of hybrid algorithm development

With the development of numerous optimization algorithms, it is difficult to test and determine which algorithm is most suitable for solving a particular optimization problem. This is because most of the algorithms work on a generalized concept and do not have domain knowledge specific to each problem. Also as per "No Free Lunch" theorem, there is no superior heuristic that can solve all types of optimization problems[39]. Considering all these, there has been an increased trend towards the development of hybrid algorithms that show remarkable improved performance due to the synergy of parent algorithms. Lesser computation, improvement of solution accuracy, enhancement of algorithm stability and the handling of searching convergence can be considered as targets of hybridization and improvement process. In continuation, this chapter introduces a novel hybrid version of Dragonfly algorithm (DA) known as Memory based Hybrid Dragonfly Algorithm (MHDA) for numerical constrained engineering problems. MHDA is hybrid optimization algorithm based on swarming behavior of dragonflies and memory concept of PSO. In this chapter, basic operation of MHDA along with the preliminary concept of DA and PSO are explained. The performance of the algorithm is validated using two test suites with standard benchmark functions.

5.3 Dragonfly Algorithm (DA)

Dragonfly algorithm is inspired by the unique and superior swarming behaviour of dragonflies. The dragonfly swarms for hunting and migration. Hunting swarm behaviour which is otherwise known as static swarm behaviour is characterized by the formation of small group of dragonflies moving locally and abruptly changing the steps. Migratory swarm behaviour which is otherwise know as dynamic swarm is characterized by a massive number of dragonflies flying in one direction over long distances. Static Swarm and dynamic swarms represent exploitation and exploration capabilities of DA. The behaviour of dragonfly follows the principles of separation, alignment, cohesion, distraction from the enemies and attraction towards the food. Each dragon fly in the swarm corresponds to the solution in the search space. Swarm movement of dragonfly is determined by five different operators such as Separation, Alignment, Cohesion, Attraction towards food sources and distraction towards enemy sources [98]. Separation (S_i) which refers to the static collision avoidance of individuals from other individuals in the neighbourhood. Alignment (A_i) refers to the velocity matching of individuals to other individuals in neighbourhood. Cohesion (C_i) refers to the tendency of individuals towards the center of the mass of the neighbourhood. Suitable weights are assigned to each operator and they are adaptively tuned to ensure the convergence of dragonflies towards the optimal solution. The neighbouring radius of the dragonflies also increases as the process of optimization progresses.The mathematical implementation of DA can be explained as follows.

Consider population of dragonflies of size N. The position of i^{th} dragonfly is given by equation (5.1)

$$X_i = (x_i^1, ..x_i^d...., x_i^N) \tag{5.1}$$

where i= 1,2,3....N, x_i^dcorrespond to the position of the i^{th} dragon fly in d^{th} dimension of the search space and N is the number of search agents.

The fitness function is evaluated based on the initial position values which are randomly generated between the lower and upper bounds of the variables. The weights for separation (s), alignment (a), cohesion(c), food (f) and enemy (e) factors for each dragonfly is initialized randomly. For updating the position and velocity of dragonflies separation, alignment and cohesion coefficients are calculated using equations (5.2)-(5.4)

$$S_i = -\sum_{j=1}^{N} X - X_i \tag{5.2}$$

$$A_i = \frac{\sum_{\mathrm{i=1}}^{\mathrm{N}} V_{\mathrm{i}}}{N} \tag{5.3}$$

$$C_i = \frac{\sum_{i=1}^{N} X_i}{N} - X \tag{5.4}$$

where X_i and V_i corresponds to the position and velocity of the i^{th} individual. X corresponds to the position of the current individual and N denotes the number of neighbouring individuals.

Attraction towards food source,F_i and distraction from enemies E_i is calculated using equations (5.5) and (5.6)

$$F_i = X^{+} - X \tag{5.5}$$

$$E_i = X^{-} + X \tag{5.6}$$

where X is the position of the current individual and X^{+}denotes the food source and X^{-}denotes the enemy source.

The distance of the neighbourhood is calculated by calculating the Euclidean distance between all the dragonflies and selecting N of them. The distance, r_{ij} is calculated by the equation (5.7)

$$r_{ij} = \sqrt{\sum_{k=1}^{d} (x_{i,k} - x_{j,k})^2} \tag{5.7}$$

If dragon fly has at least one dragonfly in the neighbourhood the velocity of the dragonfly will be updated as per equation (5.8) analogous to velocity equation of PSO and the position of the dragonfly will be updated as per equation (5.9) which is analogous to position equation of PSO.

$$\triangle X_{t+1} = (sS_i + aA_i + cC_i + fF_i + eE_i) + w\triangle X_t \tag{5.8}$$

$$X_{t+1} = X_t + \triangle X_{t+1} \tag{5.9}$$

If there is no dragonfly in the neighbourhood radius the position of the dragonfly will be updated using Levy Flight equation[99] as given in equation (5.10). The relevant information of Levy Flight equation, its strength and use are added in Appendix-A. This improves the randomness, chaotic behaviour and global search capability of dragonflies.

$$X_{t+1} = X_t + Levy(d)X_t \tag{5.10}$$

The fitness function is then evaluated based on the updated position and velocities.The position updating process is continued till the stop condition is met.

5.4 Particle Swarm Optimization (PSO)

PSO is a swarm intelligence optimization technique based on the social behaviour of organisms living in swarms [90]. Each individual in swarm is called as a particle which can move freely to explore the problem hyperspace. Each particle is associated with position, velocity and fitness function. The velocity of the particle is updated based on its own history of best solution (pbest) as well as from the history of best solution so far found by all the particles in the population (gbest). The information obtained by the particle is shared with other particles in the population and finally the particle is guided towards the optimal solution. PSO is simple, easy to implement and have few parameters to be adjusted.

Consider N dimensional search space. Let the position and velocity of the ith particle in k^{th} iteration be $x_k^i$and velocity v_k^i respectively. The velocity and position of the particle in $(k+1)th$ iteration are updated as per equation (5.11) and (5.12) respectively.

$$V_{k+1}^i = wV_k^i + C_1 r_1 (P_k^i - X_k^i) + C_2 r_2 (P_k^g - X_k^i) \tag{5.11}$$

$$X_{k+1}^i = X_k^i + V_{k+1}^i \tag{5.12}$$

where w is the inertial weight , $C_1$and C_2 represents the cognitive and social parameters, $P_k^i$and P_k^g represents the pbest of the i^{th} particle and gbest of the swarm up to k^{th} iteration respectively.ϕ_1 and ϕ_2 represents random numbers generated in the range $[0 \quad 1]$.

5.5 Memory Based Dragonfly Algorithm (MHDA)

For any optimization algorithm, proper balance between exploration and exploitation of the search space is necessary to achieve a global optimal solution. Exploration otherwise known as diversification involves global search in the search space and exploitation otherwise known as intensification involves search in a local region depending upon the current best solution. Too much of exploration and exploitation harmfully affects the performance of the algorithm by increasing the convergence time and increasing the chances to fall into local optima[100]. The conventional DA, operates on a randomly generated initial population of search agents or dragonflies and dragon flies explore the search space using Levy flight. This random initialization and levy flight search process increases solution diversity and strengthens the exploration capability of algorithm. Further, DA has only few parameters to adjust and adaptive tuning of these swarming factors helps in balancing local and global search capabilities. However, DA lacks an internal memory which can keep track of previously obtained potential solutions. During the process, DA discards all the fitness values exceeding the global best and never keeps track on possible set of solutions which has a potential to converge to global optima. This weakens the exploitation capability of the DA tending to converge very slowly and sometimes stagnate at local optima. To avoid this, a novel hybrid algorithm based on DA and PSO is proposed. Two features are added to conventional DA algorithm to improvise its performance, they are (i) an internal memory to keep track of possible solutions which has a potential to converge to global optima (ii) iteration level hybridization with PSO which runs on this set of saved solutions.

5.5.1 Implementation of internal memory

With the addition of internal memory, each dragonfly is allowed to keep track of its co-ordinates in the problem hyperspace which are associated with fitness value. This is similar to the *pbest* concept in PSO. During each iteration, the fitness value of search agents in current population is compared with the best fitness value in that iteration. Better solutions are saved and a *DA-pbest* matrix is framed. Dragonflies are also made to track best value obtained so far by any dragon fly in the neighbourhood which is same as the *gbest* concept of PSO and is stored as *DA-gbest*. The concept of *pbest* and *gbest* in DA is novel and enhances the exploitation capability of DA. This feature of internal memory provides capability to escape from local optima and provides greater performance than conventional algorithm [101].

5.5.2 Iterative level hybridization with PSO

Iteration level hybridization is a straightforward approach of iteratively executing two algorithms in sequence to enhance the optimization performance[102]. Here DA with internal memory is used to converge the search space to more promising areas and PSO is then allowed to exploit the previously limited area to find better solutions.

Due to balance between exploration offered by DA and exploitation capabilities offered by PSO, hybrid algorithm-MHDA performs better than the parent algorithms. PSO is then initialized with *DA-pbest* matrix and *DA-gbest* is set as the gbest of PSO (*PSO-gbest*). The position and velocity equations of PSO gets modified as

$$V_{k+1}^{i} = wV_{k}^{i} + C_1 r_1 (DA - pbest_{k}^{i} - X_{k}^{i}) + C_2 r_2 (DA - gbest_{k}^{g} - X_{k}^{i}) \tag{5.13}$$

$$X_{k+1}^{i} = X_{k}^{i} + V_{k+1}^{i} \tag{5.14}$$

where $DA - pbest_{k}^{i}$ is the *pbest* for i^{th} particle of PSO and $DA - gbest_{k}^{g}$ is *gbest* of the swarm up to k^{th} iteration for PSO.

Thus the MHDA combines the exploration features of DA in initial stage and exploitation capabilities of PSO in the final stage to achieve global optimal solutions. The flowchart and pseudo-code of the proposed optimization algorithm are given in Figure 5.1 and Algorithm 5.1 respectively.

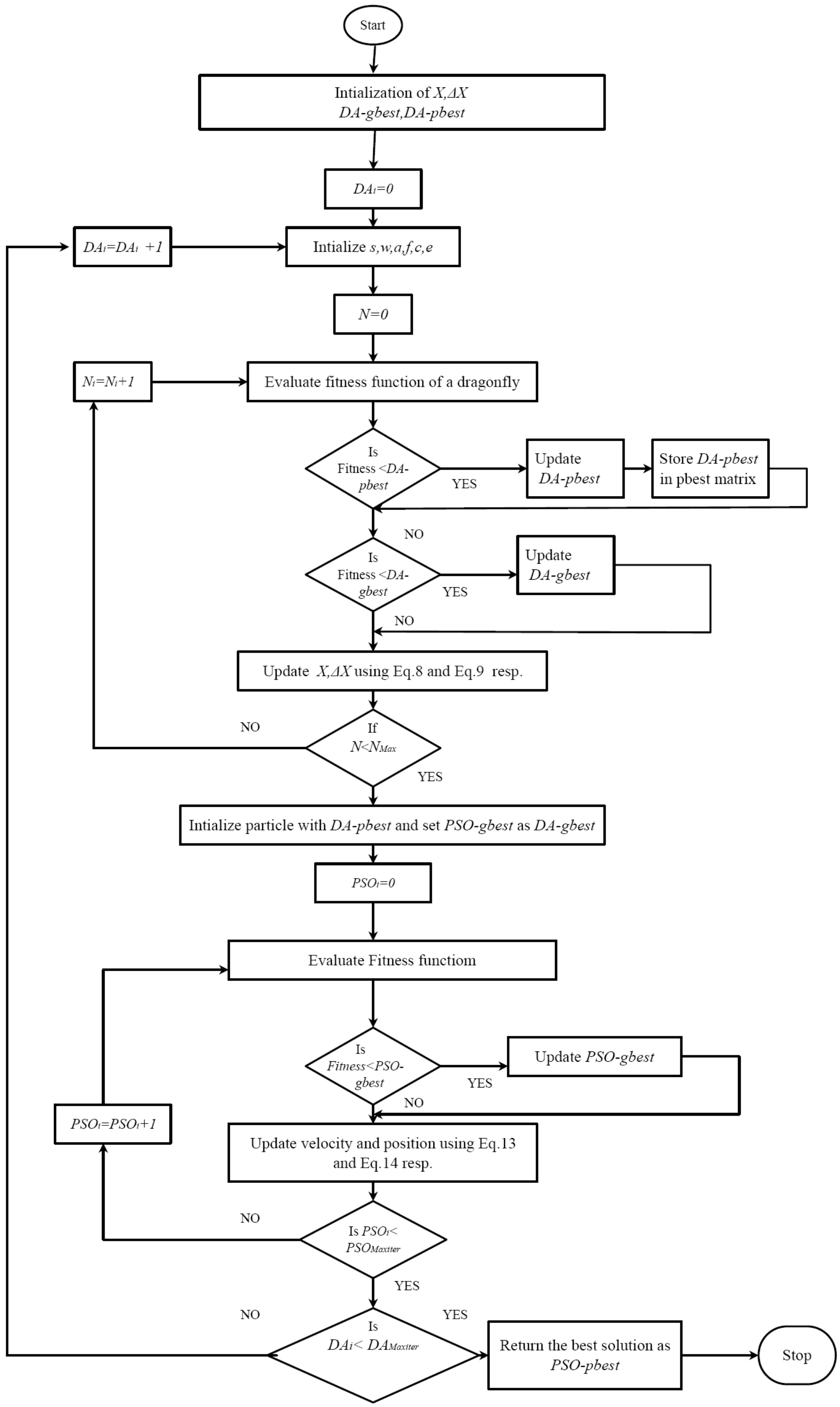

Figure 5.1 – Flowchart of MHDA

Algorithm 5.1 Pseudocode of MHDA

Initialization set of parameters Maximum iteration(Maxiter), maximum number of search agents (N_{max})number of search agents (N), number of dimensions (d), upper bound and lower bound of variables
Initialize the dragonflies populations (X) - Initialize the step vectors (ΔX)
while maximum iterations not done
For each dragonfly
Calculate fitness value
if
Fitness Value $<$ *DA-pbest* in this iteration
move the current value to *DA-pbes*t matrix
end ***if***
if
fitness value $<$ *DA-gbest*
set current value as *DA-gbest*
end **if**
end
For each dragonfly
Update the food source and enemy
Update *w, s, a, c, f,* and *e*
Calculate S, A, C, F, and E using equation (5.2)-(5.6)
Update neighbouring radius
if a dragonfly has at least one neighbouring dragonfly
Update velocity vector using equation (5.8)
Update position vector using equation. (5.9)
else
Update position vector using equation (5.10)
end ***if***
Check and correct the new positions based on the boundaries of variables
end
-------------------------End of DA and Start of PSO------------------
For each particle
Initialize particle with *DA-pbes**t*** matrix
Set *PSO-gbest* as *DA-gbest*
end
while maximum iterations or minimum error criteria is not attained
For each particle
Calculate fitness value if *fitness value* $<$ *PSO-pbest* in history
set current value as the new *PSO-pbest*
end ***if***
end
Choose the particle with the best fitness value of all the particles as the *PSO-gbest*
For each particle
Calculate particle velocity according equation (5.13)
Update particle position according equation (5.14)
end
end ***while***
------------------------------------End of PSO---
best-fitness $=$ *PSO-gbest*
end ***while***

5.6 Performance Evaluation on Benchmark Functions

The efficiency of MHDA is proved by testing on standard benchmark functions and comparing its performance with other powerful optimization algorithms. The benchmark function suite used for analysis is explained in the section 5.1. The experimental results and comparison with other algorithms are explained in section 5.6.1. Section 5.6.2 presents the statistical test results and the analysis of MHDA algorithm is explained in section 5.6.3. Section 5.6.4 explains the computational complexity of MHDA.

5.6.1 Benchmark function suite

To test the performance of MHDA, two test suites are considered. Suite I includes the function set used by the authors of conventional DA and recently proposed swarm based optimization techniques. This avoids studying the best parameter setting of each algorithm separately and to conduct a fair comparison. In Suite-I, the performance of MHDA is compared with classical DA, PSO and recently proposed swarm based optimization algorithms such as Ant Lion Optimizer(ALO)[103], Grey Wolf Optimizer(GWO)[95], Whale Optimization Algorithm (WOA)[43]. We also intend to prove that MHDA is capable of giving competitive results when compared to recently developed high performance algorithms from different families, hence suite II is considered. In Suite-II, the performance of MHDA is compared with most powerful and standard algorithms such as Cuckoo Search (CS)[104], Mean-Variance Mapping Optimization (MVMO)[105], Backtracking Search Optimization Algorithm (BSA)[106] self adaptive variants of Differential Evolution (DE) such as JADE[107], SaDE[108] and jDE[109].

5.6.1.1 Suite-I - Basic unconstrained benchmark functions

Suite-I consist of 19 benchmark functions, out of which 16 are classical benchmark functions found in the literature[103] and other 6 test problems are taken from the novel composite functions proposed in IEEE Swarm Intelligence Symposium 2005[110]. The description of functions ($F_{14} - F_{19}$) is sown in the Appendix-A. The classical benchmark set is classified into two sets- unimodal functions ($F_1 - F_7$) and multimodal functions ($F_8 - F_{13}$). The details of unimodal and multimodal benchmark functions, range, and dimension is shown in Table 5.1. Unimodal test functions have one global optima and performance of algorithm on these test function reveals its exploitation and convergence capability. Multimodal functions have more than one global optimum in the presence of many local optima. The performance of algorithm on these test function reveals its exploration and local optima avoidance capability. The last set of functions called as composite functions($F_{14} - F_{19}$) comprises of combined, shifted, rotated, biased versions of algorithms and represents the complex search space by providing large number of local minima and changing the shape of search space domain. The details of composite functions ($F_{14} - F_{19}$) are given in the Appendix-A.

Table 5.1 – Description of Unimodal Functions

Function	Dim	Range	f_{min}
Unimodal Functions			
$F_1(x) = \sum_{i=1}^{n} x_i^2$	30	[-100 100]	0
$F_2(x) = \Sigma_{i=1}^{n} \mid x_i \mid + \Pi_{i=1}^{n} \mid x_i \mid$	30	[-100 100]	0
$F_3(x) = \Sigma_{i=1}^{n} (\Sigma_{j-1}^{i} X_j)^2$	30	[-100 100]	0
$F_4(x) = max\{\mid x_i \mid, 1 \leq i \leq n\}$	30	[-100 100]	0
$F_5(x) = \Sigma_{i=1}^{n-1} [100(x_{i+1} - x_i^2)^2 + (x_i - 1)^2]$	30	[-30 -30]	0
$F_6(x) = \Sigma_{i=1}^{n} [(x_i + 0.5)]^2$	30	[-100 100]	0
$F_7(x) = \Sigma_{i=1}^{n} x_i^4 + random(0\ 1)$	30	[-1.28 1.28]	0
Multimodal Functions			
$F_8(x) = \Sigma_{i=1}^{n} - x_i sin(\sqrt{\mid x_i \mid})$	30	[-500 500]	$^{-}418.9D$
$F_9(x) = \Sigma_{i=1}^{n} [x_i^2 - 10cos(2\Pi x_i) + 10]$	30	[-5.12 5.12]	0
$F_{10}(x) = -20exp(-0.2\sqrt{\frac{1}{n}\Sigma_{i=1}^{n} x_i^2} - exp\left(\frac{1}{n}\Sigma_{i=1}^{n} cos(2\Pi x_i)\right) + 20 + e$	30	[-32 32]	0
$F_{11}(X) = \frac{1}{4000}\Sigma_{i=1}^{n} x_i^2 - \Pi_{i=1}^{n} cos(\frac{x_i}{\sqrt{i}}) + 1$	30	[-600 600]	0
$F_{12}(x) =$ $\frac{\Pi}{n}\{10\sin(\Pi y_1) + \Sigma_{i=1}^{n-1}(y_i - 1)^2[1 + 10\sin^2(\Pi y_{i+1})] + (y_n - 1)^2\} + \Sigma_{i=1}^{n} u(x_i, 10, 100, 4)$	30	[-50 50]	0
$F_{13}(x) = 0.1\{sin^2(3\Pi x_1) + \Sigma_{i=1}^{n}(x_i - 1)^2[1 + \sin^2(3\Pi x_i + 1) + (x_n - 1)^2[1 +$ $sin^2(2\Pi x_n)]\} + \Sigma_{i=1}^{n} u(x_i, 5, 100, 4)]$	30	[-1.28 1.28]	0

5.6.1.2 Suite-II-CEC 2014 unconstrained benchmark functions

Suite-II comprises 30 CEC 2014 functions with 30 dimensions (30D). The detailed explanation of different functions can be found in the technical report[111]. CEC 2014 test functions can be categorized into four types-unimodal($F_1 - F_3$), multimodal ($F_4 - F_{16}$), hybrid functions($F_{17} - F_{22}$) and composition functions ($F_{23} - F_{30}$). Unimodal functions in this set are non-separable and rotated where as multimodal functions are either separable or non-separable but are shifted or rotated. Hybrid functions are created by randomly dividing the variables into different sub components and then different basic components are used for different sub components. Composite functions in this set are created by the combination of two or more hybrid functions.

5.6.2 Experimental Results

All the experiments were executed on personal computer (Core i7, 3.4GHz, 32GB RAM) using MATLAB. The performance of MHDA was compared with other algorithms in terms of mean and standard deviation of objective function value and objective function error value on Suite-I and on Suite II respectively.

5.6.2.1 On Suite-I

In this section the performance of MHDA on benchmark function Suite-I is explained. For a fair comparison among the algorithms, maximum number of iteration and search agents was set to 1000 and 30 respectively as followed in the literature[103]. The levy flight constant and inertial weights of MHDA[w_{max}, w_{min}] was set to 1.5 and $[0.9, 0.2]$ respectively. Each function was run independently for 30 runs and mean and standard deviation (std) for unimodal, multimodal and composite functions are reported in the Table 5.2. The stopping criterion was set to maximum number of iterations. The results of other algorithms have been taken from the reference[43][103].

Table 5.2 – Comparison between MHDA and other algorithms on optimizing Suite-I benchmark functions in terms of mean and std

F	**Meas.**	**MHDA**	**DA**	**ALO**	**GWO**	**WOA**	**PSO**
F_1	Mean	**4.07E-42**	5.15E-07	2.59E−10	6.59E-28	1.41E-30	2.70E−09
	Std	**2.22E-41**	2.82E-06	1.65E−10	6.34E-05	4.91E-30	1.00E−09
F_2	Mean	6.62E-15	4.82E-06	1.842E−06	7.18E-17	**1.06E-21**	7.15E−05
F_2	Std	3.61E-14	2.50E-05	6.58E−07	2.91E-02	**2.39E-21**	2.26E−05
F_3	Mean	**2.55E-50**	5.37E-07	6.068E−10	3.29E+06	5.39E-07	4.71E−06
	Std	**1.3E-49**	2.94E-06	6.34E−10	79.14958	2.93E-06	1.49E−06
F_4	Mean	4.989E-05	1.349E-04	**1.361E−08**	5.61E-07	7.26E-02	3.25E−07
	Std	2.73E-04	4.57E-04	**1.81E−09**	1.315E+00	3.98E-11	1.02E−08
F_5	Mean	**3.34E-22**	6.71E-01	3.46E-01	2.65E+01	27.87E+00	1.23E-01
	Std	**5.67E-22**	3.66E+00	0.109584	69.90499	7.636E-01	2.16E-01
F_6	Mean	**0.00E+00**	9.05E-06	2.562E−10	8.166E-01	3.116E+00	5.23E−07
	Std	**0.00E+00**	3.31E-05	1.09E−10	1.26E-04	5.324E-01	2.74E−06
F_7	Mean	**5.25E-05**	4.5E-04	4.29E-03	2.22E-02	1.425E-03	1.39E+00

	Std	**5.02E-05**	5.71E-04	5.08E-03	1.003E-01	1.15E-03	0.001269
F_8	Mean	-2957.34	-3932.76	**-2247.86**	-6123.1	-5080.76	−4841.29
	Std	3.86E+02	2.18E+02	**5.29E+03**	4.08E+04	6.95E+00	1.15E+03
F_9	Mean	**5.91E-07**	3.36E-02	7.71E−06	3.12E-01	0.00E+00	2.78E-01
	Std	**3.23E-06**	1.81E-01	8.45E−06	4.74E+01	0.00E+00	2.18E-01
F_{10}	Mean	**6.34E-15**	2.66E-04	3.71E−15	1.06E-13	7.40E+00	1.11E−09
	Std	**2.72E-14**	8.59E-04	1.5E−15	7.78E-02	9.90E+00	2.39E−11
F_{11}	Mean	**2.40E-04**	3.83E-03	1.86E-02	4.49E-03	2.89E-04	2.73E-01
	Std	**2.25E-02**	7.154E-02	9.54E-03	6.66E-03	1.59E-03	2.04E-01
F_{12}	Mean	**2.34E-31**	7.48E-04	9.75E−12	5.34E-02	3.40E-01	9.42E−09
	Std	**4.45E-47**	3.75E-04	9.33E−12	2.07E-02	2.15E-01	2.31E−10
F_{13}	Mean	**1.39E-32**	1.06E-03	2.01E−11	6.54E-01	1.88E+00	1.35E−07
	Std	**5.57E-48**	3.99E-04	1.13E−11	4.47E-03	2.66E-01	2.88E−08
F_{14}	Mean	**5.75E-15**	1.04E+02	1.51E-04	4.38E+01	5.68E-01	100
	Std	**2.85E-04**	9.12E+01	3.82E-04	6.98E+01	5.05E-01	8.16E+01
F_{15}	Mean	1.40E+02	2.13E+02	**1.45E+01**	9.18E+01	7.53E+01	1.55E+02
F_{15}	Std	2.43E+01	1.27E+05	**3.22E+01**	9.55E+01	4.31E+01	1.13E+01
F_{16}	Mean	**1.00E+01**	5.58E+02	1.75E+02	6.14E+01	5.56E+01	1.72E+01
	Std	**3.44E+01**	1.65E+02	4.65E+01	6.86E+01	2.18E+01	3.27E+01
F_{17}	Mean	1.00E+02	2.20E-03	3.16E+02	**1.23E+01**	5.38E+01	3.14E+02
	Std	5.63E-03	4.63E-03	1.30E+01	**1.63E+02**	2.16E+01	2.00E+01
F_{18}	Mean	3.03E+02	2.50E+02	4.41E+01	**1.02E+01**	7.78E+01	8.34E+01
	Std	8.88E+00	1.85E+02	1.66E+00	**8.12E+01**	5.22E+01	1.01E+02
F_{19}	Mean	**5.00E+02**	6.79E+02	5.003E+02	4.31E+01	5.78E+01	8.61E+02
	Std	**1.36E-03**	1.99E+02	2.06E-01	8.44E+01	3.44E+01	1.25E+02

5.6.2.2 On Suite-II

The experiments are done on 30 CEC 2014 benchmark functions with 30 dimensions.The parameter setting of MHDA was kept same as in Suite-I. The parameter setting and results of other algorithms were taken from the reference[112][104]. The population size was set to 50 and maximum number of function evaluation ($MaxFE = D * 10^3$) is set as stopping criteria where D is the number of dimensions. The algorithm was run independently 51 times. The mean and standard deviation(std) of function error values between the best fitness value and true optimal value in each independent runs are reported in Table 5.3

Table 5.3 – Comparison between MHDA and other algorithms on optimizing Suite-II benchmark functions in terms of mean and std

F	Meas.	MHDA	CS	MVMO	BSA	JADE	SaDE	jDE
F_1	Mean	3.20E+03	3.50E+07	**1.07E-03**	2.04E+01	6.09E+02	3.73E+03	6.12E+04
	Std	3.02E+03	2.49E+07	**1.09E-03**	1.56E-02	1.18E+03	3.26E+03	7.64E+04
F_2	Mean	**0.00E+00**	1.95E+07	2.38E-05	1.62E+01	**0.00E+00**	**0.00E+00**	2.27E-15
	Std	**0.00E+00**	5.49E+07	1.19E-05	9.69E-01	**0.00E+00**	**0.00E+00**	7.87E-15
F_3	Mean	**0.00E+00**	3.10E+04	1.11E-03	4.19E-03	9.86E-04	**0.00E+00**	4.09E-14
	Std	**0.00E+00**	1.36E+04	1.03E-03	1.32E-02	5.95E-03	**0.00E+00**	2.60E-14
F_4	Mean	**0.00E+00**	2.03E+02	**0.00E+00**	2.93E+00	**0.00E+00**	**0.00E+00**	8.53E+00
	Std	**0.00E+00**	6.69E+01	**0.00E+00**	1.46E+00	**0.00E+00**	**0.00E+00**	2.16E+01
F_5	Mean	**2.00E+01**	2.00E+01	**2.00E+01**	5.95E+01	2.03E+01	2.03E+01	2.03E+01
	Std	**1.57E-02**	2.28E-03	**2.00E+01**	7.94E+00	3.23E-02	4.03E-02	3.26E-02
F_6	Mean	**1.76E+00**	3.23E+01	3.62E+00	3.22E+01	9.15E+00	1.49E+01	5.31E+00
	Std	**2.87E+00**	3.27E+00	3.04E+00	6.57E+00	2.21E+00	9.42E-01	4.04E+00
F_7	Mean	**0.00E+00**	1.79E+00	2.99E-03	2.56E+03	**0.00E+00**	**0.00E+00**	2.96E-04

	Std	**0.00E+00**	2.19E+00	0.00E+00	2.56E+02	**0.00E+00**	**0.00E+00**	1.48E-03
F_8	Mean	**0.00E+00**	1.71E+02	8.58E-01	4.37E-01	**0.00E+00**	**0.00E+00**	1.19E-01
	Std	**0.00E+00**	3.46E+01	9.95E-01	7.85E-02	**0.00E+00**	**0.00E+00**	3.30E-01
F_9	Mean	3.00E+01	2.80E+02	2.51E+01	**2.84E-01**	2.62E+01	3.58E+01	3.81E+01
	Std	1.82E+01	5.16E+01	2.39E+01	**4.68E-02**	4.96E+00	7.01E+00	5.71E+00
F_{10}	Mean	1.10E+03	2.66E+03	1.79E+01	**2.45E-01**	8.16E-03	1.11E+00	3.17E+00
	Std	8.24E+02	5.34E+02	9.76E+00	**4.02E-02**	1.18E-02	2.02E+00	3.18E+00
F_{11}	Mean	1.41E+02	4.13E+03	1.54E+03	**7.06E+00**	1.67E+03	2.28E+03	2.71E+03
	Std	4.35E+02	5.35E+02	1.59E+03	**1.07E+00**	2.13E+02	3.45E+02	2.75E+02
F_{12}	Mean	1.44E-01	5.11E-01	**7.21E-02**	1.07E+01	2.67E-01	4.59E-01	4.77E-01
	Std	7.19E-02	2.56E-01	**6.24E-02**	2.71E-01	3.57E-02	5.23E-02	5.41E-02
F_{13}	Mean	4.59E-01	4.81E-01	**1.57E-01**	1.54E+05	2.20E-01	3.02E-01	2.84E-01
	Std	1.23E-01	1.17E-01	**1.62E-01**	8.75E+04	3.25E-02	3.69E-02	3.55E-02
F_{14}	Mean	2.04E-01	3.08E-01	**1.99E-01**	9.10E+02	2.41E-01	2.68E-01	3.02E-01
	Std	3.33E-01	5.64E-02	**1.99E-01**	1.05E+03	3.18E-02	1.40E-01	4.15E-02
F_{15}	Mean	**2.33E+00**	9.80E+01	2.86E+00	6.91E+00	3.20E+00	4.86E+00	5.36E+00
	Std	**7.67E-01**	3.02E+01	2.69E+00	6.25E-01	4.55E-01	4.17E-01	7.43E-01
F_{16}	Mean	9.50E+00	1.27E+01	1.02E+01	1.68E+02	**9.30E+00**	1.03E+01	1.03E+01
	Std	1.18E+00	5.01E-01	9.84E+00	1.91E+02	**4.61E-01**	3.42E-01	3.23E-01
F_{17}	Mean	**4.81E+02**	1.48E+06	9.01E+02	6.20E+03	1.91E+04	8.55E+02	1.62E+03
	Std	**5.32E+02**	1.21E+06	1.03E+03	3.02E+03	1.08E+05	2.80E+02	1.49E+03
F_{18}	Mean	3.74E+01	7.67E+03	2.89E+01	1.79E+02	1.14E+02	4.92E+01	**1.86E+01**
	Std	2.08E+01	6.70E+03	2.08E+01	8.11E+01	1.97E+02	2.57E+01	**1.04E+01**
F_{19}	Mean	1.12E+01	5.33E+01	3.08E+00	3.15E+02	**4.48E+00**	5.26E+00	4.97E+00
	Std	1.87E+01	3.63E+01	3.02E+00	2.92E-07	**7.56E-01**	1.15E+00	9.61E-01

F_{20}	Mean	3.67E+02	3.93E+04	1.09E+02	2.27E+02	3.11E+03	1.85E+01	**1.36E+01**
	Std	4.08E+02	2.20E+04	5.69E+01	2.42E+00	3.01E+03	4.14E+00	**6.64E+00**
F_{21}	Mean	7.06E+02	3.54E+05	4.67E+02	**2.07E+02**	1.33E+04	4.31E+02	2.98E+02
	Std	1.05E+03	3.48E+05	4.89E+02	**6.48E-01**	4.12E+04	1.32E+02	2.25E+02
F_{22}	Mean	2.70E+02	9.47E+02	1.45E+02	**1.00E+02**	1.44E+02	1.65E+02	1.38E+02
	Std	1.80E+02	3.31E+02	1.46E+02	**5.83E-02**	7.74E+01	7.11E+01	5.38E+01
F_{23}	Mean	**3.10E+02**	3.29E+02	3.15E+02	4.09E+02	3.15E+02	3.15E+02	3.15E+02
	Std	**4.00E+01**	7.51E+00	3.15E+02	3.71E+00	4.01E-13	0.00E+00	0.00E+00
F_{24}	Mean	**2.24E+02**	2.78E+02	2.25E+02	8.77E+02	2.25E+02	2.25E+02	2.26E+02
	Std	**1.80E+01**	3.11E+01	2.25E+02	1.66E+01	3.60E+00	4.31E+00	3.34E+00
F_{25}	Mean	2.10E+02	2.23E+02	2.03E+02	1.41E+03	2.03E+02	**2.03E+02**	2.04E+02
	Std	6.91E+00	9.39E+00	2.03E+02	1.89E+02	1.13E+00	**5.52E-01**	8.81E-01
F_{26}	Mean	1.000E+02	1.00E+02	1.00E+02	2.55E+03	1.02E+02	**1.00E+02**	1.00E+02
	Std	4.720E-02	1.63E-01	1.00E+02	7.49E+02	1.39E+01	**3.55E-02**	5.05E-02
F_{27}	Mean	4.01E+02	4.27E+02	4.01E+02	5.12E+06	**3.35E+02**	5.46E+02	4.01E+02
	Std	4.01E+02	1.96E+01	4.01E+02	4.10E+06	**4.68E+01**	1.11E+02	5.44E+01
F_{28}	Mean	1.52E+03	3.49E+03	8.77E+02	**8.34E-01**	7.96E+02	8.08E+02	8.38E+02
	Std	5.77E+02	5.48E+02	8.78E+02	**1.48E+00**	4.63E+01	3.78E+01	2.99E+01
F_{29}	Mean	7.78E+02	5.44E+05	7.36E+02	**5.74E-04**	8.28E+02	8.41E+05	8.66E+02
	std	7..5E+02	2.61E+06	7.42E+02	**9.44E-04**	3.27E+02	2.66E+06	1.62E+02
F_{30}	Mean	2.37E+03	2.49E+04	2.00E+03	**9.83E+01**	1.66E+03	2.34E+03	2.79E+03
	Std	2.80E+03	2.26E+04	2.08E+03	**2.96E+01**	7.61E+02	1.38E+03	1.22E+03

5.6.3 Statistical Results

Mean and standard deviation of results give general idea about the performance of the algorithm. In order to prove that results are generated not by chance, statistical tests must be also carried out. The statistical significance of experimental results on Suite-I and Suite-II is obtained by performing Friedman's test and Wilcoxon ranksum test. Friedman test is a commonly used non parametric statistical method to rank the performance of the algorithms. Friedman's test aims to find whether any significant difference exist between the results of different algorithms. It is based on null hypothesis that there is no variation in the performance of all algorithms[113]. The best performing algorithm gets lowest rank while the worst performing algorithm gets the highest rank . The average rank obtained by each algorithm on all test functions is calculated for determining Friedman's statistic [114]. Friedman statistic is then compared with χ^2 (chi-square) distribution values with $k-1$ degrees of freedom, where k is the number of algorithms compared. If the p value returned by this comparison test is found to be less than or equal to level of significance, null hypothesis is rejected indicating the there exist significant differences between the performance of algorithms. Friedman's test is then followed by post-hoc analysis to test the pair wise comparison of algorithms using Wilcoxon's ranksum test[115] . The lowest ranked algorithm by Friedman's test is used as the control method for post-hoc analysis .The summary of statistical results on Suite-I and Suite-II benchmark functions is shown in Table 5.4 and 5.5 respectively.$+$ indicates significantly better, $-$ indicates significantly worse and Not Sgn indicates non-significant results produced by given algorithm than MHDA.

Table 5.4 – Summary of statistical results on Suite-I

Friedman's Test	
Algorithm	**Rank**
MHDA	2.263
DA	4.578
ALO	3.632
GWO	4.842
WOA	3.563
PSO	4.210

Wilcoxon ranksum test			
MHDA Vs	+	-	**Not Sgn**
DA	2	16	1
ALO	4	15	0
GWO	7	12	0
WOA	8	11	0
PSO	3	16	0

Table 5.5 – Summary of statistical results on Suite-II

Friedman's Test	
Algorithm	**Rank**
MHDA	2.230
CS	5.400
JADE	2.933
MVMO	2.700
SaDE	3.226
jDE	3.833
BSA	4.800

Wilcoxon ranksum test			
MHDA Vs	+	−	**Not Sgn**
CS	-	24	6
JADE	8	16	4
MVMO	11	13	6
SaDE	7	16	7
jDE	8	20	2
BSA	11	19	0

From the summary of statistical results of Suite-I and Suite-II, MHDA was the best performing algorithm among all the compared algorithms. Considering 5% level of significance MHDA received lowest rank of 2.263 in Suite-I test functions and 2.23 in Suite-II test functions.WOA was the second best performing algorithm on Suite-I outperforming MHDA in 11 cases . MVMO, which was one of the best qualified algorithms in CEC competition 2014 was a major competitor of MHDA in Suite-II and . Its performances were better than MHDA in 16 cases, worse than MHDA in 9 cases and gave non-significant results in 5 cases. Therefore, MHDA is proved to be a highly competitive optimization algorithm and can be used for solving hardest optimization problems.

5.6.4 Analysis of MHDA

The following observations can be made from the experimental results of Suite-I:

- Unimodal functions(F_1-F_7) - The proposed algorithm outperforms other algorithms in five out of seven benchmark problems. In function F_2 MHDA becomes third best and in F_4 MHDA becomes fourth best out of the six algorithms compared.

- Multimodal Functions (F_8-F_{13}) - The proposed algorithm outperforms other algorithms in five out of six cases. In function F_8 MHDA becomes the second best performing algorithm.

- Composite Functions (F_{14}-F_{19}) - MHDA outperforms other algorithms in four out of six cases.

The following observations can be made from the experimental results of Suite-II:

- Unimodal functions (F_1–F_3)- For this group functions the proposed MHDA gives best performance in $F_2$and F_3

- Multimodal functions (F_4–F_{16})-The proposed MHDA performs better on six functions namely$F_{4,}F_5, F_6, F_7, F_8$and F_{15} while it becomes the second performing algorithm for functions $F_{11,}F_{12}, F_{14}, F_{16}$.

- Hybrid functions(F_{17}–F_{22}) - For this group function the proposed MHDA gives best results in $F_{17}$and for other functions it is marginally worse than the best performing algorithm.

- Composition functions (F_{23}–F_{30}) - In this group the proposed MHDA performs better than all other algorithms on three functions namely $F_{23,}F_{24}, F_{26}$. It is second best in functions $F_{27}$and F_{29}.

Performance of MHDA on unimodal functions shows the exploitation capability of MHDA which helps to converge rapidly and exploit accurately. Integrated internal memory and iterative level hybridization with PSO improves the exploitation capability of MHDA.The superior performance of MHDA on multimodal functions owes to the random initialization and levy flight search process followed in DA. From the results of composite functions, it is evident that MHDA succeeds in avoiding local optima by properly balancing the exploration and exploitation capabilities. MHDA outperformed most of functions in Suite-I while giving competent results in Suite-II.

The mechanism behind the exploration and exploitation of MHDA is graphically represented by tracking the path of search agents in the search space. The Unimodal function F_1, multimodal function F_9 and composite function F_{14} from Suite-I are solved by 10 search agents for 100 iterations to explain the search process and convergence behaviour of MHDA.

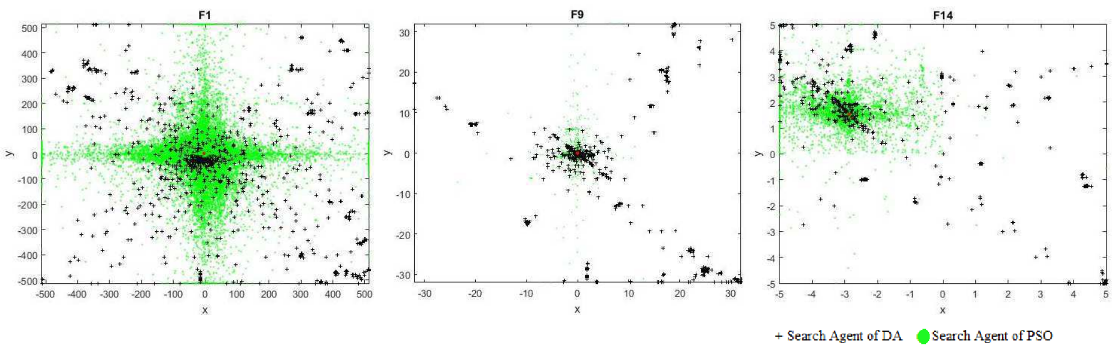

Figure 5.2 – Search process of MHDA

It has been found that search agents in MHDA tends to explore the search space very widely and then gradually converges to a point. This is because of exploration capability of DA provided in the first phase of MHDA and subsequent exploitation provided by iterative level hybridization of PSO working on $DA - pbest$ matrix. The position of potential search agents nearer to the food are saved in this memory. This helps in attracting other search agents when exploring the search space. When the search agents approach near global optimal solution they exploit very slowly on the promising area of search solution with embedded PSO operators in MHDA. This is clearly shown in figure 5.2 where the '+' indicates the search agents for DA and green dots indicates the search agents for PSO.

The convergence curves of MHDA is compared with the other six algorithms of Suite-I and is provided in Fig 2.3. All the algorithms were executed from the same initial population. It is observed that the convergence accelerates with increase in iterations. MHDA exhibits a rapid convergence in all three cases, which is due to its powerful global search mechanism in the initial stage and local search on best saved positions in the search space. From Figure 5.3 it has been found that MHDA outperforms other algorithms and converges very quickly with respect to number of iterations to global minima or near global minima.

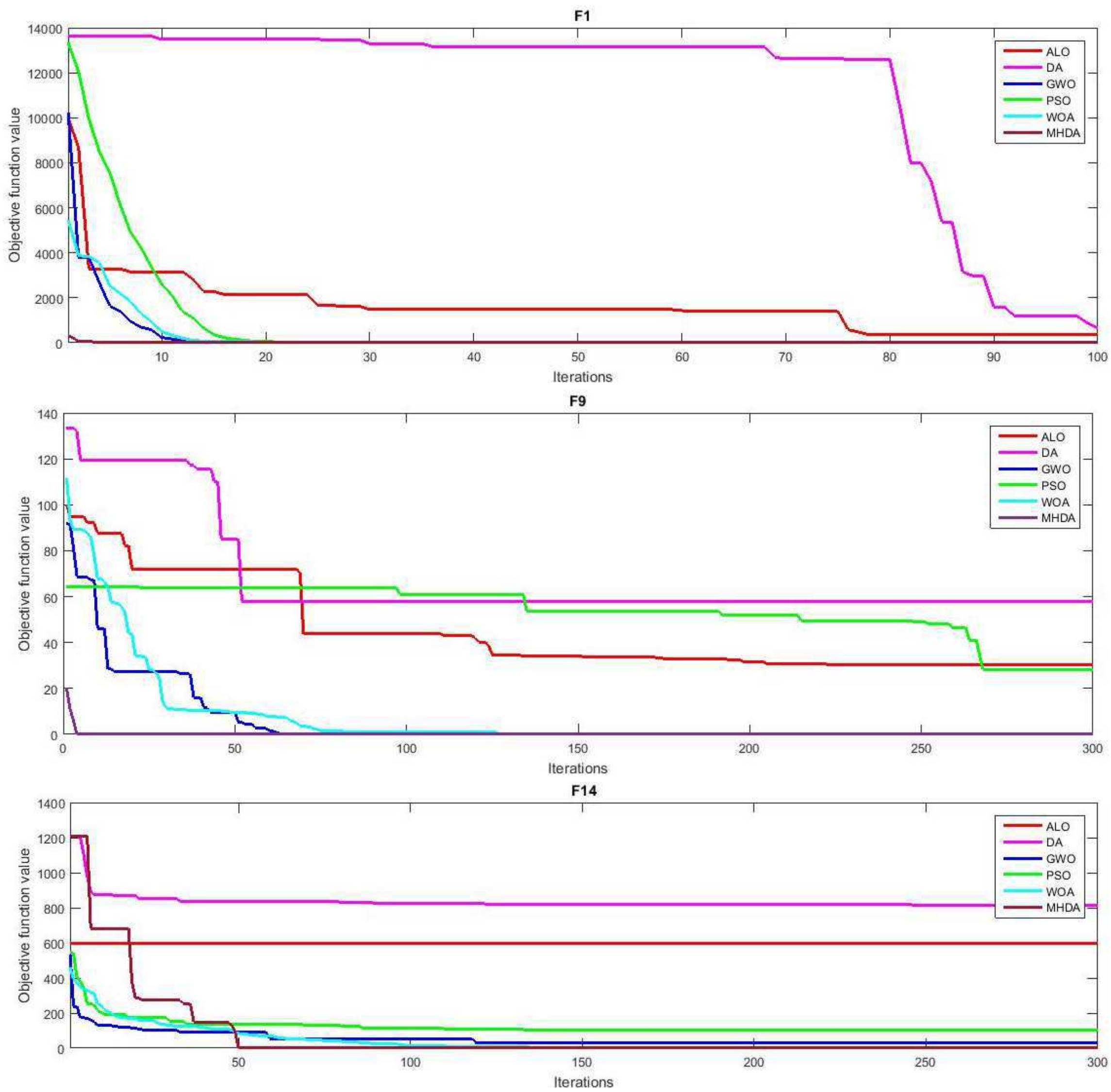

Figure 5.3 – Convergence plot of MHDA

5.6.5 Computational complexity of MHDA

MHDA is realized by combining conventional DA and PSO algorithm. Computational complexity depends on the structure and implementation of algorithm. The overall complexity can be estimated as follows. MHDA consist of four major steps (i) Fitness calculation of dragonflies (ii) Updation of dragonflies (iii) Fitness Calculation of particle (iv) Updation of particle. Assuming N as the number of search agents,t as the number of iterations the complexity of first two steps can be estimated as $O\left(N^2t\right)$. Considering K as the number of search-agents qualified for being in $DA - pbest$ matrix, the complexity of (iii) and (iv) together can be estimated as $O\left(K^2t\right)$ where $K < N$. Therefore the overall complexity of MHDA can be estimated as $O\left(N^2t + K^2t\right)$ .Usually number of search agents required for optimizing problem is small (N = 20 or 40), and t is large (1000 or 2000), the computation cost is relatively inexpensive because the algorithm complexity is linear in terms of t. Even though the complexity of MHDA is more than conventional DA at the same maximum iteration, MHDA can find optimal solutions in lesser number of iterations before it reaches maximum iteration and with greater accuracy. So, effectively the actual computation time will be reduced relative to conventional DA.

5.7 Application of MHDA in Engineering design problems

The competence of MHDA in solving real world problems especially non- linear constrained problems is demonstrated by testing on standard engineering design problems and comparing the results with other optimization algorithms. Three well known, engineering problems such as welded beam design, pressure vessel and motor design benchmark study are considered for testing MHDA algorithm.The constraints are usually handled by penalty functions. The idea of penalty functions is to transform a constrained optimization problem into an unconstrained one by adding (or subtracting) a certain value to/from the objective function based on the amount of constraint violation present in a certain solution[116]. In this paper death penalty is used for discarding infeasible solutions during optimization.

5.7.1 Welded beam design

The welded beam design problem, a standard benchmark study, aims at minimizing the fabrication cost of the welded beam by finding feasible set of four structural parameters of the beam: the thickness of the weld (h), length of the clamped bar(l), height of the bar (t) and thickness of bar(b). The related constraints are shear stress(τ), bending stress in the beam (θ), buckling load (P_c), and end deflection of the beam (δ). The variable vector (in inches) can be written as $\vec{X} = [\vec{x_1}, \vec{x_2}, \vec{x_3}, \vec{x_4}]$ where $\vec{x_1}$, $\vec{x_2}$, $\vec{x_3}$ and $\vec{x_4}$ represents h ,l ,t and b respectively. The welded beam structure shown in Figure 5.4 is taken from [117].

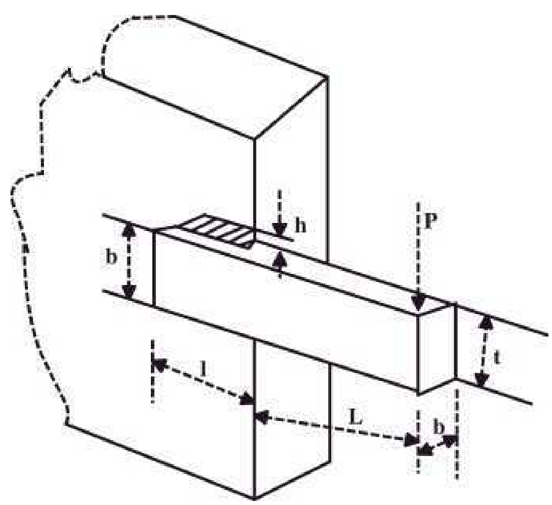

Figure 5.4 – Welded beam design problem

The mathematical formulation of the objective function along with the constraints is given below.

Minimize

$$f(\overrightarrow{X}) = 1.10471 x_2 x_1^2 + 0.04811 x_3 x_4 (14 + x_2) \quad (5.15)$$

subject to constraints,

$$g_1(\vec{X}) = \tau(\vec{X}) - \tau_{max} \leq 0 \tag{5.16}$$

$$g_2(\overrightarrow{X}) = \sigma(\vec{X}) - \sigma_{max} \leq 0 \tag{5.17}$$

$$g_3(\overrightarrow{X}) = \delta(\vec{X}) - \delta_{max} \leq 0 \tag{5.18}$$

$$g_4(\vec{X}) = x_1 - x_4 \leq 0 \tag{5.19}$$

$$g_5(\vec{X}) = P - P_c(\vec{X}) \leq 0 \tag{5.20}$$

$$g_6(\vec{X}) = 0.125 - x_1 \leq 0 \tag{5.21}$$

$$g_7(\vec{X}) = 1.1047x_1^2 + 0.04811x_3x_4(14 + x_2) - 5 \leq 0 \tag{5.22}$$

$$\text{where } \tau(\vec{X}) = \sqrt{(\tau')^2 + 2\tau'\tau" \tfrac{x_2}{2R} + (\tau")^2}$$

$$\tau' = \tfrac{P}{\sqrt{2}x_1x_2}, \tau" = \tfrac{MR}{J}, M = P(L + \tfrac{x_2)}{2}$$

$$R = \sqrt{\tfrac{x_2^2}{4} + (\tfrac{x_1+x_3}{2})^2},$$

$$J = 2\left\{\sqrt{2}x_1x_2\left[\tfrac{x_2^2}{4} + \left(\tfrac{x_1+x_3}{2}\right)^2\right]\right\},$$

$$\sigma(\vec{X}) = \tfrac{6PL}{x_4x_3^2},\ \delta(\vec{X}) = \tfrac{6PL^3}{Ex_3^2x_4}$$

$$P_c(\vec{X}) = \frac{4.013E\sqrt{\frac{x_3^2x_4^6}{36}}}{L^2}\left(1 - \tfrac{x_3}{2L}\sqrt{\tfrac{E}{4G}}\right)$$

$$P = 6000lb, L = 14in, \delta_{max} = 0.25\text{in},$$

$$E = 30E6 \text{ psi},\ G = 12E6 \text{ psi},\ \tau_{max} = 13,600 \text{ psi},\ \sigma_{max} = 30,000 \text{ psi}$$

$$0.1 \leq x_1 \leq 2, 0.1 \leq x_2 \leq 10, 0.1 \leq x_3 \leq 10, 0.1 \leq x_4 \leq 2 \tag{5.23}$$

This optimization problem is solved by using different evolutionary algorithms such as GA with self adaptive penalty[118], Evolution Strategy[119], PSO[120], Gravitational Search Algorithm (GSA)[121], Simulated Annealing(SA)[122], Co-evolutionary Particle Swarm Optimization(PSO)[123], Differential Evolution (DE)[124], Harmony-Search (HS)[125], Ant Colony Optimization(ACO)[126], Simple constrained PSO[127], Improved harmony search algorithm (IHS)[128], Cuckoo Search(CS)[129], Artificial Bee Colony Algorithm(ABC)[130], Simplex Search Method[131], Whale optimization algorithm (WO)[46], Ray optimization algorithm (RO)[132]. The maximum iteration and search agents in MHDA is set to 1500 and 50 respectively.The results of welded beam design problem using different algorithms is shown in Table 5.6. From the results it is clear that the proposed MHDA produced lowest cost of 1.6952471 and outperformed all other algorithms. The Statistical results after 30 independent runs in terms of best score, worst score ,mean and standard deviation for different algorithms is shown in Table 5.7, out of which standard deviation of MHDA was the lowest(about 5.83118E-16). This proves the reliability of MHDA in solving this optimization problem

Table 5.6 – Comparison of optimization results for welded beam design problem by different algorithms

Algorithm	**Optimum variables**				**Optimum**
	h	**l**	**t**	**b**	**Cost**
MHDA	**0.2057**	**3.2531**	**9.0366**	**0.2057**	**1.6952**
DA	0.1943	3.4668	9.0454	0.2057	1.7081
GA with Selfadaptive penalty approach	0.2088	3.4205	8.9975	0.2100	1.7483
Evolution Strategy	0.1997	3.6121	9.0375	0.2068	1.7373
SA	0.2056	3.4726	9.0366	0.2057	1.7250
Co-evolutionary PSO	0.2057	3.4705	9.0366	0.2057	1.7249

GSA	0.1822	3.8570	10.0000	0.2024	1.8800
RO	0.2037	3.5285	9.0024	0.2072	1.7353
WOA	0.2054	3.4843	9.0374	0.2063	1.7305
Simple constrained PSO	0.2057	3.4705	9.0366	0.2057	1.7249
PSO	0.2057	3.4705	9.0366	0.2057	1.7249
Improved HS	0.2057	3.4705	9.0366	0.2057	1.7248
DE	0.2057	3.4705	9.0337	0.2057	1.7249
Cuckoo Search	0.2015	3.5620	9.0414	0.2057	1.7312
ABC	0.2057	3.4705	9.0366	0.2057	1.7249
ACO	0.2057	3.4711	9.0367	0.2057	1.7249
Simplex Search Method	0.2057	3.4705	9.0366	0.2057	1.7249

.

Table 5.7 – Statistical results of different optimization algorithms for solving welded beam design problem

Algorithm	**Best Score**	**Worst Score**	**Mean**	**Std. Dev**
MHDA	**1.6952**	**1.6952**	**1.6952**	**0.0000**
DA	1.7081	2.5211	1.9408	0.2502
GA with Self adaptive penalty approach	1.7483	1.7720	1.7858	0.0112
Evolution Strategy	1.7282	1.9934	1.7927	0.0747
SA	1.7250	1.8844	1.7564	NA
Co-evolutionary PSO	1.7280	1.7821	1.7488	0.0129
Cuckoo Search	1.7312	2.3456	1.8787	0.2678
Simple constrained PSO	1.7249	NA	2.0574	0.2154
DE	1.7249	NA	1.7250	0.0000

Cuckoo Search	1.7312	2.3456	1.8787	0.2678
ABC	1.7249	NA	1.7419	0.0310
ACO	1.7292	1.7760	1.7298	0.0092

5.7.2 Pressure vessel design

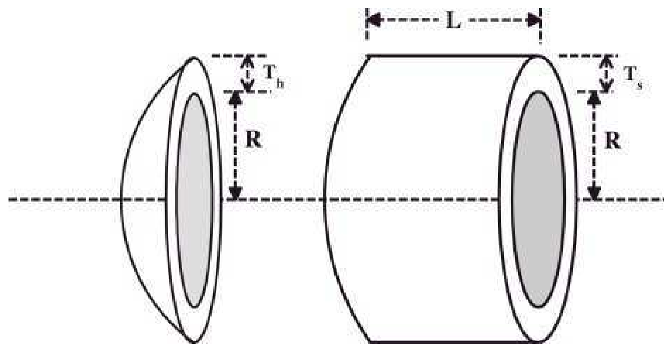

Figure 5.5 – Pressure vessel design problem

The pressure vessel design is one of the widely used structural design benchmark problem. The objective of this mixed integer optimization problem is to minimize the total cost of materials, forming and welding. The thickness of the shell (T_s), the thickness of the head (T_h),the inner radius (R) , the length of cylindrical section without considering the head (L) are the design variables involved in the optimization. Figure 5.5 showing the cross-section of pressure vessel is taken fromthe reference [133]. The variable vector (in inches) can be written as $\vec{X} = [\vec{x_1},\ \vec{x_2},\ \vec{x_3},\vec{x_4}]$ where $\vec{x_1}$, $\vec{x_2}$, $\vec{x_3}$ and $\vec{x_4}$ represents T_s ,T_h ,R and L .The mathematical formulation of the objective function along with the constraints is given below.

Minimize

$$f(\vec{X}) = 0.6224x_1x_3x_4 + 1.7781x_2x_3^2 + 3.1661x_1^2x_4 + 19.84x_1^2x_3 \tag{5.24}$$

subject to

$$g_1(\vec{X}) = -x_1 + 0.0193x_3 \leq 0 \tag{5.25}$$

$$g_2(\overrightarrow{X}) = -x_3 + 0.00954x_3 \tag{5.26}$$

$$g_3(\overrightarrow{X}) = -\Pi x_3^2 x_4 - \frac{4}{3}\Pi x_3^3 + 1296000 \leq 0 \tag{5.27}$$

$$g_4(\overrightarrow{X}) = x_4 - 240 \leq 0 \tag{5.28}$$

$$0 \leq x_1 \leq 99, 0 \leq x_2 \leq 99, 10 \leq x_3 \leq 200, 10 \leq x_4 \leq 200 \tag{5.29}$$

This optimization problem is solved by many researchers using different algorithms like non linear and discrete programming[134], Simulated Annealing[135], Harmony Search(HS) [125], Augmented Lagrange multiplier[133], GeneAS[136], GA with self adaptive penalty approach [137], Guassian QPSO[138], Co-evolutionary PSO [123],GA with dominance based tournament selection[118], Evolution Strategy [119], GA with self-adaptive penalty approach [137], Cuckoo search algorithm[129], Artificial Bee Colony algorithm (ABC) [139], Simple constrained PSO [127], Improved PSO[140], Differential Evolution (DE), Improved Ant Colony Optimization (ACO)[126], Hybrid PSO[141], PSO[120], Whale Optimization (WO) [46], Penalty guided ABC [142].

Table 5.8 – Comparison of optimization results for Pressure vessel design problem by different algorithms

Algorithm	Optimum variables				Optimum Cost
	T_s	T_h	R	L	
MHDA	**0.7782**	**0.3846**	**40.3196**	**200.0000**	**5885.3350**
DA	0.7828	0.3846	40.3196	200.0000	5923.1100
Non-linear and discrete programming	1.1250	0.6250	47.7000	117.7010	8129.1036
SA	1.1250	0.6250	58.2900	43.6930	7197.7000
HS	1.1250	0.6250	58.2789	43.7549	7198.4330
Augmented Lagrange multiplier	1.1250	0.6250	58.2910	43.6900	7198.0428

GeneAS	0.9375	0.5000	48.3290	112.6790	6410.3811
GA with Self adaptive penalty approach	0.8125	0.4375	40.3239	200.0000	6288.7445
Co-evolutionary PSO	0.8125	0.4375	42.0913	176.7465	6061.0770
GA with dominance based tournament selection	0.8125	0.4375	42.0974	176.6541	6059.9460
Evolution Strategy	0.8125	0.4375	42.0981	176.6405	6059.7456
Guassian QPSO	0.8125	0.4375	42.0984	176.6372	6059.7208
Cuckoo Search	0.8125	0.4375	42.0984	176.6364	6059.7143
Simple Constrained PSO	0.8125	0.4375	42.0984	176.6364	6059.7143
ABC	0.8125	0.4375	42.0984	176.6366	6059.7143
Improved PSO	0.8125	0.4375	42.0984	176.6366	6059.7143
DE	0.8125	0.4375	42.0984	176.6360	6059.7017
PSO	0.8125	0.4375	42.0985	176.6366	6059.1313
Hybrid PSO	0.8125	0.4375	42.1036	176.5732	6059.0925
WO	0.7828	0.3848	40.3403	200.0000	5923.1100
Penalty guided ABC	0.7782	0.3846	40.3211	199.9802	5885.4032
Hybrid PSO-GA	0.7782	0.3846	40.3196	200.0000	5885.3328

The best solutions of pressure vessel design problem found by different algorithms is shown in Table 5.8. The maximum iteration and population size is set to1500 and 50 respectively. The statistical results of different algorithms after 30 independent runs are shown in Table 5.9. From the results it is clear that the result obtained by the performance of the proposed optimization algorithm was better than other algorithms in the literature.

Table 5.9 – Statistical results of different optimization algorithms for solving pressure vessel design

Algorithm	Best Score	Worst Score	Mean	Std. Dev
MHDA	**5885.3353**	**5885.3353**	**5885.3353**	**0.0000**
DA	5923.1100	222536.0000	21342.2000	47044.2000
Non-linear and discrete programming	8129.1036	NA	NA	NA
Augmented Legrange based method	7198.0428	NA	NA	NA
GeneAS	6410.3811	NA	NA	NA
GA with self adaptive penalty approach	6288.7445	6308.1497	6293.8432	NA
GA with dominance based tournament selection	6059.9463	6469.3220	6177.2533	130.9297
Co-evolutionary PSO	6061.0770	6363.8041	6147.1332	86.4545
Evolution Strategy	6059.7456	7332.8798	6850.0049	426.0000
Cuckoo Search	6059.7140	6495.3470	6447.7360	502.6930
Improved PSO	6059.7143	NA	6289.9288	305.7800
ABC	6059.7143	NA	6245.3081	205.0000
Penalty guided ABC	5885.4033	5895.1268	5887.5570	2.7453

However considering the statistical results the performance of MHDA is superior. The standard deviation of the results after 30 independent runs is zero which indicates that the proposed hybrid optimization algorithm is very effective and reliable in solving this optimization problem.

5.7.3 Brushless DC Motor Optimization Benchmark

Brushless DC Motor (BLDC) wheel problem is well known optimization problem in electromagnetism. The objective functions and constraints for design optimization of typical brushless DC motor are available online[143].This problem aims to maximize the efficiency of the motor,η with five optimization parameters: bore stator diameter (D_s), flux density in the airgap (B_d), current density in the conductors (δ),teeth flux density (B_e)and back iron flux density (B_{cs}). The total mass (M_{tot}) , inner diameter (D_{int}), external diameter (D_{ext}) ,Maximum current (I_{max}), and temperature(T_a) and determinant used in the slot height calculation ($Discr$) which depend upon design variables are the constraints in this problem. The decision variable is represented as $X = (D_s, B_e,\delta,B_d,B_{cs}) = (x_1,x_2,x_3,x_4)$. The problem can be expressed mathematically as follows.

Minimize

$$f(x) = 1 - \eta \tag{5.30}$$

subject to

$$M_{tot} \leq 15Kg \tag{5.31}$$

$$D_{ext} \leq 0.340m \tag{5.32}$$

$$D_{int} \geq 0.076m \tag{5.33}$$

$$I_{max} \geq 125A \tag{5.34}$$

$$T_a < 125A \tag{5.35}$$

$$discr(D_s, \delta, B_d, B_e) \geq 0 \tag{5.36}$$

Table 5.10 – Comparison of optimization results for BLDC optimization benchmark problem by different algorithms

Algorithm	$x_1(mm)$	$x_2(T)$	$x_3(A/mm^2)$	$x_4(T)$	$x_5(T)$	η(%

MHDA	**201.5000**	**0.6479**	**2.0000**	**1.8000**	**0.8950**	**95.3200**
DA	201.2000	0.6481	2.0438	1.8000	0.8964	95.3100
PSO	202.1000	0.6476	2.0417	1.8000	0.9298	95.3200
ACO	201.2000	0.6481	2.0437	1.8000	0.8959	95.3200
GA	201.5000	0.6480	2.0602	1.7990	0.8817	95.3100
GA&SQP	201.2000	0.6481	2.0615	1.8000	0.8700	95.3100
BA	202.2000	0.6535	2.0514	1.8000	0.9792	95.3100
MSSO	201.2000	0.6481	2.0437	1.8000	0.8959	95.3200

The optimization results using different evolutionary algorithms are shown in the Table 5.10. It is observed that MHDA gave an efficiency of 95.32% which is probably the global optimal solution of the problem. Ant Colony Optimization(ACO) [143], Sequential Quadratic Programming(SQP) algorithm [143], PSO[143] and Modified Social Spider Optimization algorithm (MSSO) [144] was equally efficient in producing the same efficiency. The statistical results of different algorithms for this problem is shown in the Table 5.10. The average value and standard deviation, as shown in Table 5.11 for 30 independent runs and with maximum iteration of 1000 was 0.0469729 and 0.00045512 respectively. The standard deviation of MHDA was much lower than other algorithms which gave the same efficiency. This highlights the reliable nature of MHDA in optimizing this problem. The contents of this work is published in [145]

Table 5.11 – Statistical results of different optimization algorithms for solving BLDC optimization benchmark problem

Algorithm	**Best Score**	**Worst Score**	**Mean**	**Std. Dev**
MHDA	**95.32**	**95.32**	**95.32**	**2.18762E-07**
DA	95.31	95.06	95.18	8.5713E-04

BAT	NA	NA	95.23	0.056
SSO	94.98	94.81	94.88	0.08

5.8 Conclusion

This chapter summarizes the operating mechanism and performance of MHDA. Following inferences can be made from this chapter.

- Evolutionary optimization techniques are gaining significance since gradient based algorithms fails to provide global optimal solutions especially in the case of complex non-linear engineering optimization problems.
- Hybrid algorithms are more effective in finding global optimal solutions as they combines the advantages of other optimization algorithms
- A novel optimization algorithm, Memory based Dragonfly Algorithm, integrating the benefits of dragonfly algorithm and particle swarm optimization technique is proposed.
- Dragonfly algorithm operates in the direction of finding global optimum solution by exploring the search space, whereas internal memory concept and iteratively level hybridization with PSO helps to narrow down the search space with possible optimal solutions and thereby resulting in faster convergence with respect to number of iterations.
- The performance of algorithm is verified with standard unimodal,mulimodal, IEEE CEC2005 composite functions and IEEE CEC 2014 test functions.
- The performance of algorithm has been compared with other swarm algorithms

such as DA, ALO, GWO, WOA, CS, PSO and other high performance algorithms such as JADE, MVMO, SaDE, jDE, BSA.

- Statistical results further confirms that the results are not generated by chance and encourage the use of MHDA in solving optimization problems.

- MHDA is a computationally complex optimization algorithm since it operates on iterative level.However due to excellent synergy between diversification and intensification properties in search process, bear global solutions are reached in less number of iterations. The convergence analysis also proves that MHDA can find global optimal solutions in significantly lesser number of iterations compared to other optimization techniques.

- The efficiency and robustness of MHDA in solving engineering design problem is explored.

- Three engineering constrained problems such as welded beam design, pressure vessel design and brushless DC motor benchmark problem are solved using MHDA.

- The comparison results with other evolutionary algorithms proves that MHDA can be extremely effective in locating global optimal solutions.

- Statistical approach also confirms that the proposed method is reliable to solve engineering problems.

Chapter 6

Application of Surrogate Assisted Optimization in Design of High Temperature Motors

---

This chapter deals with surrogate assisted optimization in the design of high temperature motor. A novel surrogate model based on Artificial Neural Networks (ANN) and Memory based Hybrid Dragonfly Algorithm(MHDA) is built for approximating the complex relationship between the input variables and objective function. The number and locations of sampling points used for coupled electromagnetic thermal simulation is determined according to the Latin Hypercube sampling. The performance of ANN based surrogate model is then compared with conventional kriging based model. This surrogate model is used for optimization studies. The results of optimization process by ANN and MHDA provide with optimal set of design variables satisfying multiple constraints.

6.1 Introduction

The advances in mathematical modelling and computer simulation together with the availability of sophisticated optimization techniques have opened a new research field for motor design optimization. Considering the current competitive markets and application areas, it is of prime importance to reduce the "research laboratory to market time " of new and innovative optimized products. In this regard, high accuracy finite element models are used to take care of complexity of machine's structure. In the case of high temperature motors, due to the complex correlation between electromagnetic and thermal models, a coupled electromagnetic thermal model is used to give more accurate prediction of its performance. Despite advances in computing power in the recent past, this computationally intensive analysis methods can be impractical to use with optimization directly. For evaluation of every objective function, several cycles of coupled simulation needs to be run for each variation of geometrical parameter. The cost of performing optimization for complex designs becomes rather expensive with the possibilities of multiple local optima[146]. This can be effectively tackled if computationally expensive high fidelity simulations are replaced by their inexpensive approximations. Such approximations are known as meta-models or surrogate models. They are statistical regression methods that estimate the response of simulation to a limited number of intelligently chosen sample points by design of experiment. Surrogate based optimization is an effective tool for engineering optimization and can be applied to optimization of high temperature motor. This chapter propose a novel surrogate based model based on Artificial Neural Networks (ANN) and Memory based Hybrid Dragonfly Algorithm (MHDA) for design optimization of high temperature motor.

6.2 Problem Formulation

To optimize the design of motor there are three necessary things to be decided before hand[50] . They are

1. The performance criterion of motor which is to be optimized
2. Design variables and their range affecting the performance criterion
3. Accurate modelling of the relationship between design variables and performance

criterion

In the present work, minimization of winding temperature is taken as the objective function. As mentioned in the literature, windings and permanent magnets are most sensitive to temperature and their performance is adversely affected by rise in temperature. To ensure reliable operation under high ambient temperature conditions, materials that can sustain high temperature are used. Samarium cobalt permanent magnets can operate up to a temperature of 350°C and polyimide insulated wire can sustain a temperature of 220°C. Temperature tolerance of magnets is higher than the windings[147]. Moreover as the temperature of winding increases, the lifetime of insulation decreases there by affecting the performance of motor. Since cooling provisions are not available for motor considered for current application, the winding insulation must withstand the ambient temperature as well as temperature rise due to losses. Therefore to increase the reliability of high temperature motor, winding temperature needs to be optimized to minimum.

In the case of ISI vehicle, with no cooling provisions available the winding temperature of the motor can be minimized by the optimal design of motor. The optimization problem can be generalized as

$$\text{Minimize Winding temperature,}$$

$$T_{winding} \tag{6.1}$$

$$\text{subjected to constraints Torque, } T \geq 2\text{Nm}$$

$$\text{Efficiency, } \eta \geq 85$$

$$\text{Maximum flux density, } B_{max} \leq 2.25T$$

The lower and upper bound of design variables are tabulated in Table 6.1

Table 6.1 – Design variables

Symbol	Parameter	Range
l_g	Air gap(mm)	0.5-1
SD	Slot depth(mm)	8-12
δ	Current Density (A/mm^2)	1-5
TW	Tooth width (mm)	5-8
SO	Slot opening(mm)	2-3
l_m	Magnet Thickness(mm)	4-6
β_m	Magnet Arc(º)	120º-160º

Once the problem is framed, next step is modelling the relationship between design variables and objective function. The relationship between design variables and objective function is found by coupled electromagnetic thermal simulations which runs in loop until a convergence is reached between two. For optimization, there are two important issues using such computationally expensive simulations. Firstly, evaluating the objective function for every possible combination of all design variable value can become a very expensive undertaking. Secondly, number of design variables has a massive impact on the number of experiments required. It is therefore imperative that we minimize this at the outset by screening out the design variables that significantly affect the outcome[148]. This can be achieved by creating a computationally cheap model which mimic the behaviour of simulation model as accurately as possible over the complete design space of interest using fewer simulation points. Once such model is built, it can be used for other task of computational analysis such as optimization process[149].

6.3 Overview of Surrogate Modelling

Surrogate models, or metamodels, are compact scalable analytic models that approximate the multivariate input/output behavior of complex systems, based on sampled data built from limited set of computational expensive simulations [150]. Surrogate doesn't gives any idea of internal behavior of system but rather approximates the input - output response of system. It is a technique that makes use of the sampled data (observed by running the computer code) to build surrogate models, which are sufficient to predict the output of an expensive computer code at untried points in the design space[151]. There are several reported works available in literature regarding construction and implementation of surrogate models like Kriging[64], Response Surface Model (RSM)[152], Radial Basis Function (RBF)[153], Artificial Neural Networks (ANN)[154]. Surrogate based optimization have been widely used in electric machine design optimization. RSM was used by Zwe-Lee Gaing[155] for rigorous design and optimization of brushless motors. Kriging assisted surrogate model for multi-objective design of permanent magnet motor by Min Li et al. [156] . Melo et al., used Artificial Neural Network model for approximating the relationship between design variables and design objectives of flux switching permanent magnet generator[157]. Apart from electric machine design optimization, surrogate models also find several applications in the field of welding[158], fuel engine systems[159] and mechatronic systems[160]. The main considerations in the building surrogate model are selection of sample points, selection of type of model and evaluating the accuracy of model.

6.4 Design of Experiment (DoE)

The design of computer experiments allocates samples in the design space to establish combinational relationships of input design variables involved in the optimization problem so that maximum information can be retrieved with minimum bias error. Computationally extensive simulations will be carried out in the allocated samples to acquire the training set that can be used to construct surrogate model. With the increase in number of samples, the accuracy of surrogate model also increases. But, as number of samples increases the cost of computation increases. Hence a trade off must be made between number of samples and amount of information that can be retrieved must be done. The main objective of DoE for surrogate modelling is to minimize error between the constructed surrogate model and actual model with minimum number of samples[161]. There are several DoE techniques reported in the literature[162]. Full factorial, fractional factorial, central composite and Box Behnken design are considered as conventional DoE methods. Full factorial design is characterized by all possible combinations of input factors. Fractional factorial designs are used if the simulations are computationally expensive and number of design variables are very large. Central composite design starts with a full factorial or fractional factorial design (with center points) and add ”star” points to estimate curvature. Box Behnken designs is an alternate choice for fitting quadratic models that requires 3 levels of each factor. All these methods are applied to discrete design variables to explore larger design space. In cases where prior information about objective function is not known, there are other modern techniques for DoE[146]. They are Orthogonal Array and Latin Hypercube sampling. Orthogonal array method uses multiple orthogonal arrays to screen the experimental conditions and means. The advantage of this method is that it uses the least experimental data based on the number of factors and levels in factor parameter space to achieve the best combination of parameter design and optimal results. The major disadvantage associated with this method is the lack of flexibility and point replication. Lack of flexibility arises from the fact that orthogonal array, in some cases, does not exist even when the design variables are provided. Point replication occur when the orthogonal array span the same points in the design variable subspace. Alternate method is Latin Hypercube Sampling in which the domain of each random variable decomposed into interval and same probability is assigned to all the intervals. The number of intervals depends on how many samples would be generated for each variable. One value from each interval is selected at random with respect to the probability density in the interval[163]. In practice the range of every parameter for n design variables is separated as p bins, so that the total number of pn bins will be generated in the design space. The samples are randomly selected in the design space, and each will be located randomly in one of the whole bins providing a non-uniform sampling. There is exactly one sample in each bin for all one-dimensional projections of the p samples and bins hence the problem of replication does not exists. Considering these advantages over Orthogonal array[161], Latin hypercube sampling method is adopted here. Based on Latin hypercube sampling, number of computer experiments were specified. As an empirical rule, number of data collection points in a sampling plan should be around ten times the number of design variables[50]. A few literature state that the number of sample points must be at least equal to or greater than the number of model parameters to be estimated. Following the above recommendation, in this work a plan of 100 data samples is used.

6.5 Surrogate Construction

After selection of DoE approach, coupled electromagnetic thermal analysis is carried out at the sampling points to create surrogate model. The next step involves selecting an approximating functional form, $y_i\hat{(x)}$to use as a surrogate of complex computer simulations $y_i(x)$. The general form for the metamodel can be expressed as

$$y_i\hat{(x)} = y_i(x) + \varepsilon \tag{6.2}$$

where ε is the error in approximation. Among numerous techniques to create surrogate models, polynomial regression model, radial basis function, artificial neural networks and kriging model are widely used for engineering problems. The choice of right surrogate model depends on essence of the problem. Due to the suitability of Artificial Neural Networks (ANN) for approximating non-linear characteristics, we focus on ANN based surrogate model for optimization.

6.5.1 Artificial Neural Network

Artificial neural networks(ANNs) are statistical models directly inspired by, and partially modeled on biological neural networks [164]. Among different types of neural networks, Feedforward Neural Network (FNN) are most widely used. FNN is characterized by the flow of information from input nodes to output nodes through hidden nodes in a forward manner without any loops. Multi Layer Perceptrons (MLP) are FNN with multiple perceptions which makes it capable of solving non- linear problems. It has been proven that MLPs with one hidden layer are able to approximate any continuous or discontinuous function[165]. ANN yield better approximations compared to the classical response surface methods, in cases, if the nature of the problem is unknown, involves large number of design parameters, or not completely bounded design spaces[166]. A simple ANN model with input nodes $(U_1, U_2...U_n)$ single hidden layer with nodes $(H_1, H_2..H_m)$ and output node O is shown in Figure 6.1

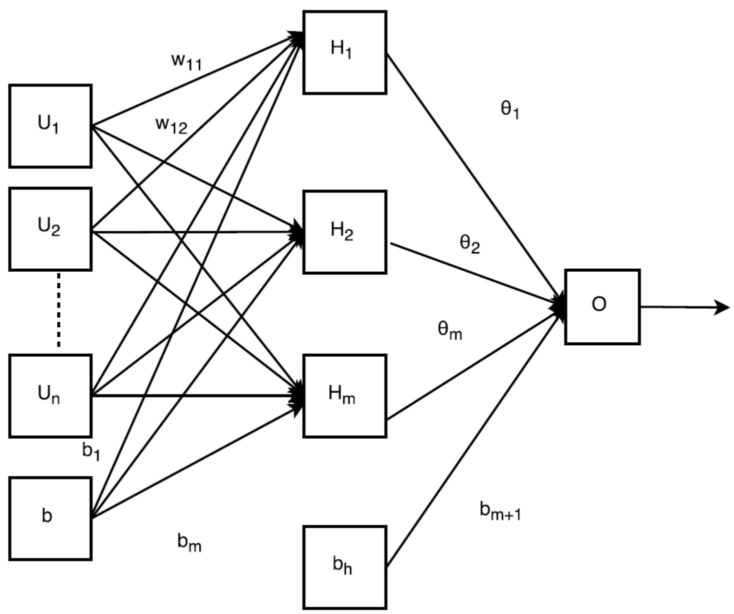

Figure 6.1 – ANN with one hidden layer

Regardless of types of ANN, the development of accurate model depends on several factors like quality of data, network architecture, model size, complexity, and training algorithm [167]. Training process, that provides learning for ANN, is an optimization process with aim of finding the optimal set of weights and biases to minimize an error, and fit within given data. Gradient based algorithms such as Back Propagation (BP) algorithm are very popular in training ANN due to its simplicity, higher speed, fine tuning and easy implementation. However, they suffer from the problems of entrapment in local optima, low convergence speed and sensitiveness to initialization[165][168]. These issues of gradient based algorithms led to the increased use of metaheuristic algorithms for training ANN[165]. Metaheuristic algorithms always starts with randomized population of points rather than a single point hence search space is effectively explored and chances of convergence to global optimum is enhanced. They don't require any gradient information as demanded by deterministic training algorithms. Moreover, metaheuristic algorithms can be applied for learning of any type of ANN with any activation function. They are also very suitable for dealing large complex problem with large number of local optima. These features make them more attractive alternative in training ANN. The efficiency of MHDA is proven in multiple test functions and engineering design problems, hence it is used in training neural networks to optimize the set of weight and biases.

6.5.2 A Novel Surrogate Model based on ANN and MHDA

In this section, the novel training algorithm known as MHDA, is used to train ANN. Two important considerations are taken into account while using this approach. They are encoding weight and biases, and defining fitness function.There are several methods of encoding the weights and biases such as vector, matrix and binary. In this context, vector representation is followed since ANNs with complex structures are not considered. In vector method, each search agent is encoded as a vector containing set of weights connecting input layer with hidden layer, set of weights connecting hidden layer with output layer and biases. The individual length of each search agent is calculated as Eq. 6.3 .

$$length = (n \times m) + (2 \times m) + 1 \tag{6.3}$$

where n is the number of input variables, m is the number of neurons in the hidden layer. The search agent vector,$\overrightarrow{SA}$ generated by MHDA can be represented as

$$\overrightarrow{SA} = \{b_1, b_2, ...b_{m+1}, w_{11}, w_{12}, ..w_{nm}, \theta_1,\theta_{2,...,}\theta_m\} \tag{6.4}$$

In MHDA, every search agent is evaluated based on fitness function. Fitness function is usually considered as Mean Square Error(MSE) which is calculated based on difference between the predicted value and actual value generated by search agents on training set[165]. MSE is calculated as per equation

$$MSE = \frac{(\sum_{i=1}^{n}(o_i^k - \hat{o_i}^k)^2)}{s} \tag{6.5}$$

where s is the number of training samples, n is the number of inputs, o_i^k is the actual value of i^{th} input when k^{th} training sample appears in the input, $\hat{o_i}^k$is the predicted value by MHDA trained ANN when i^{th} input of k^{th} training sample is applied.

MHDA is a hybrid algorithm combining conventional Dragonfly Algorithm (DA) and Particle Swarm Optimization (PSO). The procedure for training of ANNs with MHDA is explained in steps.

1. Initialization of DA: Dragonfly Algorithm is the first phase of MHDA. In this step, search agents, each having vector of weight and biases are randomly generated. Each search agent represents an ANN model.

2. Objective Function Evaluation: In this step, set of weights and biases that form the generated search agents are first assigned to ANN. The objective function in this case is chosen as MSE, as mentioned earlier. Based on training datasets, MHDA iteratively changes weights and biases to minimize the objective function

3. Saving in internal memory: The set of search agents that can give the possible minimum solution to objective function are saved in $DA - pbest$ memory. The search agent with global minimum MSE is saved as $DA - gbest$. Velocity and position are updated using Eq 6.6 and Eq 6.7

$$\triangle X_{t+1} = (sS_i + aA_i + cC_i + fF_i + eE_i) + w\triangle X_t \tag{6.6}$$

$$X_{t+1} = X_t + Levy(d)X_t \tag{6.7}$$

where X_t and X_{t+1}denotes the position of dragonfly at time t and $t+1$ respectively , $\triangle X_t$ and $\triangle X_{t+1}$ denotes step vector at time t and $t+1$ respectively, s, a, c, f, e denotes the swarming operators of DA and S, A, C, F, E denote the separation, alignment, cohesion, attraction towards food source and repulsion from enemy source which are basic swarming mechanism of dragonflies.

4. Initialization of PSO: PSO algorithm is the second phase of MHDA. PSO is initialized on on $DA - pbest$ and $DA - gbest$

5. Position and velocity are updated using Eq 6.8 and Eq 6.9

$$V_{k+1}^i = wV_k^i + C_2 r_2 (DA - gbest_k^g - X_k^i) + C_1 r_1 (DA - pbest_k^i - X_k^i) \tag{6.8}$$

$$X_{k+1}^i = X_k^i + V_{k+1}^i \tag{6.9}$$

where $V_{k+1}^i$and V_k^i denotes velocity of the particle in $k+1^{th}$ iteration and k^{th} iteration respectively, $X_{k+1}^i$and X_k^i denotes position of the particle in $k+1^{th}$ iteration and k^{th} iteration respectively, w is the inertial weight ,$C_1$and C_2 represents the cognitive and social parameters, $DA - pbest_k^i$ is the $pbest$ for i^{th} particle of PSO, $DA - gbest_k^g$ is $gbest$ of the swarm up to k^{th} iteration for PSO

6. Repeat the steps 2-5 until maximum iteration is reached. The flowchart of training process is shown in Figure 6.2

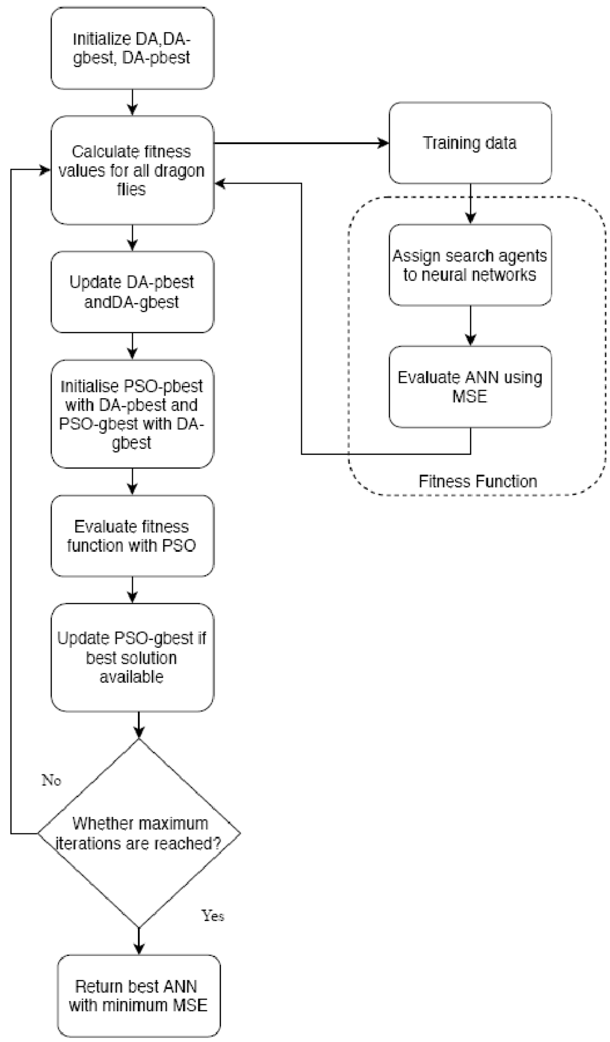

Figure 6.2 – General steps of MHDA trained ANN

The performance of MHDA trained neural network is compared with other training algorithms on standard benchmark approximation and classification functions which is detailed in the Appendix-B. The convergence curves also proves that ANN training process using MHDA is faster than other conventional algorithms such as Dragonfly Algorithm (DA), Grey Wolf Optimizer (GWO), Particle Swarm Optimization (PSO), Genetic Algorithm (GA), Ant Colony Optimizer (ACO), Evolutionary Strategy (ES). This gives the confidence in applying MHDA for training ANN in the present study.

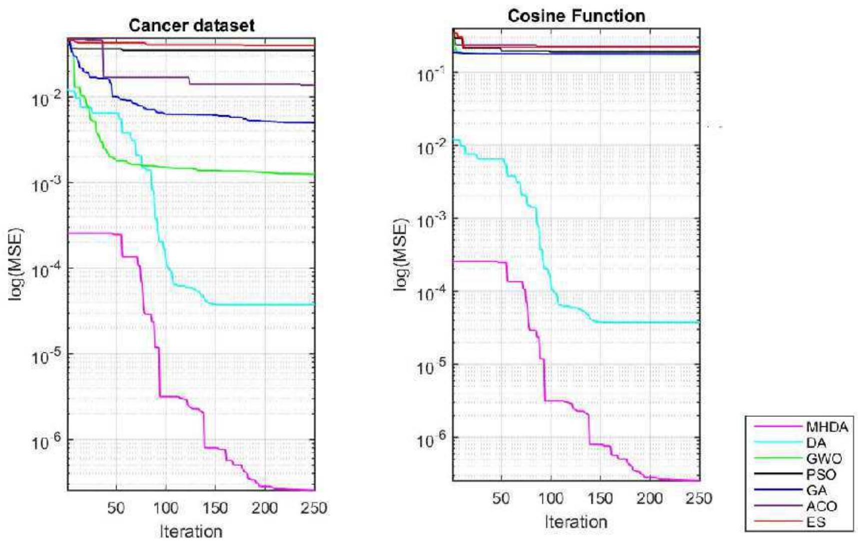

Figure 6.3 – Convergence curves for different algorithms

6.5.3 Formation of MHDA trained ANN for high temperature motor

As stated in section 6.2 the primary objective of optimization is to reduce the winding temperature of high temperature by optimal selection of design variables. MHDA trained ANN is used to find the relationship between design variables with the range mentioned in Table 6.1.The process of formation of MHDA trained ANN surrogate model based on coupled electromagnetic - thermal simulation is shown in Figure 6.4. 100 sample points are chosen as per Latin Hypercube Sampling (LHS) method with the help of statistical software. Coupled electromagnetic thermal simulation is carried out at these data points obtaining torque, winding temperature, efficiency and saturation flux density. The results obtained by the means of coupled analysis with corresponding values of design variables properly scaled are classified into training data set and validation data set. Training data set is used for training ANN and validation dataset is used for testing the performance of trained ANN.

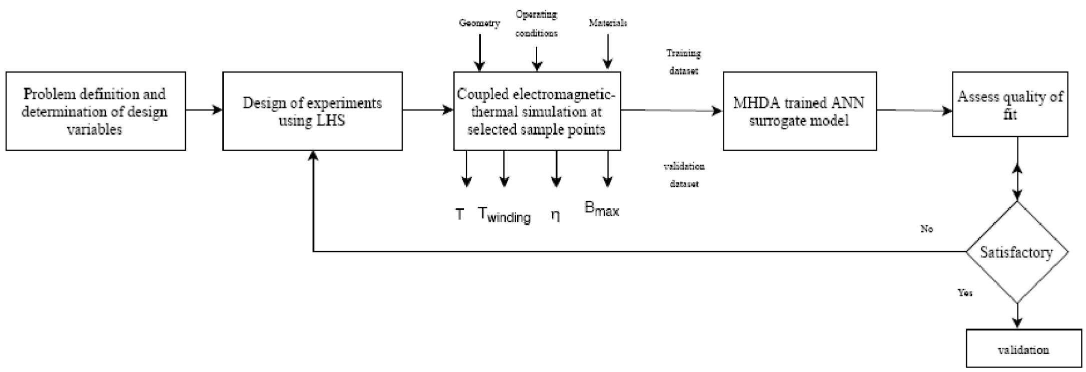

Figure 6.4 – Coupled electromagnetic thermal based MHDA trained ANN surrogate model

The applied neural network with input, hidden and output layer is shown in Figure 6.5.

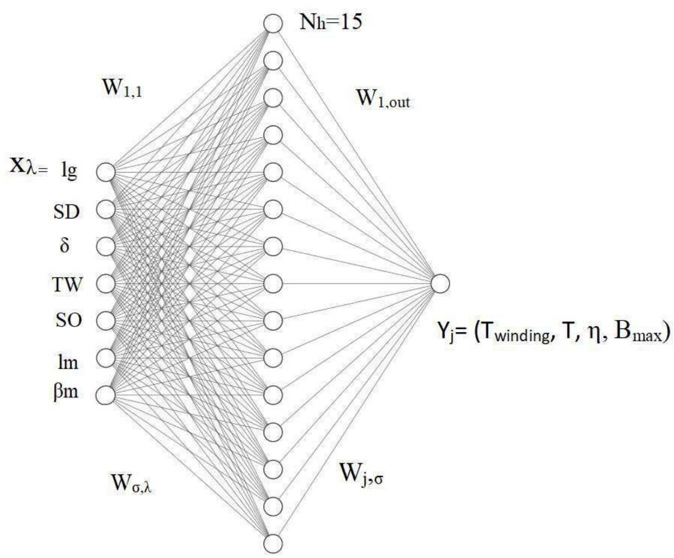

Figure 6.5 – ANN representation

where x_λ denotes number of inputs, N_h denotes number of hidden layers, Y_j denotes number of outputs. Four ANNs are considered for forming the mathematical relationship between design variables and four target functions. MHDA adjusts the weight of all interconnection to minimize the error between reference output and actual output. The training of ANN is carried out by MHDA with Mean Square Error (MSE) as the modelling error. After four ANN have been trained, following mathematical model of the form[53]

$$y_j = [1 + exp\{-\sum_{\sigma=1}^{N_h} W_{j,\sigma}[1 + exp\{-\sum_{\lambda=1}^{N_i} W_{\sigma,\lambda} X_\lambda - \upsilon_\sigma\}]^{-1} - \upsilon_j\}]^{-1} \tag{6.10}$$

representing the relationship between the design variables and target function can be built where $j = 1, 2, 3, 4$, N_h denotes number of hidden layers, $W_{\sigma,\lambda}$ denotes weight from input nodes to hidden nodes, $W_{\sigma,\lambda}$ denotes weight from hidden nodes to output node, υ_σ denotes bias at input node and υ_j denotes bias at output node.

6.5.4 Assessment and Validation of Surrogate model

Once the model is framed it is necessary to check the effectiveness of the model. This is verified using statistical indexes such as Root Mean Square Error (RMSE), Relative Root Mean Square Error (rRMSE), and determination coefficient (R^2). The mathematical expression for MSE, RMSE and R^2 are given by

$$MSE = \frac{(\sum_{i=1}^{n}(o - \hat{o})^2)}{n} \tag{6.11}$$

$$RMSE = \sqrt{\frac{(\sum_{i=1}^{n}(o - \hat{o})^2)}{n}} \tag{6.12}$$

$$R^2 = (\frac{\sum_{i=1}^{n}(\hat{o} - \bar{\hat{o}})^2 \times \sum_{i=1}^{n}(o - \bar{o})^2}{\sqrt{\sum_{i=1}^{n}(\hat{o} - \bar{\hat{o}})^2} \times \sqrt{\times \sum_{i=1}^{n}(o - \bar{o})^2}} \tag{6.13}$$

where $\hat{o}$,o are estimated value and measured value respectively,$\bar{\hat{o}}$ and $\bar{o}$ are the average of estimated and measured value respectively, n is the number of training samples, and $\bar{n}$ is the average of training samples. Good models have low RMSE and rRMSE. The value of R^2 ranges from 0 to 1. Higher values of R^2 indicates better fit to model[148]. The performance of ANN surrogate model is also compared with popular kriging surrogate model which is tabulated in Table 6.2 Kriging model is implemented with the help of SUMO toolbox in MATLAB. From the literature it was found that the the values of a normalized RMSE < 0.1 and RMSE < 0.02 implies surrogates with reasonably and excellent predictive capabilities, respectively. It is found that both surrogate models perform well in approximating the non-linear relationship between design variables and objectives. However, the performance of ANN surrogate model was relatively better when compared to kriging based model.

Table 6.2 – Comparison of surrogate models

Surrogate Model	Parameter	RMSE	R^2
ANN	Winding temperature(ºC)	0.0015	96.83
Kriging		0.06	89.63
ANN	Torque (Nm)	0.000000061	99.29
Kriging		0.002	96.78
ANN	Efficiency(%)	0.00000008	96.86
Kriging		0.0026	94.38
ANN	Maximum flux density (T)	0.00043	99.53
Kriging		0.08	96.43

6.6 Surrogate Based Optimization (SBO)

After framing the surrogate model, it is used to obtain an optimal solution subjected to a series of constraints. As mentioned earlier, minimization of winding temperature is taken as the target of the optimization process satisfying the constraints of torque, flux density and efficiency. Optimization was carried out under same torque and power. Since the efficiency of MHDA in locating global optimal solutions is already proved, same algorithm is applied here. The search agents in MHDA is set to 50 and maximum number of iterations is set to 200. MHDA is allowed to act directly on four mathematical models represented by trained neural networks. A number of machine configurations can be analyzed in this way. In order to prove the goodness of method, result obtained by ANN and MHDA is compared with results obtained by conventional algorithms such as GA and PSO. The convergence characteristics of the proposed method is compared with other algorithms such as GA and PSO. From Figure 6.6, it is found that MHDA reaches optimal solution in less number of iteration when compared to GA and PSO. The optimization results have been tabulated in Table 6.3

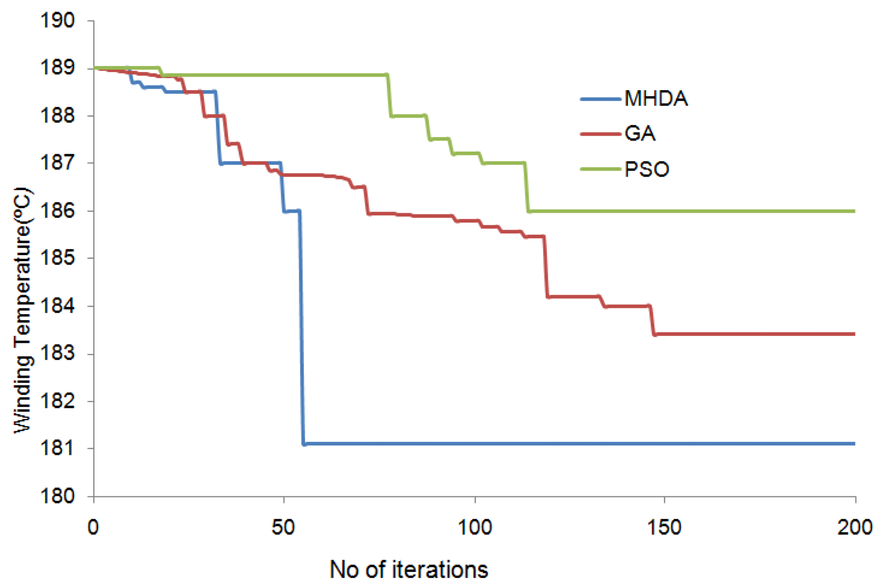

Figure 6.6 – Convergence characteristics

Table 6.3 – Comparison of optimization results by different algorithms

	Design Variable	GA	PSO	MHDA
Objective	Winding Temperature (°C)	185.2	182.1	181.6
Constraints	Torque(Nm)	2	2	2.1
	Saturation Flux Density(T)	2.1	1.99	1.98
	Efficiency(%)	76	84	85.39

The temperature rise in the winding in the optimized and prototype model is shown in Figure 6.7

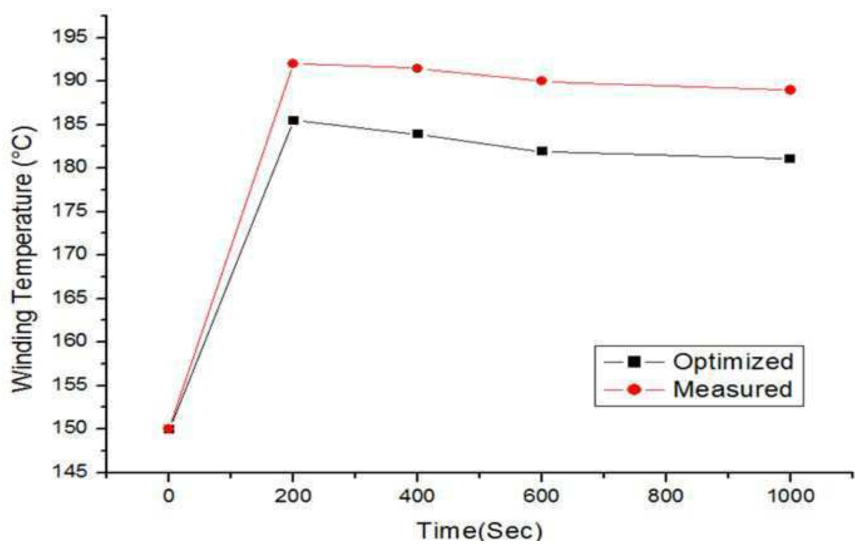

Figure 6.7 – Comparison between optimized and prototype model

Table 6.4. shows value of design variables and performance parameters for initial and optimized design.

Table 6.4 – Optimized values of design variables

Design Variable/Parameters	Basic Model	Optimal Model
$l_g(mm)$	0.5	0.75
$SD(mm)$	12	11.2
$\delta(A/mm^2)$	5	4.2
$TW(mm)$	5	6
$SO(mm)$	2.5	2.1
$l_m(mm)$	4	3.5
$\beta_m(^o)$	140	137.5
Winding Temperature(^oC)	188.6	181.6

It was found that temperature of optimized model was reduced by 7^{o}C which increases the life time of insulation by more than 20,000 hours, thereby saving the operating life of high temperature motor in the absence of any cooling mechanism. The constraints of torque, saturation flux density and efficiency was also satisfied.The results of optimization have been successfully proved by coupled electromagnetic thermal simulation. Figure 6.8 shows the temperature distribution of optimal design

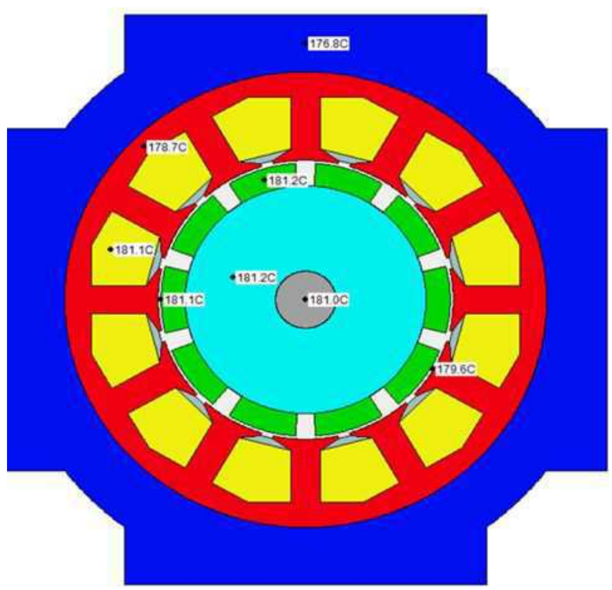

Figure 6.8 – Temperature distribution of optimized design

6.7 Conclusion

In this chapter surrogate based analysis and optimization was carried out for minimization of winding temperature of high temperature motor with Torque, Efficiency and Maximum Flux density as constraints. Following are the main points that can be concluded from the chapter.

- The process and three important steps for optimization were detailed.
- Design of experiments were presented and Latin Hypercube sampling was used to allocate the sampling points.
- Methods for construction of surrogate model were explained. Two surrogate models were considered -one based on ANN and other based on Kriging.
- MHDA was found to be an effective training algorithm for ANN when compared with other conventional algorithms.
- It was found that MHDA trained ANN surrogate model has higher precision when compared to Kriging based model
- Four ANNs are considered for forming the mathematical relationship between design variables and four target functions. MHDA algorithm is used as well to find global optimal solutions in the search space based on surrogate model.
- The temperature rise in optimized design is 7^{o}C lesser than the original design which corresponds to 20,000 hours increase in life time of insulation thereby saving the operating life of high temperature motor in the absence of any cooling mechanism.
- The results of optimization have been successfully verified using coupled electromagnetic - thermal analysis.

- Thus surrogate based optimization model accomplishes optimization process quickly and accurately.

References

[1] S. P. Ashutosh, C. Rajagopalan, V. Rakesh, S. Rajendran, S. Venugopal, K. V. Kasiviswanathan, T. Jayakumar, Evolution in the design and development of the in-service inspection device for the indian 500 MWe fast breeder reactor, Nuclear Engineering and Design 241 (9) (2011) 3719–3728.

[2] A. Shukla, H. Karki, Application of robotics in offshore oil and gas industry- a review part I, Robotics and Autonomous Systems 75, Part B (2016) 490 – 507.

[3] S. Chetal, V. Balasubramaniyan, P. Chellapandi, P. Mohanakrishnan, P. Puthiyavinayagam, C. Pillai, S. Raghupathy, T. Shanmugham, C. S. Pillai, The design of prototype fast breeder reactor, Nuclear Engineering and Design 236 (7) (2006) 852 – 860, india's Reactors: Past, Present, Future.

[4] C. A. Amy, Liquid metal pumps for enabling heat transfer at extreme temperatures, Ph.D. thesis, Georgia Institute of Technology (2017).

[5] G. Betonico, A. Bannwart, M. Ganzarolli, Determination of the temperature distribution of ESP motors under variable conditions of flow rate and loading, Journal of Petroleum Science and Engineering 129 (2015) 110 – 120.

[6] F. Ismagilov, I. K. Khairullin, V. Vavilov, D. Farrakhov, A. Yakubov, V. Bekuzin, A high-temperature frameless starter-generator integrated into an aircraft engine, Russian Aeronautics (Iz VUZ) 59 (1) (2016) 107–111.

[7] Y. Bar-Cohen, High Temperature Materials and Mechanisms, ISBN 9781466566453, CRC Press, 2014.

[8] Z.-l. Qiu, Design and research on a variable ballast system for deep-sea manned submersibles, Journal of Marine Science and Application 7 (4) (2008) 255–260.

[9] C. Sciascera, Design of short time duty permanent magnet electrical machines, Ph.D. thesis, Department of Electrical and Electronic Engineering, University of Nottingham (2017).

[10] K. Sakai, H. Karasawa, T. Yagisawa, H. Mitsui, Y. Sawada, S. Ohta, M. Kai, Development and characteristics of servomotor for use under high temperature and radiation flux conditions, Electrical Engineering in Japan 119 (4) (1997) 52–65.

[11] J. S. Sulich, M. H. Cardon, Development of a high temperature and radiation resistant linear motion servo actuator system for nuclear reactor control rod application, IRE Transactions on Nuclear Science 9 (1) (1962) 193–203.

[12] K. Swaminathan, C. Asokane, J. I. Sylvia, P. Kalyanasundaram, P. Swaminathan, An ultrasonic scanning technique for in-situ 'bowing' measurement of prototype fast breeder reactor fuel sub-assembly, IEEE Transactions on Nuclear Science 59 (1) (2012) 174–181.

[13] B. Nashine, B. Rao, Design, in-sodium testing and performance evaluation of annular linear induction pump for a sodium cooled fast reactor, Annals of Nuclear Energy 73 (2014) 527 – 536.

[14] A. G. Sarigiannidis, M. E. Beniakar, P. E. Kakosimos, A. G. Kladas, L. Papini, C. Gerada, Fault tolerant design of fractional slot winding permanent magnet aerospace actuator, IEEE Transactions on Transportation Electrification 2 (3) (2016) 380–390.

[15] C. Wong, E. Yang, X.-T. Yan, D. Gu, Autonomous robots for harsh environments: a holistic overview of current solutions and ongoing challenges, Systems Science & Control Engineering 6 (1) (2018) 213–219.

[16] J. Iqbal, A. M. Tahir, R. ul Islam, R. un Nabi, Robotics for nuclear power plants - challenges and future perspectives, in: 2012 2nd International Conference on Applied Robotics for the Power Industry (CARPI), 2012, pp. 151–156.

[17] A. E. R. BOARD, In-service inspection of nuclear power plants, AERB Safety Guide No. AERB/NPP/SG/O-2.

[18] J. Pyrhonen, T. Jokinen, V. Hrabovcova, Design of rotating electrical machines, John Wiley & Sons, 2013.

[19] R. Krishnan, Switched reluctance motor drives: modeling, simulation, analysis, design, and applications, CRC press, 2001.

[20] K. Zacny, F. Rehnmark, J. Hall, E. Cloninger, C. Hyman, K. Kriechbaum, J. Melko, J. Rabinovitch, B. Wilcox, J. Lambert, E. Mumm, G. Paulsen, V. Vendiola, K. Chow, N. Traeden, Development of venus drill, in: 2017 IEEE Aerospace Conference, 2017, pp. 1–19.

[21] T. Raminosoa, A. M. El-Refaie, D. A. Torrey, K. Grace, D. Pan, S. Grubic, K. Bodla, K. Huh, Test results for a high temperature non-permanent-magnet traction motor, IEEE Transactions on Industry Applications 53 (4) (2017) 3496–3504.

[22] K.-H. Lee, H.-R. Cha, Y.-B. Kim, Development of an interior permanent magnet motor through rotor cooling for electric vehicles, Applied Thermal Engineering 95 (2016) 348 – 356.

[23] H. Liu, L. Chow, T. Wu, Design of a permanent magnet motor with wide temperature range, in: IECON 2015 - 41st Annual Conference of the IEEE Industrial Electronics Society, 2015, pp. 003816–003820.

[24] Z. Jibin, H. Jianhui, Design of high temperature brushless DC motor system for oil well detecting, in: ICEMS'2001. Proceedings of the Fifth International Conference on Electrical Machines and Systems (IEEE Cat. No.01EX501), Vol. 2, 2001, pp. 1269–1271 vol.2.

[25] B. Wrzecionko, A. Looser, J. W. Kolar, M. Casey, High-temperature (250 degrees C/500 degrees F) 19 000 min(-1) BLDC fan for forced air-cooling of advanced automotive power electronics, Ieee-Asme Transactions on Mechatronics 20 (1) (2015) 37–49.

[26] S. Wang, Y. Li, Y.-Z. Li, J. Wang, X. Xiao, W. Guo, Conception and experimental investigation of a hybrid temperature control method using phase change material for permanent magnet synchronous motors, Experimental Thermal and Fluid Science 81 (2017) 9 – 20.

[27] N. Bianchi, Electrical machine analysis using finite elements, CRC press, 2005.

[28] H. A. Mang, Numerical methods in finite element analysis, International Journal for Numerical Methods in Engineering 11 (9) (1977) 1485–1485. doi:10.1002/nme.1620110913.

[29] Y. Wang, Coupled electromagnetic and thermal analysis and design optimization of synchronous electric machines, Master's thesis, Engineering (2014).

[30] J. Nerg, M. Rilla, J. Pyrhonen, Thermal analysis of radial-flux electrical machines with a high power density, IEEE Transactions on industrial electronics 55 (10) (2008) 3543–3554.

[31] K. Shahzad, Y. Guo, L. Li, D. Dorrell, Design of high speed permanent magnet generator for solar co-generation system using motor-CAD, in: 2017 20th International Conference on Electrical Machines and Systems (ICEMS), 2017, pp. 1–6. doi:10.1109/ICEMS.2017.8056036.

[32] A. Boglietti, A. Cavagnino, D. Staton, Thermal analysis of TEFC induction motors, in: Industry Applications Conference, 2003. 38th IAS Annual Meeting. Conference Record of the, Vol. 2, IEEE, 2003, pp. 849–856.

[33] H. Rouhani, J. Faiz, C. Lucas, Lumped thermal model for switched reluctance motor applied to mechanical design optimization, Mathematical and Computer Modelling 45 (5) (2007) 625 – 638.

[34] L. Alberti, N. Bianchi, A coupled thermal–electromagnetic analysis for a rapid and accurate prediction of im performance, IEEE Transactions on Industrial Electronics 55 (10) (2008) 3575–3582.

[35] W. Jiang, T. M. Jahns, Coupled electromagnetic-thermal analysis of electric machines including transient operation based on finite element techniques, in: 2013 IEEE Energy Conversion Congress and Exposition, 2013, pp. 4356–4363.

[36] G. Lei, J. Zhu, Y. Guo, C. Liu, B. Ma, A review of design optimization methods for electrical machines, Energies 10 (12) (2017) 1962.

[37] R. Yondo, E. Andres, E. Valero, A review on design of experiments and surrogate models in aircraft real-time and many-query aerodynamic analyses, Progress in Aerospace Sciences 96 (2018) 23 – 61.

[38] J. W. Bandler, Q. S. Cheng, S. A. Dakroury, A. S. Mohamed, M. H. Bakr, K. Madsen, J. Sondergaard, Space mapping: the state of the art, IEEE Transactions on Microwave Theory and Techniques 52 (1) (2004) 337–361.

[39] D. H. Wolpert, W. G. Macready, No free lunch theorems for optimization, IEEE Transactions on Evolutionary Computation 1 (1) (1997) 67–82. doi:10.1109/4235.585893.

[40] X.-S. Yang, A New Metaheuristic Bat-Inspired Algorithm, Springer Berlin Heidelberg, Berlin, Heidelberg, 2010, pp. 65–74.

[41] X.-S. Yang, Firefly Algorithms for Multimodal Optimization, Springer Berlin Heidelberg, Berlin, Heidelberg, 2009, pp. 169–178.

[42] A. H. Gandomi, A. H. Alavi, Krill herd: A new bio-inspired optimization algorithm, Communications in Nonlinear Science and Numerical Simulation 17 (12) (2012) 4831 – 4845.

[43] S. Mirjalili, A. Lewis, The whale optimization algorithm, Advances in Engineering Software 95 (2016) 51 – 67.

[44] S. Mirjalili, S. Saremi, S. M. Mirjalili, L. dos S. Coelho, Multi-objective grey wolf optimizer: A novel algorithm for multi-criterion optimization, Expert Systems with Applications 47 (2016) 106 – 119.

[45] A. R. Kashani, A. H. Gandomi, M. Mousavi, Imperialistic competitive algorithm: A metaheuristic algorithm for locating the critical slip surface in 2-dimensional soil slopes, Geoscience Frontiers 7 (1) (2016) 83 – 89, special Issue: Progress of Machine Learning in Geosciences.

[46] S. Mirjalili, Dragonfly algorithm: a new meta-heuristic optimization technique for solving single-objective, discrete, and multi-objective problems, Neural Computing and Applications 27 (4) (2016) 1053–1073.

[47] S. G. Min, G. Bramerdorfer, B. Sarlioglu, Analytical modeling and optimization for electromagnetic performances of fractional-slot PM brushless machines, IEEE Transactions on Industrial Electronics 65 (5) (2018) 4017–4027.

[48] P. V. M. Vrazic, G. Papa, Design of an axial flux permanent magnet synchronous machine using analytical method and evolutionary optimization, IEEE Transactions on Energy Conversion 31 (1) (2016) 150–158.

[49] W.Ji, X. Feng, J. Larsson, A. Stening, F. Gyllensten, H. Yang, Meta-modelling for enhancing design optimization of electric motors, in: ASME. International Design Engineering Technical Conferences and Computers and Information in Engineering Conference, Vol. Volume 2B, 2016.

[50] M. N. Azari, M. Mirsalim, S. M. A. Pahnehkolaei, S. Mohammadi, Optimum design of a line-start permanent-magnet motor with slotted solid rotor using neural network and imperialist competitive algorithm, IET Electric Power Applications 11 (1) (2017) 1–8.

[51] H. Shin, K. Lee, Optimal design of a 1 kw switched reluctance generator for wind power systems using a genetic algorithm, IET Electric Power Applications 10 (8) (2016) 807–817.

[52] Z. Tan, X. Song, W. Cao, Z. Liu, Y. Tong, DFIG machine design for maximizing power output based on surrogate optimization algorithm, IEEE Transactions on Energy Conversion 30 (3) (2015) 1154–1162.

[53] S. Meo, A. Zohoori, A. Vahedi, Optimal design of permanent magnet flux switching generator for wind applications via artificial neural network and multi-objective particle swarm optimization hybrid approach, Energy Conversion and Management 110 (2016) 230–239.

[54] G. Lei, X. M. Chen, J. G. Zhu, Y. G. Guo, W. Xu, K. R. Shao, Multiobjective sequential optimization method for the design of industrial electromagnetic devices, IEEE Transactions on Magnetics 48 (11) (2012) 4538–4541.

[55] G. Lei, J. Zhu, Y. Guo, K. Shao, W. Xu, Multiobjective sequential design optimization of PM-SMC motors for six sigma quality manufacturing, IEEE Transactions on Magnetics 50 (2) (2014) 717–720.

[56] G. Lei, C. Liu, J. Zhu, Y. Guo, Techniques for multilevel design optimization of permanent magnet motors, IEEE Transactions on Energy Conversion 30 (4) (2015) 1574–1584.

[57] G. Crevecoeur, L. Dupre, R. V. de Walle, Space mapping optimization of the magnetic circuit of electrical machines including local material degradation, IEEE Transactions on Magnetics 43 (6) (2007) 2609–2611.

[58] J. Gong, F. Gillon, J. T. Canh, Y. Xu, Proposal of a kriging output space mapping technique for electromagnetic design optimization, IEEE Transactions on Magnetics 53 (6) (2017) 1–4.

[59] M. Rosu, P. Zhou, D. Lin, D. M. Ionel, M. Popescu, F. Blaabjerg, V. Rallabandi, D. Staton, Multiphysics Simulation by Design for Electrical Machines, Power Electronics and Drives, Vol. 66, John Wiley & Sons, 2017.

[60] N. Bracikowski, M. Hecquet, P. Brochet, S. V. Shirinskii, Multiphysics modeling of a permanent magnet synchronous machine by using lumped models, IEEE Transactions on Industrial Electronics 59 (6) (2012) 2426–2437.

[61] Y. Wang, D. M. Ionel, D. Staton, Ultrafast steady-state multiphysics model for PM and synchronous reluctance machines, IEEE Transactions on Industry Applications 51 (5) (2015) 3639–3646.

[62] F. Lei, B. Du, X. Liu, X. Xie, T. Chai, Optimization of an implicit constrained multi-physics system for motor wheels of electric vehicle, Energy 113 (2016) 980 – 990.

[63] D. Prieto, P. Dessante, J. Vannier, B. DagusÃ©, X. Jannot, J. Saint-Michel, Multi-physic analytical model for a saturated permanent magnet assisted synchronous reluctance motor, IET Electric Power Applications 10 (5) (2016) 356–367.

[64] N. Simpson, R. Wrobel, P. H. Mellor, A multiphysics design methodology applied to a high-force-density short-duty linear actuator, IEEE Transactions on Industry Applications 52 (4) (2016) 2919–2929.

[65] Z. Huang, J. Fang, Multiphysics design and optimization of high-speed permanent-magnet electrical machines for air blower applications, IEEE Transactions on Industrial Electronics 63 (5) (2016) 2766–2774.

[66] S. Chauhan, Motor torque calculations for electric vehicle, International Journal of Scientific & Technology Research 4.

[67] Comprehensive in-service inspection system for pfbr vessels.
URL http://www.igcar.gov.in/pttc/mmg/2-tech.pdf

[68] J. F. Gieras, Material engineering, Springer Netherlands, Dordrecht, 2008, pp. 27–69.

[69] J. F. Gieras, Permanent magnet motor technology: design and applications, CRC press, 2009.

[70] F. Herrault, D. P. Arnold, I. Zana, P. Galle, M. G. Allen, High temperature operation of multi-watt, axial-flux, permanent-magnet microgenerators, Sensors and Actuators A: Physical 148 (1) (2008) 299 – 305.

[71] K. Kiyota, A. Chiba, Design of switched reluctance motor competitive to 60-kW IPMSM in third-generation hybrid electric vehicle, IEEE Transactions on Industry Applications 48 (6) (2012) 2303–2309.

[72] B. Kerdsup, N. H. Fuengwarodsakul, Performance and cost comparison of reluctance motors used for electric bicycles, Electrical Engineering 99 (2) (2017) 475–486.

[73] A. M. Omekanda, B. Lequesne, H. Klode, S. Gopalakrishnan, I. Husain, Switched reluctance and permanent magnet brushless motors in highly dynamic situations: A comparison in the context of electric brakes, in: Conference Record of the 2006 IEEE Industry Applications Conference Forty-First IAS Annual Meeting, Vol. 3, 2006, pp. 1570–1577.

[74] D. C. Hanselman, Brushless Permanent Magnet Motor Design, Magna Physics Pub, 1994.

[75] G. Pellegrino, A. Vagati, P. Guglielmi, B. Boazzo, Performance comparison between surface-mounted and interior pm motor drives for electric vehicle application, IEEE Transactions on Industrial Electronics 59 (2) (2012) 803–811.

[76] N. Zhao, W. Liu, Loss calculation and thermal analysis of surface-mounted pm motor and interior pm motor, IEEE Transactions on Magnetics 51 (11) (2015) 1–4.

[77] J. Goss, D. Staton, R. Wrobel, P. Mellor, Brushless AC interior-permanent magnet motor design: Comparison of slot/pole combinations and distributed vs. concentrated windings, in: 2013 IEEE Energy Conversion Congress and Exposition, 2013, pp. 1213–1219.

[78] S. Ranjini, R. Chellapandian, S. Murugan, S. Venugopal, Design and analysis of brushless servomotor for in-service inspection of PFBR, in: 2015 Annual IEEE India Conference (INDICON), 2015, pp. 1–5. doi:10.1109/INDICON.2015.7443307.

[79] S. Ranjini, S. Murugan, Design and performance comparison of permanent magnet brushless motors and switched reluctance motors for extended temperature applications, Progress In Electromagnetics Research M 67 (2018) 137– 146.

[80] K. S. S. Ranjini, S. Murugan, Electromagnetic and thermal analysis of permanent magnet motor for extended temperature applications, in: 2018 4th International Conference on Electrical Energy Systems (ICEES), IEEE, 2018, pp. 557–562.

[81] Z. Zhang, High temperature, buried permanent magnet, brushless DC motor, Master's thesis, Texas A&M University (2010).

[82] S. Qiang, L. Chenguang, Data acquisition system for electric vehicle's driving motor test bench based on VC++, Physics Procedia 33 (2012) 1725 – 1731, 2012 International Conference on Medical Physics and Biomedical Engineering (ICMPBE2012).

[83] R. Marko, B. MiloÅ¡, B. Miroslav, R. Leposava, Electrical motor testing station with electromagnetic load emulator: An overview of design, construction and calibration with examples of use, in: 3rd International Symposium on Environmental Friendly Energies and Applications (EFEA), 2014, pp. 1–6. doi:10.1109/EFEA.2014.7059959.

[84] A. Cavagnino, G. Bramerdorfer, J. A. Tapia, Optimization of electric machine designs part i, IEEE Transactions on Industrial Electronics 64 (12) (2017) 9716–9720. doi:10.1109/TIE.2017.2753359.

[85] M. Dorigo, S. Thomas, Ant Colony Optimization, MIT Press eBooks, 2004.

[86] C. Blum, X. Li, Swarm Intelligence in Optimization, Springer Berlin Heidelberg, Berlin, Heidelberg, 2008, pp. 43–85.

[87] G.-C. Luh, C.-Y. Lin, Structural topology optimization using ant colony optimization algorithm, Applied Soft Computing 9 (4) (2009) 1343 – 1353.

[88] M. R. J. Sattari, H. Malakooti, A. Jalooli, R. M. Noor, A Dynamic Vehicular Traffic Control Using Ant Colony and Traffic Light Optimization, Springer International Publishing, Cham, 2014, pp. 57–66.

[89] C. S. Greene, B. C. White, J. H. Moore, Ant Colony Optimization for Genome-Wide Genetic Analysis, Springer Berlin Heidelberg, Berlin, Heidelberg, 2008, pp. 37–47.

[90] R. Eberhart, J. Kennedy, A new optimizer using particle swarm theory, in: Micro Machine and Human Science, 1995. MHS '95., Proceedings of the Sixth International Symposium on, 1995, pp. 39–43.

[91] R. Kuo, C. Huang, Application of particle swarm optimization algorithm for solving bi-level linear programming problem, Computers & Mathematics with Applications 58 (4) (2009) 678 – 685.

[92] M. R. AlRashidi, M. E. El-Hawary, A survey of particle swarm optimization applications in electric power systems, IEEE Transactions on Evolutionary Computation 13 (4) (2009) 913–918.

[93] X. Wang, X. Qiu, Application of particle swarm optimization for enhanced cyclic steam stimulation in a offshore heavy oil reservoir, International Journal of Information Technology, Modeling and Computing (IJITMC) 1 (2) (2013) 37–47.

[94] M. G. H. Omran, A. P. Engelbrecht, A. Salman, Particle Swarm Optimization for Pattern Recognition and Image Processing, Springer Berlin Heidelberg, Berlin, Heidelberg, 2006, pp. 125–151.

[95] S. Mirjalili, S. M. Mirjalili, A. Lewis, Grey wolf optimizer, Advances in Engineering Software 69 (2014) 46 – 61.

[96] A. Sharma, A. Sharma, B. Panigrahi, D. Kiran, R. Kumar, Ageist spider monkey optimization algorithm, Swarm and Evolutionary Computation 28 (2016) 58 – 77.

[97] G.-G. Wang, Moth search algorithm: a bio-inspired metaheuristic algorithm for global optimization problems, Memetic Computing (2016) 1–14.

[98] C. W. Reynolds, Flocks, herds and schools: A distributed behavioral model, in: Proceedings of the 14th Annual Conference on Computer Graphics and Interactive Techniques, SIGGRAPH '87, ACM, New York, NY, USA, 1987, pp. 25–34.

[99] X.-S. Yang, Firefly Algorithm, Lévy Flights and Global Optimization, Springer London, London, 2010, pp. 209–218.

[100] X.-S. Yang, Chapter 2 - analysis of algorithms, in: X.-S. Yang (Ed.), Nature-Inspired Optimization Algorithms, Elsevier, Oxford, 2014, pp. 23 – 44.

[101] R. P. Parouha, K. N. Das, A memory based differential evolution algorithm for unconstrained optimization, Applied Soft Computing 38 (2016) 501 – 517.

[102] H. Ma, D. Simon, M. Fei, X. Shu, Z. Chen, Hybrid biogeography-based evolutionary algorithms, Engineering Applications of Artificial Intelligence 30 (2014) 213 – 224.

[103] S. Mirjalili, The ant lion optimizer, Advances in Engineering Software 83 (2015) 80 – 98.

[104] U. Mlakar, I. F. Jr., I. Fister, Hybrid self-adaptive cuckoo search for global optimization, Swarm and Evolutionary Computation 29 (2016) 47 – 72.

[105] I. Erlich, J. L. Rueda, S. Wildenhues, F. Shewarega, Evaluating the mean-variance mapping optimization on the IEEE-CEC 2014 test suite, in: 2014 IEEE Congress on Evolutionary Computation (CEC), 2014, pp. 1625–1632.

[106] P. Civicioglu, Backtracking search optimization algorithm for numerical optimization problems, Applied Mathematics and Computation 219 (15) (2013) 8121 – 8144.

[107] J. Zhang, A. C. Sanderson, JADE: Adaptive differential evolution with optional external archive, IEEE Transactions on Evolutionary Computation 13 (5) (2009) 945–958.

[108] A. K. Qin, V. L. Huang, P. N. Suganthan, Differential evolution algorithm with strategy adaptation for global numerical optimization, IEEE Transactions on Evolutionary Computation 13 (2) (2009) 398–417.

[109] J. Brest, S. Greiner, B. Boskovic, M. Mernik, V. Zumer, Self-adapting control parameters in differential evolution: A comparative study on numerical benchmark problems, IEEE Transactions on Evolutionary Computation 10 (6) (2006) 646–657.

[110] J. J. Liang, P. N. Suganthan, K. Deb, Novel composition test functions for numerical global optimization, in: Proceedings 2005 IEEE Swarm Intelligence Symposium,SIS 2005., 2005, pp. 68–75.

[111] P. J.Liang, B.Qu, Problem definitions and evaluation criteria for the CEC2014 special session and competition on single objective real parameter numerical optimization, Tech. rep., Computational Intelligence Laboratory,Zhengzhou University,Zhengzhou,China TechnicalReport,Nanyang Technological University,Singapore. (2014).

[112] D. Chen, F. Zou, R. Lu, P. Wang, Learning backtracking search optimisation algorithm and its application, Information Sciences 376 (2017) 71 – 94.

[113] J. Demsar, Statistical comparisons of classifiers over multiple data sets, Journal of Machine Learning Research 7 (2006) 1–30.

[114] Z. Li, W. Wang, Y. Yan, Z. Li, Ps-abc: A hybrid algorithm based on particle swarm and artificial bee colony for high-dimensional optimization problems, Expert Systems with Applications 42 (22) (2015) 8881 – 8895.

[115] J. Derrac, S. Garcia, D. Molina, F. Herrera, A practical tutorial on the use of nonparametric statistical tests as a methodology for comparing evolutionary and swarm intelligence algorithms, Swarm and Evolutionary Computation 1 (1) (2011) 3 – 18.

[116] G. D. Pillo, L. Grippo, Exact penalty functions in constrained optimization, SIAM Journal on Control and Optimization 27 (6) (1989) 1333–1360.

[117] S. Rao, Engineering Optimization: Theory and Practice: Fourth Edition, John Wiley and Sons, 2009.

[118] C. A. C. Coello, E. M. Montes, Constraint-handling in genetic algorithms through the use of dominance-based tournament selection, Advanced Engineering Informatics 16 (3) (2002) 193 – 203.

[119] Mezura-Montes, C. A. C. Coello, An empirical study about the usefulness of evolution strategies to solve constrained optimization problems, International Journal of General Systems 37 (4) (2008) 443–473.

[120] X. Hu, R. C. Eberhart, Y. Shi, Engineering optimization with particle swarm, in: Swarm Intelligence Symposium, 2003. SIS '03. Proceedings of the 2003 IEEE, 2003, pp. 53–57.

[121] E. Rashedi, H. Nezamabadi-pour, S. Saryazdi, GSA: A gravitational search algorithm, Information Sciences 179 (13) (2009) 2232 – 2248.

[122] A.-R. Hedar, M. Fukushima, Derivative-free filter simulated annealing method for constrained continuous global optimization, Journal of Global Optimization 35 (4) (2006) 521–549.

[123] Q. He, L. Wang, An effective co-evolutionary particle swarm optimization for constrained engineering design problems, Engineering Applications of Artificial Intelligence 20 (1) (2007) 89 – 99.

[124] E. Mezura-Montes, C. A. C. Coello, J. Reyes, L. Davila, Multiple trial vectors in differential evolution for engineering design, Engineering Optimization 39 (5) (2007) 567–589.

[125] K. S. Lee, Z. W. Geem, A new meta-heuristic algorithm for continuous engineering optimization: harmony search theory and practice, Computer Methods in Applied Mechanics and Engineering 194 (36) (2005) 3902 – 3933. doi:https://doi.org/10.1016/j.cma.2004.09.007.
URL http://www.sciencedirect.com/science/article/pii/S0045782504004682

[126] A. Kaveh, S. Talatahari, An improved ant colony optimization for constrained engineering design problems, Engineering Computations 27 (1) (2010) 155–182.

[127] C. C. L.C. Cagnina, S.C. Esquivel, Solving engineering optimization problems with the simple constrained particle swarm optimizer, Informatica 32 (2008) 319–326.

[128] M. Mahdavi, M. Fesanghary, E. Damangir, An improved harmony search algorithm for solving optimization problems, Applied Mathematics and Computation 188 (2) (2007) 1567 – 1579.

[129] A. H. Gandomi, X.-S. Yang, A. H. Alavi, Cuckoo search algorithm: a metaheuristic approach to solve structural optimization problems, Engineering with Computers 29 (1) (2013) 17–35.

[130] D. Karaboga, B. Basturk, On the performance of artificial bee colony (ABC) algorithm, Applied Soft Computing 8 (1) (2008) 687 – 697.

[131] V. K. Mehta, B. Dasgupta, A constrained optimization algorithm based on the simplex search method, Engineering Optimization 44 (5) (2012) 537–550.

[132] A. Kaveh, M. Khayatazad, A new meta-heuristic method: Ray optimization, Computers & Structures 112-113 (2012) 283 – 294.

[133] Kannan, Kramer, An augmented lagrange multiplier based method for mixed integer discrete continuous optimization and its applications to mechanical design, ASME. J. Mech. Des. 116(2 (1994) 405–411.

[134] Sandgren, Nonlinear integer and discrete programming in mechanical design optimization, ASME. J. Mech. Des 112(2) (1990) 223–229.

[135] C. Zhang, H.-P. Wang, Mixed-discrete non-linear optimization using simulated annealing, Engineering Optimization 21 (4) (1993) 277–291.

[136] K. Deb, GeneAS: A Robust Optimal Design Technique for Mechanical Component Design, Springer Berlin Heidelberg, Berlin, Heidelberg, 1997, pp. 497–514.

[137] C. A. C. Coello, Use of a self-adaptive penalty approach for engineering optimization problems, Computers in Industry 41 (2) (2000) 113 – 127.

[138] L. dos, S. Coelho, Gaussian quantum-behaved particle swarm optimization approaches for constrained engineering design problems, Expert Systems with Applications 37 (2) (2010) 1676 – 1683.

[139] B. Akay, D. Karaboga, Artificial bee colony algorithm for large-scale problems and engineering design optimization, Journal of Intelligent Manufacturing 23 (4) (2012) 1001–1014.

[140] S. He, E. Prempain, Q. H. Wu, An improved particle swarm optimizer for mechanical design optimization problems, Engineering Optimization 36 (5) (2004) 585–605.

[141] A. Kaveh, S. T. Talatahari, Engineering optimization with hybrid particle swarm anoptimization optimization, Asian Journal of Civil Engineering 10 (2009) 267–283.

[142] H. Garg, Solving structural engineering design optimization problems using an artificial bee colony algorithm, Journal of Industrial and Management Optimization 10 (3) (2014) 777–794.

[143] Benchmark[Online], A benchmark for a mono and multi objective optimization of the brushless dc wheel motor., accessed 11-November-2016(http://l2ep.univ-lille1.fr/come/benchmark-wheel-motor/OptRest.htm) (2005).

[144] C. E. Klein, E. H. V. Segundo, V. C. Mariani, L. dos S. Coelho, Modified social-spider optimization algorithm applied to electromagnetic optimization, IEEE Transactions on Magnetics 52 (3) (2016) 1–4.

[145] S. Ranjini, S. Murugan, Memory based hybrid dragonfly algorithm for numerical optimization problems, Expert Systems with Applications 83 (2017) 63–78.

[146] S. Koziel, L. Leifsson, Surrogate-based aerodynamic shape optimization by variable-resolution models, AIAA journal 51 (1) (2012) 94–106.

[147] Q. Li, M. Dou, B. Tan, H. Zhang, D. Zhao, Electromagnetic-thermal integrated design optimization for hypersonic vehicle short-time duty pm brushless dc motor, International Journal of Aerospace Engineering 2016.

[148] A. Forrester, A. Keane, et al., Engineering design via surrogate modelling: a practical guide, John Wiley & Sons, 2008.

[149] D. Stephens, D. Gorissen, K. Crombecq, T. Dhaene, Surrogate based sensitivity analysis of process equipment, Applied Mathematical Modelling 35 (4) (2011) 1676 – 1687.

[150] D. Gorissen, I. Couckuyt, P. Demeester, T. Dhaene, K. Crombecq, A surrogate modeling and adaptive sampling toolbox for computer based design, Journal of Machine Learning Research 11 (Jul) (2010) 2051–2055.

[151] Z.-H. Han, K.-S. Zhang, Surrogate-based optimization, in: Real-world applications of genetic algorithms, InTech, 2012.

[152] A. Khuri, Response Surface Methodology, Springer Berlin Heidelberg, Berlin, Heidelberg, 2011, pp. 1229–1231.

[153] H.-M. Gutmann, A radial basis function method for global optimization, Journal of Global Optimization 19 (3) (2001) 201–227.

[154] Z. Zainuddin, O. Pauline, Function approximation using artificial neural networks, in: Proceedings of the 12th WSEAS International Conference on Applied Mathematics, MATH'07, World Scientific and Engineering Academy and Society (WSEAS), Stevens Point, Wisconsin, USA, 2007, pp. 140–145.

[155] Z. L. Gaing, C. H. Lin, M. H. Tsai, M. F. Hsieh, M. C. Tsai, Rigorous design and optimization of brushless PM motor using response surface methodology with quantum-behaved pso operator, IEEE Transactions on Magnetics 50 (1) (2014) 1–4.

[156] M. Li, F. Gabriel, M. Alkadri, D. A. Lowther, Kriging-assisted multi-objective design of permanent magnet motor for position sensorless control, IEEE Transactions on Magnetics 52 (3) (2016) 1–4.

[157] A. Melo, D. Costola, R. Lamberts, J. Hensen, Development of surrogate models using artificial neural network for building shell energy labelling, Energy Policy 69 (2014) 457 – 466.

[158] L. Portelette, J.-C. Roux, V. Robin, E. Feulvarch, A gaussian surrogate model for residual stresses induced by orbital multi-pass tig welding, Computers & Structures 183 (2017) 27 – 37.

[159] H. Taghavifar, Towards multiobjective nelder-mead optimization of a HSDI diesel engine: Application of latin hypercube design-explorer with svm modeling approach, Energy Conversion and Management 143 (2017) 150 – 161.

[160] F. Sanchez, M. Budinger, I. Hazyuk, Dimensional analysis and surrogate models for the thermal modeling of multiphysics systems, Applied Thermal Engineering 110 (2017) 758 – 771. doi:https://doi.org/10.1016/j.applthermaleng.2016.08.117.
URL http://www.sciencedirect.com/science/article/pii/S1359431116314776

[161] T. Zheng, Improved winding design of a double fed induction generator (dfig) wind turbine using surrogate optimisation algorithm, Ph.D. thesis, School of Electrical and Electronic Engineering,New Castle University (2015).
URL http://hdl.handle.net/10443/3274

[162] D. C. Montgomery, Design and analysis of experiments, John wiley & sons, 2017.

[163] B. Tang, Orthogonal array-based latin hypercubes, Journal of the American statistical association 88 (424) (1993) 1392–1397.

[164] W. S. McCulloch, W. Pitts, A logical calculus of the ideas immanent in nervous activity, The bulletin of mathematical biophysics 5 (4) (1943) 115–133. doi:10.1007/BF02478259.

[165] S. Mirjalili, S. M. Mirjalili, A. Lewis, Let a biogeography-based optimizer train your multi-layer perceptron, Information Sciences 269 (Supplement C) (2014) 188 – 209.

[166] M. Y. M. Ahmed, N. Qin, Surrogate-based aerodynamic design optimization: Use of surrogates in aerodynamic design optimization, in: 13th International Conference on AEROSPACE SCIENCES & AVIATION TECHNOLOGY, ASAT- 13, 2009.

[167] M. Braik, A. Sheta, A. Arieqat, A comparison between GAs and PSO in training ANN to model the TE chemical process reactor, in: AISB 2008 Convention communication, interaction and social intelligence, Vol. 1, 2008, p. 24.

[168] A. Askarzadeh, A. Rezazadeh, Artificial neural network training using a new efficient optimization algorithm, Applied Soft Computing 13 (2) (2013) 1206 – 1213.

[169] I. Ramadhani, E. Minarto, Sungkono, Memory based hybrid dragonfly algorithm (MHDA): a new technique for determining model parameter in vertical electrical sounding (VES) data, Journal of Physics: Conference Series 1245 (2019) 012020. doi:10.1088/1742-6596/1245/1/012020.

[170] J. Wang, W. Yang, P. Du, Y. Li, Research and application of a hybrid forecasting framework based on multi-objective optimization for electrical power system, Energy 148 (2018) 59 – 78.

APPENDIX-A

Levy Flight Function

Lévy flights, also referred to as Lévy motion, stand for a class of non-Gaussian random processes whose stationary increments are distributed according to a Lévy stable distribution. Levy flight is a statistical description of motion that extend beyond the more traditional Brownian motion discovered over one hundred years earlier. Gaussian distributions, Levy distributions do not fall off as rapidly at long distances. Levy flight laws has been used for a broad class of processes such as in physical, chemical, biological, statistical and also in financial.

The Levy flight equation is calculated as follows:

$Levy(x) = 0.01 \times \frac{r_1 \times \sigma}{|r_2|^{\frac{1}{\beta}}}$

where r1 and r2 are two random numbers in [0,1], β is a constant (equal to 1.5 in this work) and α is calculated as follows:

$\alpha = \left(\frac{\Gamma(1+\beta) \times \sin\left(\frac{\pi\beta}{2}\right)}{\Gamma\left(\frac{1+\beta}{2}\right) \times \beta \times 2^{\left(\frac{\beta-1}{2}\right)}} \right)^{1/\beta}$

where Γ(x) = (x-1)!.

Composite Test Functions

In this section we give the details of composite test functions($F_{14} - F_{19}$) used in Suite-I. The basic functions for each composite function and controlling factors σ , λ for different functions are given below.

- F_{14}

$$f_1, f_2 ... f_{10} \quad = \quad Sphere\ Function$$

$$[\sigma_1, \sigma_2 ..... \sigma_{10}] \quad = \quad [1, 1, 1, ...1]$$

$$[\lambda_1, \lambda_2, ... \lambda_{10}] \quad = \quad \left[\frac{5}{100}, \frac{5}{100} ... \frac{5}{100}\right]$$

- F_{15}

$$f_1, f_2 ... f_{10} \quad = \quad Griewank's\ Function$$

$$[\sigma_1, \sigma_2 ..... \sigma_{10}] \quad = \quad [1, 1, 1, ...1]$$

$$[\lambda_1, \lambda_2, ...\lambda_{10}] \quad = \quad \left[\frac{5}{100}, \frac{5}{100} ... \frac{5}{100}\right]$$

- F_{16}

$$f1, f2 ... f10 \quad = \quad Griewank's\ Function$$

$$[\sigma_1, \sigma_2 ..... \sigma_{10}] \quad = \quad [1, 1, 1, ...1]$$

$$[\lambda_1, \lambda_2, ...\lambda_{10}] \quad = \quad [1, 1, 1, ...1]$$

- F_{17}

$$f_1, f_2 = Ackley's\ Function, f_3, f_4 = Rastrigin's\ Function f_5, f_6 = Weierstrass\ Function \\ , f_7, f_8 = Griewank's\ Function f_9, f_{10} = Sphere\ Function$$

$$[\sigma_1, \sigma_2 ..... \sigma_{10}] \quad = \quad [1, 1, 1, ...1]$$

$$[\lambda_1, \lambda_2, ...\lambda_{10}] \quad = \quad \left[\frac{5}{32}, \frac{5}{32}, 1, 1, \frac{5}{0.5}, \frac{5}{0.5}, \frac{5}{100}, \frac{5}{100}, \frac{5}{32}, \frac{5}{32}, \frac{5}{100}, \frac{5}{100}\right]$$

- F_{18}

$$f_1, f_2 = Rastrigin's\ Function, f_3, f_4 = Weierstrass\ Function f_5, f_6 = Griewank's\ Function \\ f_7, f_8 = Ackley's\ Function f_9, f_{10} = Sphere\ Function$$

$$[\sigma_1, \sigma_2 ..... \sigma_{10}] \quad = \quad [1, 1, 1, ...1]$$

$$[\lambda_1, \lambda_2, ...\lambda_{10}] \quad = \quad \left[\frac{1}{5}, \frac{1}{5}, \frac{5}{0.5}, \frac{5}{0.5}, \frac{5}{100}, \frac{5}{100}, \frac{5}{32}, \frac{5}{32}, \frac{5}{100}, \frac{5}{100}\right]$$

- F_{19}

$$f_1, f_2 = Rastrigin's\ Function, f_3, f_4 = Weierstrass\ Function f_5, f_6 = Griewank's\ Function$$
$$f_7, f_8 = Ackley's\ Function f_9, f_{10} = Sphere\ Function$$

$$[\sigma_1, \sigma_2 .....\sigma_{10}] = [0.1, 0.2, 0.3, 0.4, 0.5, 0.6, 0.7, 0.8, 0.9, 1]$$

$$[\lambda_1, \lambda_2, ...\lambda_{10}] = [0.1 * \frac{1}{5}, 0.2 * \frac{1}{5}, 0.3 * \frac{5}{0.5}, 0.4 * \frac{5}{0.5}, 0.5 * \frac{5}{100}, 0.6 * \frac{5}{100}, 0.7 * \frac{5}{32}, 0.8 * \frac{5}{32} 0.9 * \frac{5}{100}, 1 * \frac{5}{100}]$$

The mathematical formulation of basic functions used in the creation of composite functions are given below.

- Sphere Function

$f(x) = \sum_{i=1}^{d} x_i^2, x \in [-100, 100]^d$

- Rastrigin's Function

$f(x) = n * 10 + \sum_{i=1}^{d} (x_i - 10cos(2\Pi x_i)) x \in [-5, 5]^d$

- Griewank's Function

$f(x) = \frac{1}{4000} \sum_{i=1}^{d} x_i^2 - \prod_{i=1}^{d} cos(\frac{x}{\sqrt{1}}) + 1, x \in [-100, 100]^d$

- Ackley's Function

$f(x) = -20exp[-\frac{1}{5} \sqrt{\frac{1}{d} \sum_{i=1}^{d} cos(2\Pi x_i)}] + 20 + e, x \in [-32, 32]^d$

- Weierstrass Function

$f(x) = \sum_{i=1}^{d} \sum_{k=0}^{k=kmax} \left[a^k cos(2\Pi b^k (x_i + 0.5))\right] - D \sum_{k=0}^{k=kmax} \left[a^k cos(2\Pi b^k 0.5)\right]$

APPENDIX-B

Experimental Set up for training ANN

In this section, the performance of the proposed approach is verified using standard datasets. This involves eight classification datasets and three approximation functions.The classification dataset includes XOR, Balloon, Iris Heart, and Cancer, dataset taken from UCI machine learning repositoryand approximation dataset includes a one-dimensional sigmoid, one-dimensional cosine with one peak and one-dimensional sine with four peaks.The performance of MHDA is compared with recently proposed meta-heuristic algorithms such as Grey Wolf Optimizer (GWO), Dragonfly Algorithm (DA) and classical optimization algorithms such as Genetic algorithm (GA), Ant Colony Optimization(ACO) algorithms, Particle Swarm Optimization (PSO), Evolutionary Strategy (ES) and gradient based algorithm such as Back Propagation (BP) algorithm. The performance of MHDA trained ANN is also compared with well known Extreme Learning Machine (ELM) algorithm. All the experiments are executed on a personal computer (Core i7, 3.4GHz, 32GB RAM) using MATLAB and run 10 different times, each with 250 iterations. The number of neurons in the hidden layers is selected based on the method followed in literature. Prior to training, preprocessing of data is highly essential, as training algorithm works best when all the data are selected in the same range. As per min-max technique normalized value, p' in the range of $[min_A, max_A]$can be written as

$$p' = \frac{p - min_A}{max_A - min_A} \tag{7.1}$$

Classification dataset

Table 1 shows the specification of classification dataset. The number of attributes, training samples, test samples and classes for five different classification problems are explained. 3 bit XOR dataset is a standard non-linear classification problem and simplest among the dataset. ANN structure of 3-7-1 is used to solve this problem. Balloon dataset is based on different conditions of an experiment in blowing up a balloon. ANNs with a structure of 4-9-1 is used to classify this dataset. Iris dataset consists of 3 classes with 150 training or test samples. Each sample consist of 4 attributes. ANN of 4-9-3 is used to solve this problem. The purpose of cancer dataset is to classify whether a tumor is benign or malignant. It has 9 integer attributes and ANN of 9-19-1 is used to solve this dataset. Heart dataset consists of 22 attributes with 80 training samples and 187 test samples. ANN of 22-45-1 is used to classify this problem.

Table 1: Specification of classification dataset

Classification dataset	**No: of attributes**	**No: of training samples**	**No: of test samples**	**No: of classes**
3 bits XOR	3	8	8	2
Balloon	4	16	16	2
Iris	4	150	150	2
Cancer	9	599	100	2
Heart	22	80	187	2

Approximation Functions

ANNs with structure 1-15-1are trained using MHDA for approximating test functions such as sigmoid, cosine and sine. The number of training and test samples of different functions are explained in Table 2. The sigmoid dataset is in the range of [-3 3] with an interval of 0.1, whereas cosine dataset is in the range of [1.25 2.75] with an interval of 0.05. Sine dataset is a complicated dataset with the range of [-2Π,2Π] and with an interval of 0.1.

Table 2: Specification of functionapproximation dataset

Function Approximation Dataset	**No: of training samples**	**No: of test samples**
Sigmoid $y = 1/1 + e{-}^{x}$	$61 : x\ in[-3 : 0.1 : 3]$	$121 : xin[-3 : 0.05 : 3]$
Cosine $y = (cos(x\pi/2))^7$	$31 : x\ in[1.25 : 0.05 : 2.75]$	$38 : xin[1.25 : 0.04 : 2.75]$
Sine $y = sin(2x)$	$126 : x\ in[-2\pi : 0.1 : 2\pi]$	$252 : xin[-2\pi : 0.05 : 2\pi]$

Results and Discussions

Table 3: Performance of MHDA trained ANN
3(a)Classification dataset

Algorithm	Measure	XOR	Balloon	Iris	Cancer	Heart
	Mean	1.17E-03	3.50E-06	1.70E-02	7.26E-02	5.37E-02
BP	Std.Dev	4.12E+04	1.44E-06	1.70E-03	5.61E-03	8.78E+03
	Accuracy	**100%**	**100%**	78.66%	94%	72.5%
	Mean	8.41E-02	5.80E-04	2.29E-01	3.49E-02	1.89E-01
PSO	Std.Dev	3.60E-02	7.00E-04	5.72E-02	2.50E-03	8.90E-03
	Accuracy	37.5%	**100%**	37.33%	11%	68.75%
	Mean	1.00E-04	**5.08E-24**	8.99E-02	3.10E-03	9.30E-02
GA	Std.Dev	1.00E-04	1.06E-23	1.24E-01	1.50E-03	2.25E-02
	Accuracy	**100%**	**100%**	89.33%	98%	58.75%
	Mean	1.80E-01	4.85E-03	4.06E-01	1.35E-02	2.28E-01
ACO	Std.Dev	2.53E-02	7.80E-03	5.38E-02	2.10E-03	5.00E-03
	Accuracy	62.5%	**100%**	32.66%	40%	00%
	Mean	1.19E-01	1.91E-02	3.14E-01	4.03E-02	4.32E-02
ES	Std.Dev	1.16E-02	1.70E-01	5.21E-02	2.50E-03	2.00E-04
	Accuracy	62.5%	**100%**	46.66%	6%	71.25%
	Mean	9.40E-03	9.38E-15	2.29E-02	1.20E-03	1.23E-01
GWO	Std.Dev	2.95E-02	2.81E-14	3.20E-03	7.45E-05	7.70E-03
	Accuracy	**100%**	**100%**	91.333%	**99%**	75%
	Mean	8.89E-05	1.62E-09	1.23E-03	1.78E-02	1.60E-01
DA	Std.Dev	0.00E+00	0.00E+00	8.10E-08	1.00E-04	7.00E-04
	Accuracy	**100%**	**100%**	90.89 %	28%	70.32%
	Mean	**1.92E-06**	8.94E-19	**2.887E-04**	**1.10E-03**	4.**95E-02**
MHDA	Std.Dev	0.00E+00	0.00E+00	2.1E-09	0.00E+00	5.50E-02
	Accuracy	**100%**	**100%**	**92.22%**	**99%**	**77.36%**

The experimental results of proposed approach on classification and approximation datasets are shown in Table 3 (a) and 3 (b) respectively. It can be seen that classification rate of ANNs trained by GA,GWO,DA and MHDA on XOR dataset is 100%; however considering MSE values, the performance of MHDA is better. Due to the simplicity of dataset, all algorithms could give a classification rate of 100% on balloon dataset. GA outperformed all algorithms in terms of mean and standard deviation, and performance of MHDA was found second best to GA. The classification accuracy of MHDA was higher in the cancer dataset and iris dataset.

The breast cancer dataset has the highest difficulty compared to the previously discussed datasets in terms of the number of weights, biases, and training samples.

3(b)Approximation function

Algorithm	Measure	Sigmoid	Cosine	Sine
BP	Mean	3.70E-04	7.90E-03	2.03E-02
	Std.Dev	1.26E-04	3.80E-03	7.50E-03
	Test Error	1.3894	2.5663	23.3423
PSO	Mean	2.30E-02	5.90E-02	5.27E-01
	Std.Dev	9.40E-03	2.10E-02	7.29E-02
	Test Error	3.3563	2.009	124.89
GA	Mean	1.10E-03	1.09E-02	4.21E-01
	Std.Dev	1.00E-03	6.30E-03	6.12E-02
	Test Error	0.44969	0.7105	111.25
ACO	Mean	2.35E-02	5.09E-02	5.30E-01
	Std.Dev	1.00E-02	1.08E-02	5.33E-02
	Test Error	3.9974	2.4498	117.71
ES	Mean	7.56E-02	8.67E-02	7.07E-01
	Std.Dev	1.64E-02	2.22E-02	7.74E-02
	Test Error	8.8015	3.1461	142.31
GWO	Mean	1.00E-04	3.20E-03	2.62E-01
	Std.Dev	1.20E-03	2.16E-03	1.15E-01
	Test Error	0.27134	0.6692	149.6
DA	Mean	1.37E-09	4.18E-05	2.29E-01
	Std.Dev	3.60E-03	5.60E-03	3.00E-03
	Test Error	0.20864	2.2713	37.8121
MHDA	Mean	2.91E-12	1.14E-07	1.89E-01
	Std.Dev	**2.51E-12**	**9.97E-07**	**5.00E-08**
	Test Error	**0.0661**	**0.6635**	**34.7**

3(c)Statistical analysis

Algorithm	**Mean Rank**
MHDA	1.375
DA	3.25
GWO	3.625
GA	3.875
BP	4
PSO	6.25
ES	6.75
ACO	6.875

MHDA trained ANN has highest classification accuracy in this dataset, which strongly support the superiority of MHDA.The results of other algorithms have been taken from the reference. The above results confirm the superior performance of MHDA in avoiding local optima and reaching global optimal solutions. In case of approximation functions, best error rate belongs to MHDA training algorithm which proves the accuracy of the proposed method. The low value of mean and standard deviation shows the local optimal avoidance of MHDA.

<u>Thesis Highlight</u>

Name of the Student: Sree Ranjini K S

Name of the CI/OCC: IGCAR, Kalpakkam **Enrolment No.: ENGG02201404011**

Thesis Title: Design, Development and Optimization of High Temperature Motors for In-service Inspection Devices

Discipline: Engineering Sciences **Sub-Area of Discipline:** Motor design and Optimization

Date of viva voice: 03/02/2020

In-Service Inspection (ISI) of Fast Breeder Reactor (FBR) using semi-automated device is a typical application characterized by an ambient temperature of 150°C. High ambient temperature makes manual inspection of the plant infeasible. Any inspection under these circumstances can only be carried out by customized remote inspection techniques coupled with semi-automated devices. A compact, high temperature traction motor withstanding high temperatures and providing required torque, meeting the space constraints of the device is required to drive the device in the limited space.

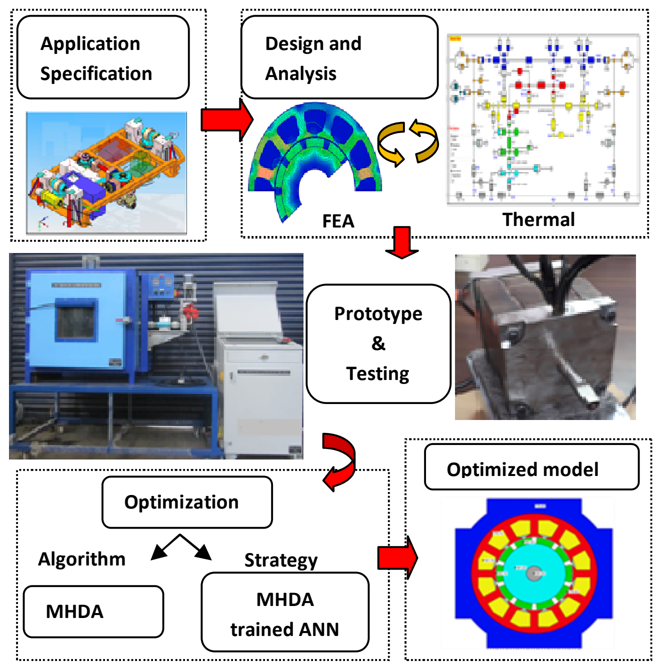

Figure 1. Methodology adopted in the design and development of an optimized model of high temperature motor.

Based on the application specifications, a comparative study of permanent magnet and permanent magnet free motors was done. It was found that permanent magnet motors were more suitable for the application in terms of torque density, higher efficiency and thermal performance. Special care has been taken in the selection of materials used for the design. A 12/10 slot/pole permanent magnet motor was designed and analyzed and the performance was verified with coupled electromagnetic-thermal analysis. The performance of the motor was verified experimentally using indigenously built high temperature motor test facility. Minimizing the winding temperature increases the lifetime of insulation thereby ensuring high reliability of motor. Hence the design of motor was optimized for reduced winding temperature keeping the constraints of torque, saturation flux density and efficiency. For this an efficient optimization strategy including a surrogate model and a novel hybrid optimization algorithm- Memory based Hybrid Dragonfly Algorithm (MHDA) has been proposed. A surrogate model is built based on neural networks and MHDA to save the computational cost of coupled simulation. The optimized design is then validated by coupled Finite Element Analysis-thermal analysis. In summary, a high temperature motor was designed, developed and tested. An efficient optimization strategy was proposed for optimization purpose. This can be incorporated in any of modern motor design software in order to ease the optimization process and accurately find the optimal solution.